Part 5
Uncoupled Spins

10 Single Spin-1/2

The next four chapters concern the dynamics of one-spin systems, i.e. isolated nuclei that are assumed not to interact with each other, to a good approximation. Many very important NMR experiments, such as NMR imaging, may be treated well within this approximation.

We start by considering the simplest possible case: systems of isolated spins-1/2.

10.1 Zeeman Eigenstates

According to the quantum theory of angular momentum (Chapter 7), a single spin-1/2 has two eigenstates of angular momentum along the z-axis, denoted $|\alpha\rangle$ and $|\beta\rangle$. These states are defined:

$$|\alpha\rangle = |\frac{1}{2}, +\frac{1}{2}\rangle$$
$$|\beta\rangle = |\frac{1}{2}, -\frac{1}{2}\rangle \tag{10.1}$$

using the notation $|I, M\rangle$, as given in Section 7.7. The states $|\alpha\rangle$ and $|\beta\rangle$ are called the *Zeeman eigenstates* of the single spin-1/2 and obey the following eigenequations:

$$\hat{I}_z|\alpha\rangle = +\frac{1}{2}|\alpha\rangle$$
$$\hat{I}_z|\beta\rangle = -\frac{1}{2}|\beta\rangle \tag{10.2}$$

Equation 10.2 indicates that the state $|\alpha\rangle$ is an eigenstate of angular momentum along the z-axis, with eigenvalue $+1/2$. A spin that is in the state $|\alpha\rangle$ is said to be *polarized along the z-axis*. Similarly, the state $|\beta\rangle$ is an eigenstate of angular momentum along the z-axis, with eigenvalue $-1/2$. A spin that is in the state $|\beta\rangle$ is said to be *polarized along the $-z$-axis*.

In diagrams, the spin states $|\alpha\rangle$ and $|\beta\rangle$ are represented by arrows pointing along the positive or negative z-axis:

Spin Dynamics: Basics of Nuclear Magnetic Resonance, Second Edition Malcolm H. Levitt

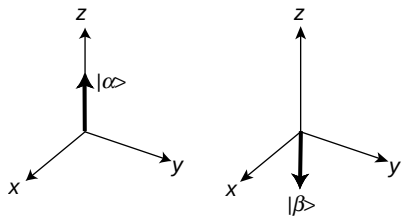

Figure 10.1
The two Zeeman eigenstates of a single spin-1/2.

The state $|\alpha\rangle$ is sometimes called the 'spin-up' state; the state $|\beta\rangle$ is sometimes said to be 'spin-down'.

10.2 Measurement of Angular Momentum: Quantum Indeterminacy

Suppose a spin is in a certain quantum state and the z-component of angular momentum is measured. I leave aside the technical issue as to how this is actually done; suffice it to say that such observations are possible.[1]

Consider first the situation in which the spin is in state $|\alpha\rangle$ when the z-component of angular momentum is measured. The state $|\alpha\rangle$ is an eigenstate of the operator $\hat{I}_z$, with eigenvalue $+1/2$. According to the postulates of quantum mechanics (Section 7.1.3), the observation of z-angular momentum on a spin in state $|\alpha\rangle$ always gives the same result, namely the eigenvalue $+1/2$ (in units of $\hbar$, as usual). The z-angular momentum of state $|\alpha\rangle$ is said to be *sharp*, or *well defined*.

Similarly, the observation of z-angular momentum on a spin in the state $|\beta\rangle$ always gives the same result, namely $-1/2$.

What happens if the spin is in state $|\alpha\rangle$, but the x-component of angular momentum is observed instead of the z-component? Since the state $|\alpha\rangle$ is *not* an eigenstate of the operator $\hat{I}_x$, the result is *fundamentally unpredictable*. The result is always either $+1/2$ or $-1/2$, but it is *impossible* to predict which of the two answers will be given. The diagram below shows the results of many identical observations, all on spins prepared in identical physical states $|\alpha\rangle$:

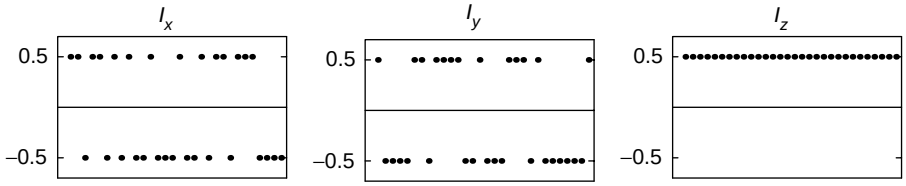

Figure 10.2
Observations of spins in state $|\alpha\rangle$.

Similarly, if the spins are prepared in identical states $|\beta\rangle$, the measurement of z-angular momentum gives the reproducible value $-1/2$, and measurements of the x- or y-components give results that are equally and randomly distributed between the values $\pm 1/2$:

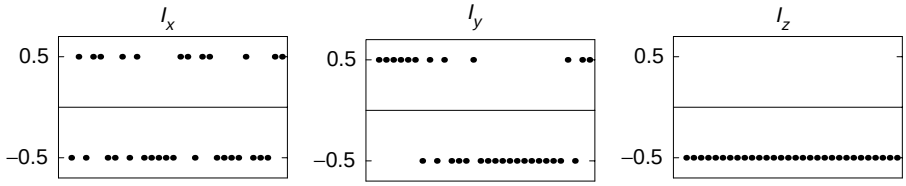

Figure 10.3
Observations of spins in state $|\beta\rangle$.

The irreproducibility of these results is not due to instrumental imperfections. Nor is it due to something 'inside' the spin that decides whether the result is going to be $+1/2$ or $-1/2$. This possibility has been ruled out by more subtle experimental observations (see *Further Reading*).

The random outcome of certain observations is now broadly accepted as a *feature or reality itself*. Even though the quantum state is a complete description of the physical system, it is *not sufficient* to give unambiguous results for all observations. In plain language, sometimes *even the spin* does not 'know' what the answer is going to be! Colloquially speaking, if the spin is in state $|\alpha\rangle$ and the z-component of angular momentum is measured, then the spin 'knows the answer'. It says '$+1/2$'. But if the x-component of angular momentum is measured, the spin says: 'I don't know. I'll choose $+1/2$ or $-1/2$ at random'.

This feature of quantum mechanics is a very deep mystery. Probably it is beyond human understanding. Many scientists, such as Einstein, could never reconcile themselves to it ('God does not play dice'). Nevertheless, it is supported by massive experimental evidence and is now broadly accepted (see *Further Reading*).

No pictorial representation of a spin state is completely satisfactory. The diagrams in Figure 10.1 use an arrow to indicate the spin polarization, i.e. the direction along which the angular momentum is well-defined. The state $|\alpha\rangle$ is represented by an arrow along the z-axis, and the state $|\beta\rangle$ is represented by an arrow pointing along the $-z$-axis. These 'spin arrows' must not be overinterpreted. An arrow along the z-axis does *not* imply that the angular momentum along the x-axis is zero. In fact, the angular momentum along the x-axis is *undefined*: measurements give the result $\pm 1/2$, with equal probability. It is impossible to accomodate this feature in a pictorial representation.

Some books try to depict the quantum indeterminacy by drawing the spin state as a sort of cone. Such diagrams are always incorrect on closer examination and are best avoided.

⚠ These 'spin polarization arrows' do *not* behave like ordinary vectors. For example, the arrow diagrams do *not* imply that $|\alpha\rangle$ and $|\beta\rangle$ are related by a sign change:

$$|\alpha\rangle = -|\beta\rangle \qquad \text{⚠WRONG!} \tag{10.3}$$

The 'arrow' is a pictorial device for depicting the direction of well-defined spin angular momentum, and nothing else.

10.3 Energy Levels

If the magnetic field is along the z-axis and has magnitude B^0, the spin Hamiltonian is proportional to $\hat{I}_z$:

$$\widehat{\mathcal{H}}^0 = \omega^0 \hat{I}_z \tag{10.4}$$

where the (chemically shifted) Larmor frequency is given by $\omega^0 = -\gamma B^0(1+\delta)$. The states $|\alpha\rangle$ and $|\beta\rangle$ are eigenstates of the spin Hamiltonian, obeying the eigenequations

$$\widehat{\mathcal{H}}^0|\alpha\rangle = +\frac{1}{2}\omega^0|\alpha\rangle$$

$$\widehat{\mathcal{H}}^0|\beta\rangle = -\frac{1}{2}\omega^0|\beta\rangle$$

The eigenvalues $\pm\frac{1}{2}\omega^0$ are the *energies* of the states. The two states $|\alpha\rangle$ and $|\beta\rangle$ have well-defined (sharp) energies. An energy level diagram may be constructed, in which each 'energy level' belongs to a different state. The energy level splitting of the spin in the magnetic field is known as the *Zeeman splitting* and is equal to the Larmor frequency ω^0 (as usual, in units of $\hbar$):

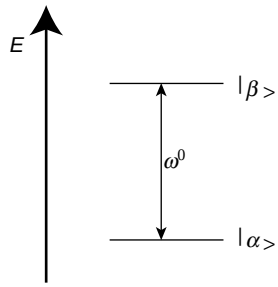

Figure 10.4
Energy levels for a spin-1/2 in a magnetic field.

This diagram is appropriate for a spin of positive gyromagnetic ratio γ, and hence negative Larmor frequency ω^0. Note that the state $|\alpha\rangle$ has lower energy than the state $|\beta\rangle$ in this case.

10.4 Superposition States

10.4.1 General spin states

A spin-1/2 particle is not restricted to the $|\alpha\rangle$ or $|\beta\rangle$ state, but may be in a *superposition* of the two energy eigenstates:

$$|\psi\rangle = c_\alpha|\alpha\rangle + c_\beta|\beta\rangle \tag{10.5}$$

where c_α and c_β are complex numbers, called *superposition coefficients*. The only restriction on the values of the superposition coefficients is that the state must be *normalized*:

$$|c_\alpha|^2 + |c_\beta|^2 = 1 \tag{10.6}$$

10.4.2 Vector notation

The state $|\psi\rangle = c_\alpha|\alpha\rangle + c_\beta|\beta\rangle$ is conveniently written as a two-dimensional column vector with complex components:

$$|\psi\rangle = \begin{pmatrix} c_\alpha \\ \\ c_\beta \end{pmatrix}$$

In this notation, the Zeeman eigenstates are written

$$|\alpha\rangle = \begin{pmatrix} 1 \\ \\ 0 \end{pmatrix} \qquad |\beta\rangle = \begin{pmatrix} 0 \\ \\ 1 \end{pmatrix}$$

The bra state $\langle\psi|$ is written as a *row vector*, with elements given by the complex conjugates of the corresponding ket column vector:

$$\langle\psi| = |\psi\rangle^\dagger = (\,c_\alpha{}^* \,, \quad c_\beta{}^*\,)$$

Note that the adjoint operation corresponds to taking the transpose (which turns a row vector into a column vector), followed by taking the complex conjugate.

The normalization condition corresponds to the usual multiplication rule for row and column vectors:

$$\langle\psi|\psi\rangle = (\,c_\alpha{}^*, \quad c_\beta{}^*\,)\begin{pmatrix} c_\alpha \\ c_\beta \end{pmatrix} = c_\alpha{}^* c_\alpha + c_\beta{}^* c_\beta = |c_\alpha|^2 + |c_\beta|^2 = 1$$

10.4.3 Some particular states

Consider the following superposition state:

$$|+x\rangle = \frac{1}{\sqrt{2}}|\alpha\rangle + \frac{1}{\sqrt{2}}|\beta\rangle$$

or in vector notation:

$$|+x\rangle = \frac{1}{\sqrt{2}}\begin{pmatrix} 1 \\ 1 \end{pmatrix}$$

This state is called $|+x\rangle$ because it is an eigenstate of the operator $\hat{I}_x$ with eigenvalue $+1/2$:

$$\hat{I}_x|+x\rangle = \frac{1}{2}\begin{pmatrix} 0 & 1 \\ 1 & 0 \end{pmatrix}\frac{1}{\sqrt{2}}\begin{pmatrix} 1 \\ 1 \end{pmatrix} = \frac{1}{2\sqrt{2}}\begin{pmatrix} 1 \\ 1 \end{pmatrix} = \frac{1}{2}\cdot\frac{1}{\sqrt{2}}\begin{pmatrix} 1 \\ 1 \end{pmatrix} = \frac{1}{2}|+x\rangle$$

For this state, the x-component of spin angular momentum is 'sharp', whereas the y- and z-components are not:

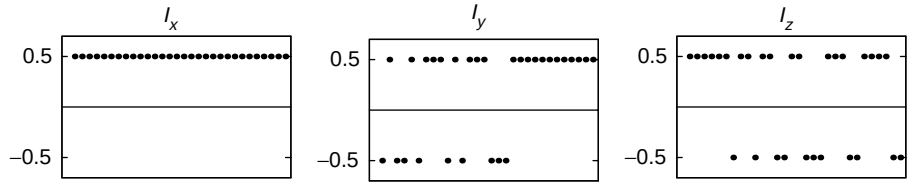

Figure 10.5
Observations of spins in state $|+x\rangle$.

This state, therefore, can be depicted as an arrow along the $+x$-axis:

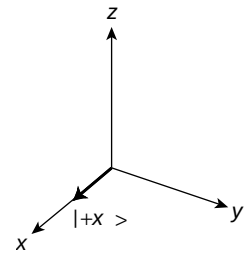

Figure 10.6
Pictorial representation of the state $|+x\rangle$.

Similarly, consider the state $|-y\rangle$, defined as

$$|-y\rangle = \frac{1}{2}(1+\mathrm{i})|\alpha\rangle + \frac{1}{2}(1-\mathrm{i})|\beta\rangle = \frac{1}{2}\begin{pmatrix} 1+\mathrm{i} \\ 1-\mathrm{i} \end{pmatrix}$$

This is an eigenstate of the operator $\hat{I}_y$ with eigenvalue $-1/2$:

$$\hat{I}_y|-y\rangle = \frac{1}{2\mathrm{i}}\begin{pmatrix} 0 & 1 \\ -1 & 0 \end{pmatrix}\frac{1}{2}\begin{pmatrix} 1+\mathrm{i} \\ 1-\mathrm{i} \end{pmatrix} = -\frac{1}{2}\cdot\frac{1}{2}\begin{pmatrix} 1+\mathrm{i} \\ 1-\mathrm{i} \end{pmatrix} = -\frac{1}{2}|-y\rangle$$

The y-component of spin angular momentum is 'sharp', whereas the x- and z-components are not:

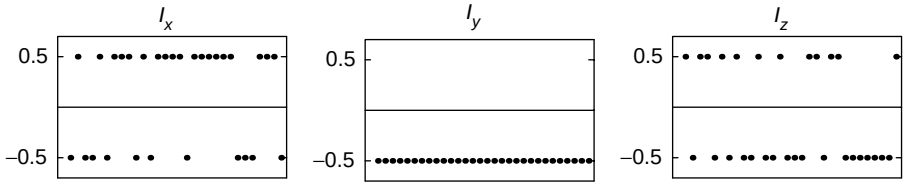

Figure 10.7
Observations of spins in state $|-y\rangle$.

This state, therefore, can be depicted as a arrow along the $-y$-axis:

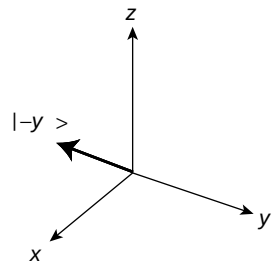

Figure 10.8
Pictorial representation of the state $|-y\rangle$.

If the magnetic field is along the z-axis, then superposition states such as $|+x\rangle$ and $|-y\rangle$ do not have sharp energies. Therefore, it is not possible to attach these states to energy level diagrams. The spin is 'in between' the energy levels. Nevertheless, the superposition states have just as much physical reality as the Zeeman eigenstates, and they play a very important role in NMR.

A variety of spin-1/2 quantum states, and ways of depicting these states, is shown below:

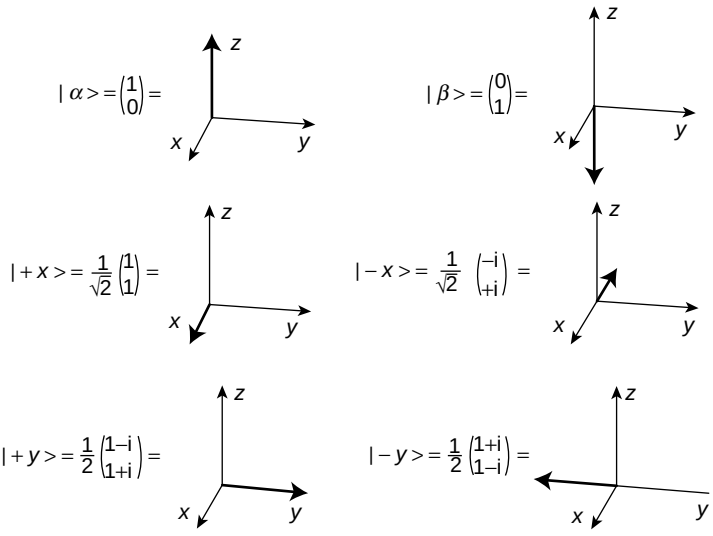

Figure 10.9
A selection of spin states.

It is possible to construct quantum states with well-defined angular momentum in *any* spatial direction, not just along the x-, y- or z-axes. For example, the state

$$|\theta, \phi\rangle = \begin{pmatrix} \cos\tfrac{1}{2}\theta\, \mathrm{e}^{-\mathrm{i}\frac{1}{2}\phi} \\ \sin\tfrac{1}{2}\theta\, \mathrm{e}^{+\mathrm{i}\frac{1}{2}\phi} \end{pmatrix}$$

obeys the following eigenequation:

$$\left(\hat{I}_z \cos\theta + \hat{I}_x \sin\theta\cos\phi + \hat{I}_y \sin\theta\sin\phi\right)|\theta, \phi\rangle = +\frac{1}{2}|\theta, \phi\rangle$$

and has the following geometric representation:

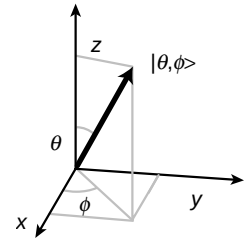

Figure 10.10
Pictorial representation of the state $|\theta, \phi\rangle$.

10.4.4 Phase factors

Two states $|\psi\rangle$ and $|\psi\rangle'$ differ by a *phase factor* if they can be expressed as follows:

$$|\psi\rangle' = \mathrm{e}^{\mathrm{i}\phi}|\psi\rangle$$

For example, the state

$$|-y\rangle' = \frac{1}{\sqrt{2}}\begin{pmatrix} \mathrm{i} \\ 1 \end{pmatrix}$$

is related to the state

$$|-y\rangle = \frac{1}{2}\begin{pmatrix} 1+\mathrm{i} \\ 1-\mathrm{i} \end{pmatrix}$$

by the phase factor $\exp\{\mathrm{i}\pi/4\}$.

States related by a phase factor obey the same eigenequation and give the same results for most observations (within the limits of quantum indeterminacy, as described above). Nevertheless, there are certain situations in which the phase factors are relevant, so it is best to retain them.

It is not convenient to show the phase of the state on 'arrow diagrams'. The states $|-y\rangle$ and $|-y\rangle'$, given above, both have sharp y angular momentum of $-1/2$, and must both be depicted as arrows pointing along the negative y-axis. The arrow diagrams are always incomplete in this sense.

⚠ Changing the sign of a spin state is equivalent to multiplying it by the phase factor $\exp\{\mathrm{i}\pi\} = -1$. As just mentioned, this does *not* change the direction of the spin polarization 'arrow'. The 'arrow' for $-|\alpha\rangle$ is the same as the arrow for $|\alpha\rangle$; both point along the z-axis. Multiplying $|\alpha\rangle$ by -1 does *not* change it into the state $|\beta\rangle$ (see Equation 10.3).

10.5 Spin Precession

In general, the spin state $|\psi\rangle$ depends on time – the spin precesses.

Suppose that one knows the spin state $|\psi\rangle(t_\mathrm{a})$ at an initial time point t_a, and wishes to predict the spin state at a later time point t_b. The interval between the time points is given by $\tau = t_\mathrm{b} - t_\mathrm{a}$:

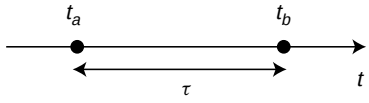

Figure 10.11
Two time points.

The law of motion of the spin is the time-dependent Schrödinger equation:

$$\frac{\mathrm{d}}{\mathrm{d}t}|\psi\rangle(t) = -\mathrm{i}\widehat{\mathcal{H}}|\psi\rangle(t) \tag{10.7}$$

If there is no r.f. field, the spin Hamiltonian is

$$\widehat{\mathcal{H}} = \widehat{\mathcal{H}}^0 = \omega^0 \hat{I}_z$$

The equation of motion of the spin, in the absence of an r.f. field, is therefore:

$$\frac{\mathrm{d}}{\mathrm{d}t}|\psi\rangle(t) = -\mathrm{i}\omega^0 \hat{I}_z|\psi\rangle(t)$$

This is a simple first-order differential equation. The solution is

$$|\psi\rangle(t_\mathrm{b}) = \exp\{-\mathrm{i}\omega^0\tau\hat{I}_z\}|\psi\rangle(t_\mathrm{a}) \tag{10.8}$$

The exponential operator was already encountered in Section 7.8. It is equal to a *rotation operator* for the spin around the z-axis:

$$\widehat{R}_z(\phi) = \exp\{-\mathrm{i}\phi\hat{I}_z\} \tag{10.9}$$

The solution of the Schrödinger equation, in the absence of r.f. fields, is therefore:

$$|\psi\rangle(t_b) = \widehat{R}_z\left(\omega^0\tau\right)|\psi\rangle(t_a) \tag{10.10}$$

In the absence of r.f. fields, the Schrödinger equation says that *the spin rotates around the z-axis, through the angle* $\omega^0\tau$. We will examine the physical meaning of this in a moment.

As described in Section 7.8, the matrix representation of the rotation operator is:

$$\widehat{R}_z(\phi) = \exp\{-i\phi\hat{I}_z\} = \begin{pmatrix} \exp\{-i\frac{1}{2}\phi\} & 0 \\ 0 & \exp\{+i\frac{1}{2}\phi\} \end{pmatrix} \tag{10.11}$$

This matrix is now used to do some explicit calculations.

10.5.1 Dynamics of the eigenstates

The motion of these states depends on the value of $\omega^0\tau$, where τ is the elapsed interval between times t_a and t_b. For simplicity, consider a special case. Suppose that the elapsed interval τ is given by

$$\tau = \left|\frac{\pi}{2\omega^0}\right|$$

The absolute value is necessary because a time interval τ is always positive, whatever the sign of the Larmor frequency. If the gyromagnetic ratio γ is positive, then the Larmor frequency $\omega^0 = -\gamma B^0$ is negative, so the (positive) interval τ is given by

$$\tau = -\frac{\pi}{2\omega^0}$$

In this case, the relevant angle is

$$\omega^0\tau = -\pi/2$$

The relationship between states at times t_a and t_b is therefore

$$|\psi\rangle(t_b) = \widehat{R}_z(-\pi/2)|\psi\rangle(t_a)$$

where the rotation operator has a matrix representation:

$$\widehat{R}_z(-\pi/2) = \begin{pmatrix} \exp\{+i\pi/4\} & 0 \\ 0 & \exp\{-i\pi/4\} \end{pmatrix} = \frac{1}{\sqrt{2}}\begin{pmatrix} 1+i & 0 \\ 0 & 1-i \end{pmatrix}$$

Suppose that the spin is in an eigenstate $|\psi\rangle(t_a) = |\alpha\rangle$ at time t_a. At time t_b, it is in the state

$$|\psi\rangle(t_b) = \widehat{R}_z(-\pi/2)|\psi\rangle(t_a) = \frac{1}{\sqrt{2}}\begin{pmatrix} 1+i & 0 \\ 0 & 1-i \end{pmatrix}\begin{pmatrix} 1 \\ 0 \end{pmatrix} = \frac{1}{\sqrt{2}}(1+i)\begin{pmatrix} 1 \\ 0 \end{pmatrix} = \exp\{+i\pi/4\}|\alpha\rangle$$

The new state $|\psi\rangle(t_b)$ is still an eigenstate of $\hat{I}_z$, with eigenvalue $+1/2$. Apart from the phase factor $\exp\{+i\pi/4\}$, the spin 'didn't move'. The eigenstate $|\alpha\rangle$ is *stationary*:

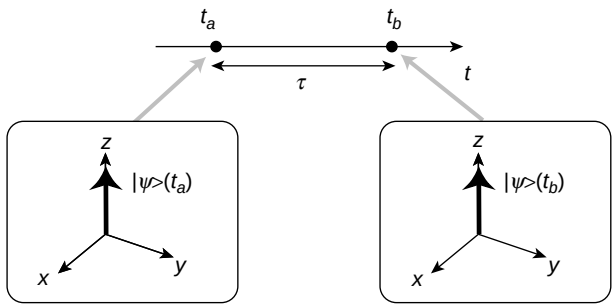

Figure 10.12
The state $|\alpha\rangle$ is stationary under free evolution.

(The phase factor is not shown.)

This result is general. If the spin is in an eigenstate of the Hamiltonian, it remains in that eigenstate, only accumulating a phase factor, for as long as the Hamiltonian remains constant.

10.5.2 Dynamics of the superposition states

If the spin is initially in the superposition state

$$|\psi\rangle(t_\mathrm{a}) = |+x\rangle = \frac{1}{\sqrt{2}}\begin{pmatrix}1\\1\end{pmatrix}$$

it evolves over the interval τ according to

$$\begin{aligned}|\psi\rangle(t_\mathrm{b}) &= \widehat{R}_z(-\pi/2)|\psi\rangle(t_\mathrm{a}) = \widehat{R}_z(-\pi/2)|+x\rangle \\ &= \frac{1}{\sqrt{2}}\begin{pmatrix}1+\mathrm{i} & 0\\ 0 & 1-\mathrm{i}\end{pmatrix}\frac{1}{\sqrt{2}}\begin{pmatrix}1\\1\end{pmatrix} = \frac{1}{2}\begin{pmatrix}1+\mathrm{i}\\1-\mathrm{i}\end{pmatrix} = |-y\rangle\end{aligned}$$

The initial state $|+x\rangle$ evolves into the state $|-y\rangle$ over the time τ. This can be depicted pictorially as a rotation of the spin polarization around the z-axis:

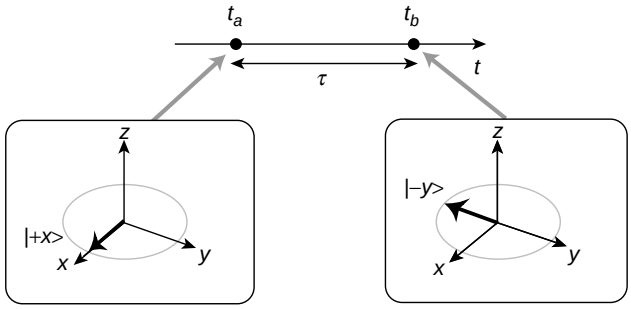

Figure 10.13
Precession transforms the state $|+x\rangle$ into the state $|-y\rangle$.

If the evolution is continued for a further three intervals τ, the pattern of the motion is more obvious:

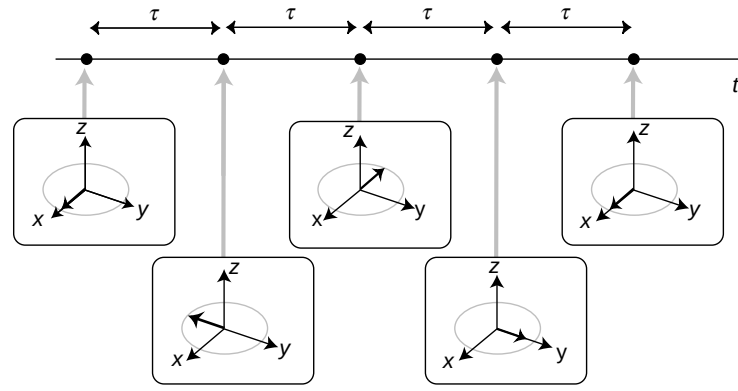

Figure 10.14
Precession of superposition states.

(The reader should verify this by calculation.)

This *precession* of the spin angular momentum axis was described in Section 2.4. Note the negative sense of the precession. The precession frequency is equal to the Larmor frequency ω^0, which is a negative number for positive-γ spins.

The free precession of the spin starting in state $|+x\rangle$ may therefore be written as

$$|-y\rangle = \widehat{R}_z(-\pi/2)|+x\rangle \qquad |-x\rangle = \widehat{R}_z(-\pi/2)|-y\rangle$$
$$|+y\rangle = \widehat{R}_z(-\pi/2)|-x\rangle \qquad |+x\rangle = \widehat{R}_z(-\pi/2)|+y\rangle$$

and so on. If γ is positive, each interval τ leads to spin precession through the angle $-\pi/2$ about the z-axis.

The precessional motion of the spin angular momentum is a consequence of quantum mechanics. Nevertheless, it resembles many everyday classical phenomena, as mentioned in Chapter 2 (bicycle riding, precession of a child's top, etc.).

To summarize: if the spin is initially in an energy eigenstate ($|\alpha\rangle$ or $|\beta\rangle$), then it remains in that state, only accumulating a complex phase factor. If the spin is in a superposition state, then it precesses around the z-axis at the Larmor frequency.

10.6 Rotating Frame

The equation of motion is more complicated in the presence of r.f. pulses, since the spin Hamiltonian is time dependent in that case. In order to solve the spin dynamics in the presence of an r.f. field, a special trick is needed. This mathematical trick is equivalent to viewing the nuclear spins from a reference frame revolving around the z-axis. Under suitable approximations, the spin Hamiltonian *appears* to be time independent in the rotating frame.

The rotating frame is useful because the resonant part of the r.f. field is rotating (see Section 8.4.2). By viewing the spins from a frame that rotates 'with the field', it is possible to make the r.f. field look as if it is static:

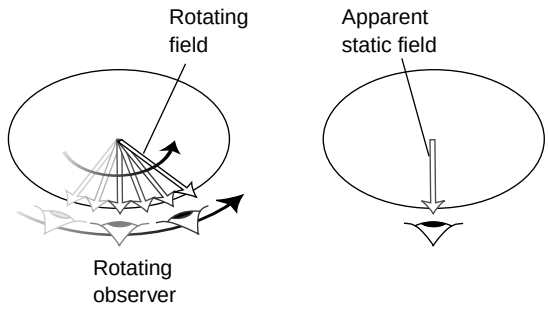

Figure 10.15
The rotating reference frame.

In this way, a difficult time-dependent problem is reduced to a simpler form.

The use of the rotating frame is a necessary evil, and requires some notational complexity. The reader may prefer to skip to the main results (Equations 10.15 and 10.16).

Consider two reference frames, i.e. a fixed reference frame, with axes $\mathbf{e}_x$, $\mathbf{e}_y$, $\mathbf{e}_z$, and a rotating reference frame, with axes denoted $\mathbf{e}'_x$, $\mathbf{e}'_y$, $\mathbf{e}'_z$:

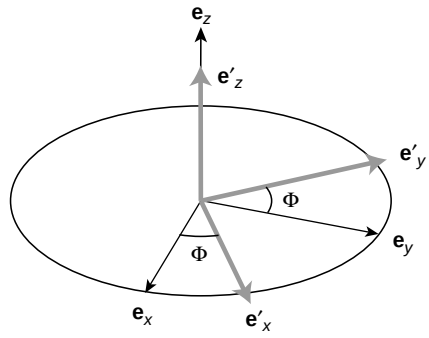

Figure 10.16
The rotating frame axes $\mathbf{e}'_x$, $\mathbf{e}'_y$ and $\mathbf{e}'_z$.

The frame axes are related as

$$\mathbf{e}'_x = \mathbf{e}_x \cos\Phi(t) + \mathbf{e}_y \sin\Phi(t)$$
$$\mathbf{e}'_y = \mathbf{e}_y \cos\Phi(t) - \mathbf{e}_z \sin\Phi(t)$$
$$\mathbf{e}'_z = \mathbf{e}_z$$

where $\Phi(t)$ is a time-dependent angle. We consider the case where the frame rotates with a constant frequency ω_{ref} around the z-axis:

$$\Phi(t) = \omega_{\text{ref}} t + \phi_{\text{ref}} \tag{10.12}$$

The appropriate choice of frame phase ϕ_{ref} is discussed below.

For brevity, the symbol (t) indicating time dependence is now dropped.

Consider a spin with a Larmor frequency exactly equal to the reference frequency ω_{ref}. If this spin were prepared in a state $|+x\rangle$, then it would precess at the frequency ω_{ref}, keeping its polarization arrow always along the rotating axis $\mathbf{e}'_x$. By the arguments of the previous section, this spin state must have the form

$$|+x'\rangle = \widehat{R}_z(\Phi)|+x\rangle$$

in which the angle Φ increases in time, as given in Equation 10.12.

Now imagine that one were viewing the spin *from the rotating frame*. Clearly, the spin would appear to be static, and identical to the state $|+x\rangle$. This statement can be formalized by writing

$$\widetilde{|+x'\rangle} = |+x\rangle$$

where the $\widetilde{\ }$ symbol ('tilde') is taken to mean 'as viewed from the rotating frame'. It follows that the spin state 'as viewed from the rotating frame' must be related to the spin state 'as viewed from the laboratory frame' through

$$\widetilde{|+x'\rangle} = \widehat{R}_z(-\Phi)|+x'\rangle$$

This relationship may be generalized: Any spin state 'viewed from the rotating frame' is related to the spin state 'viewed from the fixed frame' through

$$|\widetilde{\psi}\rangle = \widehat{R}_z(-\Phi)|\psi\rangle \tag{10.13}$$

This equation may now be used to derive the equation of motion of the spin states 'as seen from the rotating frame', $|\widetilde{\psi}\rangle$.

I will now use the term *rotating-frame spin states* to mean 'spin states as seen from the rotating frame'.

Consider the time derivative of the rotating-frame state $|\widetilde{\psi}\rangle$. By the usual chain rule for differentiation, it is given by

$$\frac{\mathrm{d}}{\mathrm{d}t}|\widetilde{\psi}\rangle = \frac{\mathrm{d}}{\mathrm{d}t}\left\{\widehat{R}_z(-\Phi)|\psi\rangle\right\} = \left\{\frac{\mathrm{d}}{\mathrm{d}t}\widehat{R}_z(-\Phi)\right\}|\psi\rangle + \widehat{R}_z(-\Phi)\left\{\frac{\mathrm{d}}{\mathrm{d}t}|\psi\rangle\right\} \tag{10.14}$$

From Equation 10.9, the time derivative of the rotation operator is

$$\frac{\mathrm{d}}{\mathrm{d}t}\widehat{R}_z(-\Phi) = \frac{\mathrm{d}}{\mathrm{d}t}\exp\{+\mathrm{i}\Phi\hat{I}_z\} = \mathrm{i}\hat{I}_z\left\{\frac{\mathrm{d}}{\mathrm{d}t}\Phi\right\}\exp\{+\mathrm{i}\Phi\hat{I}_z\} = \mathrm{i}\omega_{\mathrm{ref}}\hat{I}_z\widehat{R}_z(-\Phi)$$

The first term on the right-hand-side of Equation 10.14 is therefore

$$\left\{\frac{\mathrm{d}}{\mathrm{d}t}\widehat{R}_z(-\Phi)\right\}|\psi\rangle = \mathrm{i}\omega_{\mathrm{ref}}\hat{I}_z\widehat{R}_z(-\Phi)|\psi\rangle = \mathrm{i}\omega_{\mathrm{ref}}\hat{I}_z|\widetilde{\psi}\rangle$$

The second term on the right-hand side may be calculated by the time-dependent Schrödinger equation:

$$\widehat{R}_z(-\Phi)\left\{\frac{\mathrm{d}}{\mathrm{d}t}|\psi\rangle\right\} = -\mathrm{i}\widehat{R}_z(-\Phi)\widehat{\mathcal{H}}|\psi\rangle = -\mathrm{i}\widehat{R}_z(-\Phi)\widehat{\mathcal{H}}\widehat{R}_z(\Phi)|\widetilde{\psi}\rangle$$

where the last line uses the inverse of the relationship in Equation 10.13. All of these equations may be combined to give the *rotating-frame Schrödinger equation*:

$$\frac{\mathrm{d}}{\mathrm{d}t}|\widetilde{\psi}\rangle = -\mathrm{i}\hat{\tilde{\mathcal{H}}}|\widetilde{\psi}\rangle \tag{10.15}$$

where the operator $\hat{\tilde{\mathcal{H}}}$ is given by

$$\hat{\tilde{\mathcal{H}}} = \hat{R}_z(-\Phi)\hat{\mathcal{H}}\hat{R}_z(\Phi) - \omega_{\text{ref}}\hat{I}_z \tag{10.16}$$

Equation 10.15 is identical to the time-dependent Schrödinger equation (Equation 10.7), except for the substitution of the rotating-frame state $|\tilde{\psi}\rangle$ for the fixed-frame state $|\psi\rangle$, and the substitution of the operator $\hat{\tilde{\mathcal{H}}}$ for the spin Hamiltonian $\hat{\mathcal{H}}$. Therefore, it is natural to call the operator $\hat{\tilde{\mathcal{H}}}$ the *rotating-frame spin Hamiltonian*. It plays the same role in the rotating frame as the ordinary Hamiltonian does in the fixed frame.

Equation 10.15 and Equation 10.16 are the main results of this section. They give a recipe for deriving the dynamics of the spin states 'as viewed from the rotating frame'. One simply uses the ordinary time-dependent Schrödinger equation, but substitutes the rotating-frame spin Hamiltonian $\hat{\tilde{\mathcal{H}}}$ for the ordinary spin Hamiltonian.

What is the physical significance of the two terms in Equation 10.16? The first term may be interpreted as the usual Hamiltonian, rotated about the z-axis through the angle Φ. This rotation arises because the system is viewed from a frame which is itself rotating. Any static spin operators appear to be rotating backwards when viewed from this frame. The second term in Equation 10.16 is more subtle. It produces an additional correction to the spin dynamics, over and above the transformations of the spin operators. This correction arises because the frame is not executing a linear motion, but is rotating and, therefore, accelerating in the technical sense.

An analogy with the everyday world may help. We all live on a rotating frame, because the Earth is rotating about the north–south axis. In everyday life, we find it convenient to use our own planetary rotating frame, rather than a frame that is fixed with respect to the stars. For example, when we say 'go west' or 'go east', we are using implicitly the rotating reference frame (otherwise we would have to use different directions every few minutes, as the Earth rotates). This procedure corresponds to using only the first term in Equation 10.16. One simply forgets that the Earth is rotating, because we are rotating with it. However, just occasionally, the second term makes its presence felt, often in a rather non-intuitive way. For example, the circulation of the winds and the ocean currents are manifestations of planetary rotation. Sometimes fictitious forces, called 'Coriolis forces', are invented to account for such effects, but the real cause is simply the rotation of the planet. For nuclear spins, described in the rotating frame, the second term in Equation 10.16 takes into account the ficititious 'Coriolis forces'.

So far, the equations were developed for the rotating frame in a rather general way. We must now be more specific in our choice of frame. As discussed in Section 8.4.2, the frame frequency ω_{ref} is equal to the frequency of the resonant component of the r.f. pulse (i.e. the component that rotates in the same sense as the spin precession). If γ is positive, then the Larmor frequency $\omega^0 = -\gamma B^0$ is negative, so ω_{ref} is also negative. On the other hand, if γ is negative, then the Larmor frequency and ω_{ref} are both positive. In addition, one has to choose the phase of the rotating frame at time $t = 0$ (ϕ_{ref} in Equation 10.12). There are a number of different conventions for this initial phase.

The convention followed in this book is as follows:

$$\begin{aligned} \phi_{\text{ref}} &= \pi \qquad (\text{for } \gamma > 0) \\ \phi_{\text{ref}} &= 0 \qquad (\text{for } \gamma < 0) \end{aligned} \tag{10.17}$$

The convention for ϕ_{ref} has no practical consequences, but makes some calculations more convenient, as will be seen.

10.7 Precession in the Rotating Frame

We now examine the precessional motion of the spin in the presence of the static magnetic field, as seen from the rotating reference frame.

The spin Hamiltonian in the static field is

$$\hat{\mathcal{H}}^0 = \omega^0 \hat{I}_z$$

so that the rotating-frame Hamiltonian is

$$\hat{\tilde{\mathcal{H}}}^0 = \omega^0 \hat{R}_z(-\Phi)\hat{I}_z\hat{R}_z(\Phi) - \omega_{\text{ref}}\hat{I}_z = (\omega^0 - \omega_{\text{ref}})\hat{I}_z$$

The last equation follows because the rotation operator $\hat{R}_z(\Phi)$ commutes with the angular momentum operator $\hat{I}_z$ (see Section 7.7.2).

The frequency $\omega^0 - \omega_{\text{ref}}$ is the difference between the Larmor frequency and that of the frame. It is called the *relative Larmor frequency*, *offset frequency*, or *resonance offset*, and is denoted Ω^0:

$$\Omega^0 = \omega^0 - \omega_{\text{ref}} \tag{10.18}$$

The rotating-frame spin Hamiltonian, in the presence of the static field, is therefore

$$\hat{\tilde{\mathcal{H}}}^0 = \Omega^0 \hat{I}_z \tag{10.19}$$

This has just the same form as the laboratory-frame spin Hamiltonian, except that the offset frequency Ω^0 is involved instead of the Larmor frequency ω^0. The previous discussion may therefore be used without modification. The rotating-frame spin states $|\tilde{\psi}\rangle$ precess around the z-axis at the offset frequency Ω^0. Over a time interval τ, the spin precesses through the angle $\Omega^0\tau$ in the rotating frame:

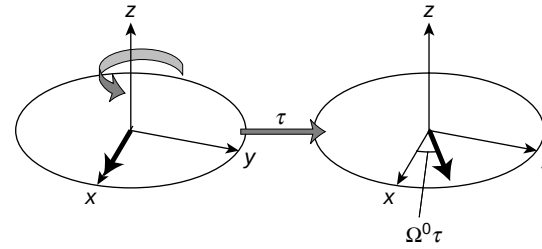

Figure 10.17
Precession in the rotating frame.

The offset frequency Ω^0, unlike the Larmor frequency ω^0, is under experimental control at fixed magnetic field. Adjustment of the spectrometer reference frequency changes the offset Ω^0. For example, if the spectrometer reference frequency is set exactly equal to the Larmor frequency ($\omega^0 = \omega_{\text{ref}}$), then the resonance offset is zero. This is called the case of *exact resonance*.

The offset frequency Ω^0 is related to the chemical shift of the spin and the setting for the reference frequency. Suppose that the spectrometer reference frequency corresponds to the chemical shift δ_{ref}, i.e.

$$\omega_{\text{ref}} = -\gamma B^0(1 + \delta_{\text{ref}}) \tag{10.20}$$

In this case, the offset frequency is given by

$$\Omega^0 = -\gamma B^0(\delta - \delta_{\text{ref}}) \tag{10.21}$$

where $-\gamma B^0$ is the Larmor frequency, including the sign.

Sections 3.4 and 3.5 examined the relationship between the offset frequency Ω^0 and the chemical shift scale. For spins of positive γ, peaks on the left-hand side of the spectrum (high δ) correspond to spins precessing in the negative sense in the rotating frame, whereas peaks on the right-hand side of the spectrum (low δ) correspond to spins precessing in the positive sense in the rotating frame. Spins with chemical shifts equal to δ_{ref} have an offset frequency $\Omega^0 = 0$:

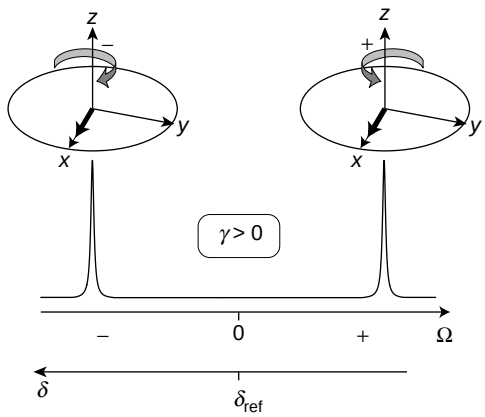

Figure 10.18
Rotating frame precession and the frequency axis for $\gamma > 0$.

For spins with negative γ, the offset frequency axis runs in the opposite direction:

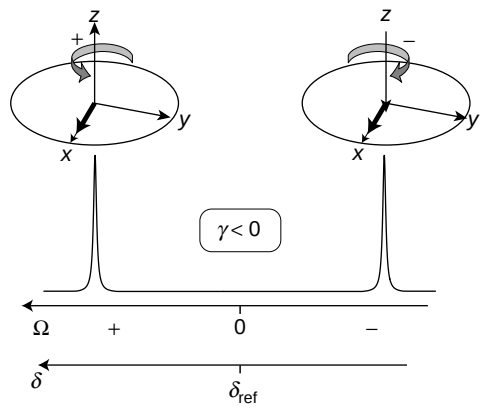

Figure 10.19
Rotating frame precession and the frequency axis for $\gamma < 0$.

10.8 Radio-Frequency Pulse

When an r.f. pulse is applied, the spin experiences two magnetic fields: a static field generated by the magnet and an oscillating field from the excitation coil. The static field is many orders of magnitude larger than the oscillating field.

Why does the weak r.f. field produce a large effect on the nuclear spin, in the presence of the much larger static field?

The key point is that the r.f. field is *resonant* with the precession of the spin. As the spin precesses, the rotating r.f. field 'keeps up' with it. This allows the effect of the weak r.f. field to accumulate as time goes on. If the pulse is applied for long enough, then the weak r.f. field can give rise to a large change in the spin state.

In practice, a significant change in the spin polarization is induced after several microseconds of r.f. irradiation. This corresponds to hundreds of Larmor precession cycles.

The effect is analogous to a child's swing. Each small push on the swing only produces a small effect, but if the pushes are applied at a frequency that corresponds to the natural oscillation frequency of the swing, the accumulated effect after many pushes can be large.

In this section, we examine the mathematics of this process. The use of the rotating frame makes the calculation easier. Nevertheless, the following derivation displays some mathematical complexity and some readers may want to skip to the main result (Equation 10.26).

10.8.1 Rotating-frame Hamiltonian

Consider an r.f. pulse of phase ϕ_{p} applied along the x-axis of the fixed reference system. As described in Section 8.4.2, the r.f. field oscillates in amplitude at the spectrometer reference frequency ω_{ref}. This oscillation may be described as two components rotating in opposite senses. The *resonant* field component rotates in the same sense as the nuclear spin precession. The *non-resonant* field component rotates in the opposite sense. Under normal circumstances, it is possible to neglect the non-resonant component, and this is what we will do now.[2]

With this approximation, the spin Hamiltonian during an r.f. pulse is given by

$$\widehat{\mathcal{H}}(t) = \omega^0 \hat{I}_z + \widehat{\mathcal{H}}_{\mathrm{RF}}(t)$$

where

$$\widehat{\mathcal{H}}_{\mathrm{RF}}(t) \cong -\frac{1}{2}\gamma B_{\mathrm{RF}} \sin\theta_{\mathrm{RF}} \left\{\cos\left(\omega_{\mathrm{ref}} t + \phi_{\mathrm{p}}\right)\hat{I}_x + \sin\left(\omega_{\mathrm{ref}} t + \phi_{\mathrm{p}}\right)\hat{I}_y\right\} \tag{10.22}$$

and B_{RF} is the peak value of the oscillating r.f. field, in units of tesla (see Section 8.4.2).

It is convenient to write the r.f. part of the spin Hamiltonian in a different form. We can use the sandwich relationship in Section 6.6.2 to write Equation 10.22 as

$$\widehat{\mathcal{H}}_{\mathrm{RF}}(t) \cong -\frac{1}{2}\gamma B_{\mathrm{RF}} \sin\theta_{\mathrm{RF}}\ \widehat{R}_z\left(\Phi_p\right)\hat{I}_x\widehat{R}_z\left(-\Phi_p\right)$$

where the time-dependent angle Φ_p is given by

$$\Phi_p(t) = \omega_{\mathrm{ref}} t + \phi_{\mathrm{p}}$$

In the rotating frame, the appropriate spin Hamiltonian is given by applying Equation 10.16. The result is

$$\hat{\tilde{\mathcal{H}}} = -\frac{1}{2}\gamma B_{\mathrm{RF}} \sin\theta_{\mathrm{RF}} \hat{R}_z\left(-\Phi + \Phi_p\right) \hat{I}_x \hat{R}_z\left(\Phi - \Phi_p\right) + (\omega^0 - \omega_{\mathrm{ref}})\hat{I}_z$$

where Φ is specified in Equation 10.12.

If all the terms are gathered up, and substitutions are made, we get

$$\hat{\tilde{\mathcal{H}}} \cong -\frac{1}{2}\gamma B_{\mathrm{RF}} \sin\theta_{\mathrm{RF}} \hat{R}_z\left(-\phi_{\mathrm{ref}} + \phi_{\mathrm{p}}\right) \hat{I}_x \hat{R}_z\left(\phi_{\mathrm{ref}} - \phi_{\mathrm{p}}\right) + \Omega^0 \hat{I}_z \tag{10.23}$$

where Ω^0 is the resonance offset.

Note that the time dependence has vanished from this expression.[2] This is the point of the rotating frame: it transforms a time-dependent quantum-mechanical problem into a time-independent one.

As a final simplification, we can substitute in the value of ϕ_{ref}, as specified in Equation 10.17. For positive γ spins, ϕ_{ref} is equal to π, which has the effect of changing the sign of the first term in the equation. Equation 10.23 becomes

$$\hat{\tilde{\mathcal{H}}} \cong \omega_{\mathrm{nut}} \hat{R}_z\left(\phi_{\mathrm{p}}\right) \hat{I}_x \hat{R}_z\left(-\phi_{\mathrm{p}}\right) + \Omega^0 \hat{I}_z \tag{10.24}$$

where the nutation frequency is defined as

$$\omega_{\mathrm{nut}} = |\tfrac{1}{2}\gamma B_{\mathrm{RF}} \sin\theta_{\mathrm{RF}}| \tag{10.25}$$

The nutation frequency is a measure of the r.f. field amplitude and is always positive, which proves to be convenient.[3]

For negative γ spins, ϕ_{ref} is equal to zero, so exactly the same equations apply.

The sandwich property may be used again to write Equation 10.24 as

$$\hat{\tilde{\mathcal{H}}} \cong \Omega^0 \hat{I}_z + \omega_{\mathrm{nut}} \left(\hat{I}_x \cos\phi_{\mathrm{p}} + \hat{I}_y \sin\phi_{\mathrm{p}}\right) \tag{10.26}$$

The final form of the rotating-frame Hamiltonian during the pulse, Equation 10.26, is very simple, and should be memorized.

10.8.2 *x*-pulse

Consider a strong pulse of frequency ω_{ref}, duration τ_{p} and phase $\phi_{\mathrm{p}} = 0$ (an '*x*-pulse', in the usual NMR jargon). The amplitude of the pulse is specified through the nutation frequency ω_{nut}:

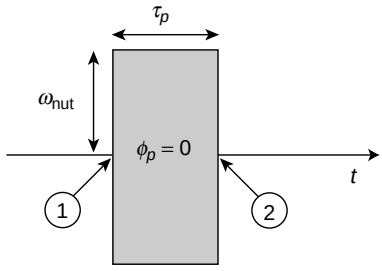

Figure 10.20
A pulse of phase $\phi_{\mathrm{p}} = 0$ and duration τ_{p}.

Consider the case in which the pulse is applied exactly on resonance ($\Omega^0 = 0$). This is ensured by setting the reference frequency to the exact Larmor frequency ($\omega_{\mathrm{ref}} = \omega^0$).

The time points ① and ② indicate the start and end of the pulse, which is assumed to be perfectly rectangular.

The rotating-frame spin Hamiltonian during the pulse is

$$\hat{\tilde{\mathcal{H}}} = \omega_{\text{nut}} \hat{I}_x$$

The motion of the spin states may be calculated through the rotating-frame Schrödinger equation (Equation 10.15). Suppose that the spin state before the pulse is given by $|\tilde{\psi}\rangle_{①}$, and the spin state after the pulse is given by $|\tilde{\psi}\rangle_{②}$. By direct integration of the Schrödinger equation, these states are related by

$$|\tilde{\psi}\rangle_{②} = \widehat{R}_x(\beta_{\text{p}})|\tilde{\psi}\rangle_{①} \tag{10.27}$$

where the *pulse propagator* $\widehat{R}_x(\beta_{\text{p}})$ is defined as

$$\widehat{R}_x(\beta_{\text{p}}) = \exp\{-\text{i}\beta_{\text{p}}\hat{I}_x\} \tag{10.28}$$

and the angle β_{p} is given by

$$\beta_{\text{p}} = \omega_{\text{nut}}\tau_{\text{p}} \tag{10.29}$$

The angle β_{p} is called the *flip angle* of the pulse, and is by definition always positive. It is proportional to the amplitude of the pulse, through the factor ω_{nut}, and is also proportional to the duration of the pulse τ_{p}.

In order to discover what the pulse does, we can use the matrix representation of the rotation operator $\widehat{R}_x(\beta_{\text{p}})$. This is derived in Appendix A.4, and is equal to

$$\widehat{R}_x(\beta) = \begin{pmatrix} \cos\frac{1}{2}\beta & -\text{i}\sin\frac{1}{2}\beta \\ -\text{i}\sin\frac{1}{2}\beta & \cos\frac{1}{2}\beta \end{pmatrix} \tag{10.30}$$

This matrix representation may be used to calculate what the pulse does to spins prepared in various states.

1. *A* $(\pi/2)_x$ *pulse applied to a spin in state* $|\alpha\rangle$. The notation $(\pi/2)_x$ implies that the flip angle is $\beta_{\text{p}} = \pi/2$ and the phase is $\phi_{\text{p}} = 0$. The transformation of the state may be calculated as follows:

$$\widehat{R}_x(\pi/2)|\alpha\rangle = \frac{1}{\sqrt{2}}\begin{pmatrix} 1 & -\text{i} \\ -\text{i} & 1 \end{pmatrix}\begin{pmatrix} 1 \\ 0 \end{pmatrix} = \frac{1}{\sqrt{2}}\begin{pmatrix} 1 \\ -\text{i} \end{pmatrix} = \text{e}^{-\text{i}\pi/4}\frac{1}{2}\begin{pmatrix} 1+\text{i} \\ 1-\text{i} \end{pmatrix} = \text{e}^{-\text{i}\pi/4}|-y\rangle$$

Apart from the unimportant phase factor, the pulse transforms the state $|\alpha\rangle$ into the state $|-y\rangle$, i.e. rotates the polarization of the spin by $\pi/2$ around the x-axis:

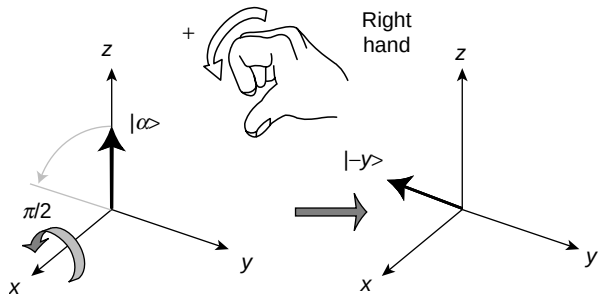

Figure 10.21
The state $|\alpha\rangle$ is transformed into the state $|-y\rangle$ by a $(\pi/2)_x$ pulse.

Note the sense of the *positive* rotation: *anticlockwise* looking down the rotation axis towards the origin.

2. *A π_x pulse applied to a spin in state $|\alpha\rangle$*. This time the flip angle is $\beta_{\mathrm{p}} = \pi$ and the phase is $\phi_{\mathrm{p}} = 0$. The transformation of the state is

$$\widehat{R}_x(\pi)|\alpha\rangle = \begin{pmatrix} 0 & -\mathrm{i} \\ -\mathrm{i} & 0 \end{pmatrix} \begin{pmatrix} 1 \\ 0 \end{pmatrix} = -\mathrm{i} \begin{pmatrix} 0 \\ 1 \end{pmatrix} = -\mathrm{i}|\beta\rangle$$

Apart from the phase factor, the pulse transforms the state $|\alpha\rangle$ into the state $|\beta\rangle$:

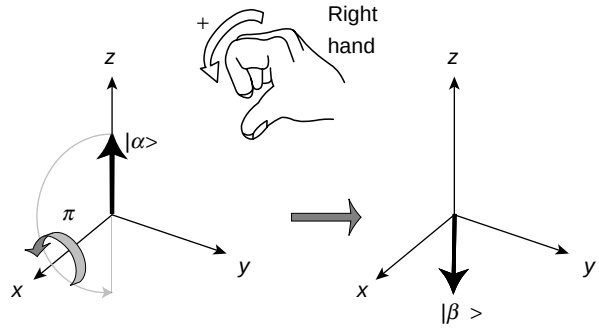

Figure 10.22
The state $|\alpha\rangle$ is transformed into the state $|\beta\rangle$ by a π_x pulse.

3. *A $(\pi)_x$ pulse applied to a spin in state $|+x\rangle$*. The transformation this time is:

$$\widehat{R}_x(\pi)|+x\rangle = \begin{pmatrix} 0 & -\mathrm{i} \\ -\mathrm{i} & 0 \end{pmatrix} \frac{1}{\sqrt{2}} \begin{pmatrix} 1 \\ 1 \end{pmatrix} = -\mathrm{i}\frac{1}{\sqrt{2}} \begin{pmatrix} 1 \\ 1 \end{pmatrix} = -\mathrm{i}|+x\rangle$$

Apart from the phase factor, the pulse leaves the state $|+x\rangle$ unchanged:

Do you get the idea? Whatever the intial state of the spin in the rotating frame, the action of the pulse can always be calculated geometrically, just by rotating the angular momentum around the x-axis through an angle equal to the flip angle of the pulse. Only the phase factors are left out, and these are usually unimportant.

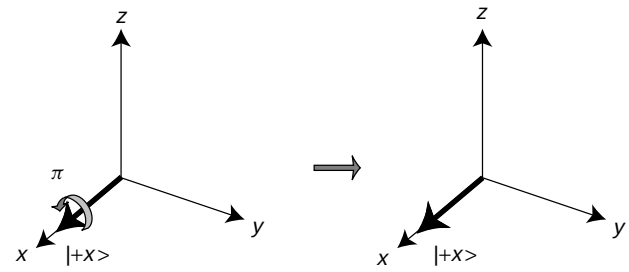

Figure 10.23
A π_x pulse applied to $|+x\rangle$ has no effect.

10.8.3 Nutation

The above calculations concern the rotating-frame spin states $|\widetilde{\psi}\rangle$. In order to examine the motion of the spin states in the fixed reference frame, we have to transform back again. From

$$|\widetilde{\psi}\rangle_{②} = \widehat{R}_x(\beta_{\mathrm{p}})|\widetilde{\psi}\rangle_{①}$$

and the relationship in Equation 10.13 between the fixed-frame and the rotating-frame states, we get

$$|\psi\rangle_{②} = \widehat{R}_z\Big(\Phi(t_{②})\Big)\widehat{R}_x(\beta_{\mathrm{p}})\widehat{R}_z\Big(-\Phi(t_{①})\Big)|\psi\rangle_{①}$$

where $t_{①}$ and $t_{②}$ are the time coordinates at the beginning and end of the pulse ($t_{②} = t_{①} + \tau_{\mathrm{p}}$). This relationship is *much* more complicated. The rotation of the spin polarization around the x-axis, induced by the pulse, occurs simultaneously with the rapid rotation around the z-axis, due to the motion of the frame. These two simultaneous rotations generate a sort of spiralling motion. This motion may be visualized by imagining that the tip of the spin polarization arrow leaves a track behind. The track has the following form:

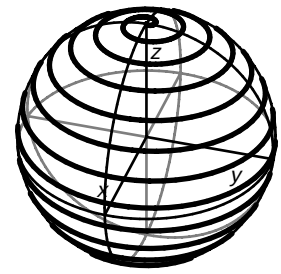

Figure 10.24
The track left behind by the tip of the spin polarization arrow under an r.f. pulse, in the fixed frame.

The diagram uses unrealistic parameters to bring out the nature of the motion more clearly. In practice, there are many thousands of revolutions around the z-axis for every revolution around the x-axis.

This complicated double rotational motion is called *nutation* in classical mechanics. This is the origin of the term *nutation frequency* for the quantity ω_{nut}.

Since the motion of the spin states during the pulse is so much more complicated in the static frame, it is customary to analyse the entire NMR experiment in the rotating frame.

10.8.4 Pulse of general phase

Now consider a pulse that is exactly on resonance ($\Omega^0 = 0$), but which has a general r.f. phase ϕ_p. The rotating-frame spin Hamiltonian during the pulse is

$$\hat{\tilde{\mathcal{H}}} = \omega_\mathrm{nut}\left(\hat{I}_x \cos\phi_\mathrm{p} + \hat{I}_y \sin\phi_\mathrm{p}\right) \tag{10.31}$$

From the form of this operator, one can see that the effect of the phase shift is to change the axis about which the spin polarizations rotate. The rotation axis is still in the xy-plane, but subtends an angle ϕ_p with the x-axis:

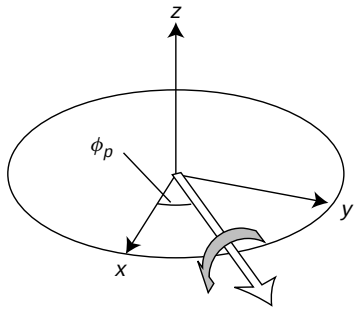

Figure 10.25
Rotation axis for a pulse of general phase.

For example, a pulse of phase $\phi_\mathrm{p} = \pi/2$ rotates the spin polarization around the y-axis, a pulse of phase $\phi_\mathrm{p} = \pi$ rotates the spin polarization around the $-x$-axis, and so on. This property is the origin of the jargon for pulse phases summarized in Table 4.1.

The *propagator for an on-resonance pulse of general phase* is given by

$$\begin{aligned}\widehat{R}_{\phi_p}(\beta_\mathrm{p}) &= \exp\{-\mathrm{i}\omega_\mathrm{nut}\tau_\mathrm{p}\left(\hat{I}_x\cos\phi_\mathrm{p} + \hat{I}_y\sin\phi_\mathrm{p}\right)\} \\ &= \exp\{-\mathrm{i}\beta_\mathrm{p}\left(\hat{I}_x\cos\phi_\mathrm{p} + \hat{I}_y\sin\phi_\mathrm{p}\right)\}\end{aligned}$$

The results of Section 7.6.3 may be used to set this in the form

$$\widehat{R}_{\phi_p}(\beta_\mathrm{p}) = \widehat{R}_z(\phi_\mathrm{p})\widehat{R}_x(\beta_\mathrm{p})\widehat{R}_z(-\phi_\mathrm{p}) \tag{10.32}$$

This is a product of three rotation operators: two about the z-axis and one about the x-axis.

The matrix representation of the operator $\widehat{R}_{\phi_p}(\beta_\mathrm{p})$ is easily derived by multiplying together these three matrices. The result is

$$\widehat{R}_{\phi_p}(\beta_\mathrm{p}) = \begin{pmatrix} \cos\tfrac{1}{2}\beta_\mathrm{p} & -\mathrm{i}\sin\tfrac{1}{2}\beta_\mathrm{p}\mathrm{e}^{-\mathrm{i}\phi_\mathrm{p}} \\ -\mathrm{i}\sin\tfrac{1}{2}\beta_\mathrm{p}\mathrm{e}^{+\mathrm{i}\phi_\mathrm{p}} & \cos\tfrac{1}{2}\beta_\mathrm{p} \end{pmatrix} \tag{10.33}$$

The reader should be able to verify the properties:

$$\widehat{R}_y(\pi/2)|\alpha\rangle = \text{phase factor} \times |+x\rangle$$

$$\widehat{R}_{\bar{x}}(\pi/2)|+y\rangle = \text{phase factor} \times |\beta\rangle$$

which have the following geometrical representation:

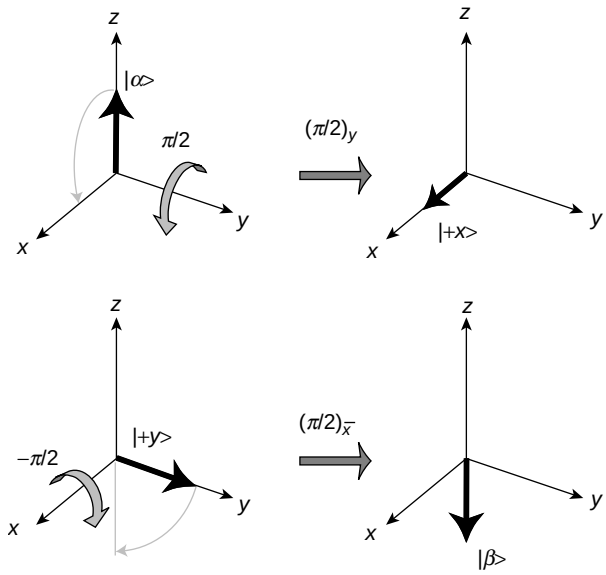

Figure 10.26
More examples of pulses acting on spins.

The notation 'y' implies a phase $\phi_p = \pi/2$; the notation '$\bar{x}$' implies a phase $\phi_p = \pi$, and so on. Note carefully the *negative* rotation in the last example (point the thumb of your right hand along the *negative* x-axis, and see which way your fingers curl).

10.8.5 Off-resonance effects

Up to now, we have assumed that the r.f. pulse was exactly on resonance, $\Omega^0 = 0$. In general, it is not possible to ensure exact resonance for all spins at the same time, so this condition cannot always be satisfied. We must consider the case $\Omega^0 \neq 0$, i.e. the problem of *off-resonance* effects.

I will not consider this case very thoroughly, but simply emphasize the results and their experimental significance.

The spin Hamiltonian during a general rectangular pulse is given by

$$\hat{\tilde{\mathcal{H}}} = \Omega^0 \hat{I}_z + \omega_{\text{nut}} \left(\hat{I}_x \cos\phi_p + \hat{I}_y \sin\phi_p \right)$$

By analogy with the previous discussion, one can guess what happens. The rotation axis of the spin polarization now has a z-component as well as an x- and a y-component. The axis is therefore 'tilted' out of the xy-plane. The sense of the 'tilt' depends on the sign of Ω^0. If Ω^0 is positive, the axis is tilted in the positive x-direction, i.e. 'above' the plane. If Ω^0 is negative, then the axis is tilted in the negative x-direction, i.e. 'below' the plane:

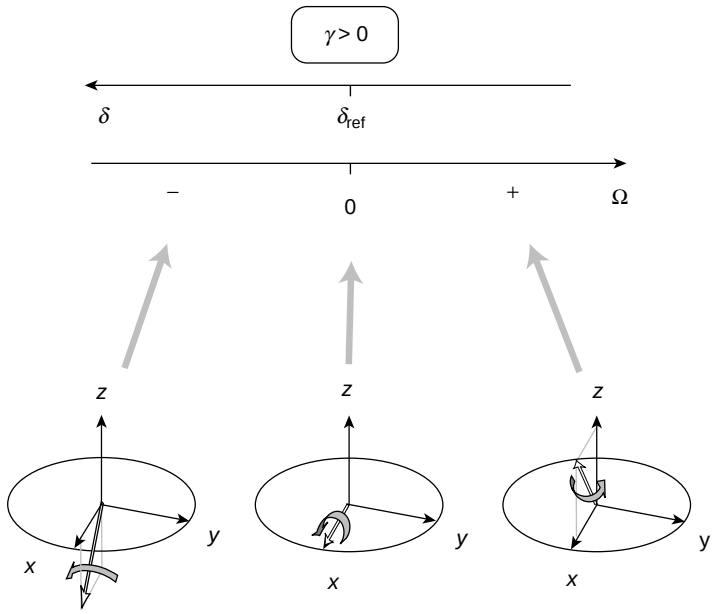

Figure 10.27
Rotation axes for off-resonance pulses.

(These diagrams apply to the case $\gamma > 0$.)

I will not derive the propagator in this case explicitly. The following results are stated without proof, although they may easily be verified from the matrix representations. The rotating-frame spin Hamiltonian for an off-resonant pulse may be written

$$\hat{\tilde{\mathcal{H}}} = \boldsymbol{\omega}_{\text{eff}} \cdot \hat{\mathbf{I}}$$

where $\boldsymbol{\omega}_{\text{eff}}$ is the *effective rotation axis*, given by

$$\boldsymbol{\omega}_{\text{eff}} = \omega_{\text{eff}} \left\{ \mathbf{e}'_x \sin\theta_{\text{p}} \cos\phi_{\text{p}} + \mathbf{e}'_y \sin\theta_{\text{p}} \sin\phi_{\text{p}} + \mathbf{e}'_z \cos\theta_{\text{p}} \right\} \tag{10.34}$$

and $\{\mathbf{e}'_x, \mathbf{e}'_y, \mathbf{e}'_z\}$ are the axes of the rotating reference frame. The vector operator $\hat{\mathbf{I}}$ is defined as

$$\hat{\mathbf{I}} = \mathbf{e}'_x \hat{I}_x + \mathbf{e}'_y \hat{I}_y + \mathbf{e}'_z \hat{I}_z$$

The *tilt* of the rotation axis away from the z-axis is given by

$$\theta_{\text{p}} = \arctan\left(\frac{\omega_{\text{nut}}}{\Omega^0}\right) \tag{10.35}$$

The *magnitude* of the rotation frequency around the tilted axis is given by

$$\omega_{\text{eff}} = \left\{ (\omega_{\text{nut}})^2 + (\Omega^0)^2 \right\}^{1/2} \tag{10.36}$$

The tilt θ_{p} is defined such that $\theta_{\text{p}} = \pi/2$ in the exact on-resonance case ($\Omega^0 = 0$).

Using these parameters, the rotating-frame spin Hamiltonian may be written as

$$\hat{\tilde{\mathcal{H}}} = \omega_{\text{eff}} \hat{R}_z(\phi_{\text{p}}) \hat{R}_y(\theta_{\text{p}}) \hat{I}_z \hat{R}_y(-\theta_{\text{p}}) \hat{R}_z(-\phi_{\text{p}})$$

The rotating-frame spin states before and after the pulse are related through

$$|\widetilde{\psi}\rangle_{②} = \widehat{R}_{\text{off}}|\widetilde{\psi}\rangle_{①}$$

where $\widehat{R}_{\text{off}}$ is the off-resonance pulse propagator, given by

$$\widehat{R}_{\text{off}} = \widehat{R}_z(\phi_{\text{p}})\widehat{R}_y(\theta_{\text{p}})\widehat{R}_z(\omega_{\text{eff}}\tau_{\text{p}})\widehat{R}_y(-\theta_{\text{p}})\widehat{R}_z(-\phi_{\text{p}}) \tag{10.37}$$

The off-resonance pulse propagator, therefore, may be written as a product of *five* rotations about orthogonal axes. The frequency of the rotation is no longer equal to the nutation frequency ω_{nut}, but is given by the square root of the sum of the squares of the nutation frequency and the offset Ω^0. Therefore, the rotation frequency for a pulse applied off-resonance is always *larger* than the nutation frequency, so that the rotation angle is always larger than the nominal flip angle $\beta_{\text{p}} = |\omega_{\text{nut}}\tau_{\text{p}}|$. However, the rotation occurs about a tilted axis, which makes it less effective.

Rather than delving into the mathematics of these transformations, I show below what happens to the polarization of a spin in state $|\alpha\rangle$ exposed to a $\pi/2$ pulse with different resonance offsets Ω^0. For clarity, the track of the *tip* of the polarization arrow is drawn during the pulse, but not the polarization arrow itself. The diagrams depict the motion of the spin polarization around the rotation axis, which is shown as an 'open' arrow. All pictures are shown in the rotating frame, and the value of $\Omega^0/\omega_{\text{nut}}$ is given above each diagram:

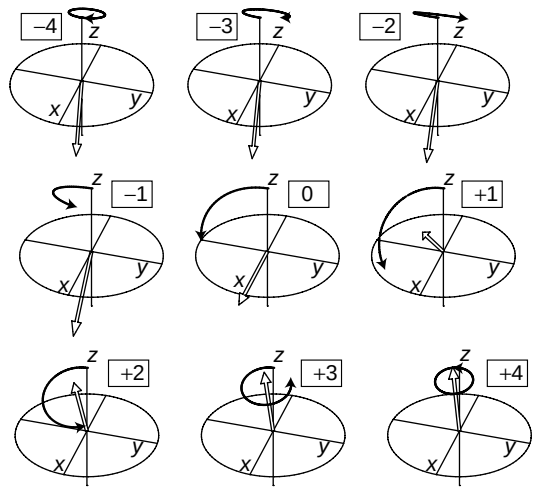

Figure 10.28
Off-resonance pulses acting on spins initially in the state $|\alpha\rangle$. The white arrow indicates the rotation axis. The black arrow indicates the trace left by the tip of the spin polarization arrow. The labels show the value of $\Omega^0/\omega_{\text{nut}}$. The pulse has an on-resonance flip angle $\omega_{\text{nut}}\tau_{\text{p}} = \pi/2$.

When the pulse is far off resonance, nothing much happens. The tilt angle ϕ_{p} is small, and the spin polarization simply wobbles a number of times about an axis which is close to the z-axis. As the frequency of the pulse approaches resonance, the excursions of the polarization arrow become larger until, at exact resonance, the pulse transforms the state $|\alpha\rangle$ exactly into the state $|-y\rangle$, as calculated before. When the frequency of the pulse is changed further, the axis tilts in the opposite sense, and for large offsets there is only a minor disturbance of the spin.

Another way to think about this is in terms of the *transition probability* for the spin states. The quantity

$$\text{P}_{\alpha\to\beta} = |\langle\beta|\widehat{R}_{\text{off}}(\Omega^0)|\alpha\rangle|^2$$

corresponds to the probability that a spin in state $|\alpha\rangle$ before the pulse is found in the state $|\beta\rangle$ after the pulse. Figure 10.29 shows the transition probability $\text{P}_{\alpha\to\beta}$ as a function of resonance offset Ω^0, in the case of a π pulse:

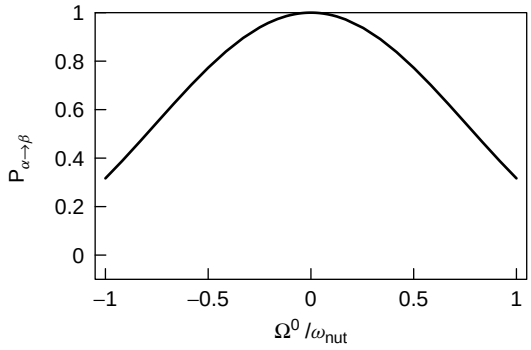

Figure 10.29
Transition probability for the process $|\alpha\rangle \to |\beta\rangle$ as a function of resonance offset, in the case of a π pulse.

Exactly on resonance, the transition probability is unity because the pulse transforms the state $|\alpha\rangle$ into the state $|\beta\rangle$. Off resonance, the transition probability declines, since the pulse becomes less effective.

Figure 10.30 explores the behaviour of the transition probability $P_{\alpha\to\beta}$ for larger resonance offsets or, equivalently, for weaker r.f. fields:

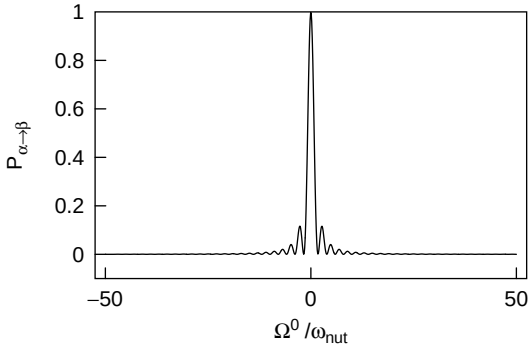

Figure 10.30
Transition probability for the process $|\alpha\rangle \to |\beta\rangle$ as a function of resonance offset, in the case of a π pulse.

This shows clearly that a realistic r.f. pulse is frequency selective. Only spins that precess at a frequency close to that of the r.f. irradiation are significantly affected by the pulse. In terms of the 'swing' analogy, this corresponds to the everyday experience that small pushes must be timed very well to get a swing going.

The *bandwidth* of the pulse is proportional to the nutation frequency, and hence to the peak r.f. amplitude.[4] If the pulse is *strong* (large peak r.f. amplitude), then the pulse is less frequency selective. If the pulse is *weak* (small peak r.f. amplitude), then the pulse is more frequency selective.

These results have a large effect on the methodology of NMR. Generally speaking, it is desirable to use r.f. fields that are as large as possible, so as to 'cover' all spins in the practical chemical shift range. Strong pulses allow a reasonably uniform manipulation of all spins in the spectrum, irrespective of their chemical shifts. In terms of the swing analogy, this corresponds to the use of brute force to correct for deficiencies in one's timing.

The nutation frequency is limited by technical considerations. The largest achievable nutation frequency is usually around 200 kHz, which is smaller than the difference in Larmor frequency between different isotopes. An r.f. field applied near the Larmor frequency of one isotope generally has an insignificant influence on the spins of a different isotope. This fact accounts for the design of multinuclear magnetic resonance spectrometers, which employ multiple transmitter circuits and multiply tuned probes, in order to irradiate the sample with a set of r.f. fields, each close to resonance for a different spin isotope.

In the rest of this book, I assume that r.f. pulses are strong, and use the form of the pulse propagator given in Equation 10.33.

Some NMR experiments employ a *weak* r.f. pulse (small value of ω_{nut}), in order to influence only those spins whose Larmor frequency falls in a narrow defined range. This is called a *frequency-selective pulse*.

The above calculations considered a *rectangular r.f. pulse of constant phase*, defined as one for which the r.f. amplitude climbs infinitely fast at the start of the pulse, falls infinitely fast to zero at the end of the pulse, and in which the phase and amplitude are constant during the pulse. It may be shown that a rectangular r.f. pulse does not have optimal frequency selectivity. Much effort has gone into the development of *shaped* r.f. pulses, whose waveforms are smoother and more complicated than a rectangular pulse, but which can achieve a cleaner frequency selection. Such methods are widely used in NMR imaging.

Notes

1. Atoms may be sorted according to their spin angular momentum by allowing them to float through a region of inhomogeneous magnetic field (*Stern–Gerlach* experiments). See the text by Cohen-Tannoudji *et al.* in *Further Reading*.

2. The treatment given here neglects the effect of the non-resonant rotating component of the r.f. field. This approximation is very good as long as the r.f. field is weak compared with the static field, which is almost always the case.

3. The choice of rotating frame phase ϕ_{ref} (Equation 10.17) leads to a consistently positive nutation frequency ω_{nut} (Equation 10.25). With this convention, all pulses execute positive right-handed rotations around the rotating-frame axes. The NMR community is evenly split between those who use positive right-handed rotations for pulses (as in this book), and those who prefer negative right-handed rotations (so that, for example, a rotation by $\pi/2$ around the x-axis transforms a vector along the z-axis into a vector along the positive y-axis). All conventions lead, of course, to equivalent results, providing that they are used consistently.

4. The relationship between the pulse bandwidth (the width of the frequency response) and the r.f. nutation frequency ω_{nut} is not straightforward. There are essentially two main regimes, determined by the value of the flip angle $\beta_{\text{p}} = \omega_{\text{nut}}\tau_{\text{p}}$, where τ_{p} is the pulse duration. If the flip angle is smaller than around $\pi/2$ (the *linear regime*), then the pulse bandwidth is determined by the inverse of the pulse duration, rather than the nutation frequency – i.e. the shorter the pulse, the wider its bandwidth. However, most r.f. pulses operate in the *non-linear regime*, in which the flip angles are large ($\beta_{\text{p}} \geq \pi/2$). In the non-linear regime, it is the nutation frequency ω_{nut} that determines the bandwidth of the frequency response, not the pulse duration.

Further Reading

- For more on the quantum mechanics of a single spin-1/2, see C. Cohen-Tannoudji, B. Diu and F. Laloë, *Quantum Mechanics*, Wiley, London, 1977.
- For a review of current thinking about the observation process in quantum mechanics, see A. Whitaker, *Einstein, Bohr and the Quantum Dilemma*, Cambridge University Press, 1996.
- For more discussion of the rotating frame, and a treatment of selective pulses and shaped pulses, see R. Freeman, *Spin Choreography. Basic Steps in High Resolution NMR*, Spektrum, Oxford, 1997.
- For a review of shaped pulses, see R. Freeman, *Prog. NMR Spectrosc.* **32**, 59–106 (1998).

Exercises

10.1 In the following calculation, the spin-1/2 state $|\theta\rangle$ is defined as

$$|\theta\rangle = \cos\tfrac{1}{2}\theta|\alpha\rangle + \mathrm{i}\sin\tfrac{1}{2}\theta|\beta\rangle$$

(i) Show that the spin-1/2 state $|\theta\rangle$ is an eigenstate of $\hat{I}_z\cos\theta + \hat{I}_y\sin\theta$ and give the eigenvalue.
(ii) Give a pictorial representation of the state $|\theta\rangle$.
(iii) What pulse transforms the state $|\theta\rangle$ into the state $|\pi/2\rangle$? Derive the result geometrically and then verify it mathematically.

10.2 A sample containing protons is exposed to an r.f. magnetic field with peak amplitude $B_{\mathrm{RF}} = 469.8\,\mu\mathrm{T}$. The frequency of the r.f. field is exactly resonant with the proton Larmor precession.
(i) What is the nutation frequency of the protons in units of hertz?
(ii) How long should the r.f. field be applied in order to generate a pulse with a flip angle of $\pi/2$?
(iii) What is the flip angle of the protons if the pulse duration is kept as in (ii) but the peak r.f. field is increased to $B_{\mathrm{RF}} = 939.6\,\mu\mathrm{T}$?

10.3 A single spin-1/2 in state $|\alpha\rangle$ is exposed to a three-pulse sequence $(\pi/2)_x\pi_y(\pi/2)_x$.
(i) Calculate the spin state after the three-pulse sequence.
(ii) Show that the final spin state is an eigenstate of $\hat{I}_z$. What is the eigenvalue?
(iii) Interpret the trajectory of the spin geometrically.

10.4 A single spin-1/2 in state $|\alpha\rangle$ is exposed to a $\pi/2$ pulse of phase $\pi/2$, followed by a π pulse of phase $5\pi/4$.
(i) Calculate the spin state after the two-pulse sequence.
(ii) Show that the final spin state is an eigenstate of $\hat{I}_y$. What is the eigenvalue?
(iii) Interpret the trajectory of the spin geometrically.

10.5 A pulse with nutation frequency $\omega_{\mathrm{nut}}/2\pi = 10\,\mathrm{kHz}$ is applied to a single spin-1/2 in state $|\alpha\rangle$. The resonance offset of the pulse is exactly $\Omega^0/2\pi = 10\,\mathrm{kHz}$. If the spin has a 50% probability of making a transition to the state $|\beta\rangle$, what is the pulse duration?

11 Ensemble of Spins-1/2

11.1 Spin Density Operator

Consider a sample containing only magnetically equivalent spins-1/2, such as the protons in a tube of pure water (neglecting rare isotopes). To a good approximation, the $\sim 10^{22}$ spins do not influence each other. The spin magnetic moments precess and nutate, independently of each other.[1]

A collection of independent, identical systems is called an *ensemble*. The proton spins in a tube of water behave, to a very good approximation, as an *ensemble of isolated spins*-1/2.

At any particular moment, each of the protons has a different polarization state. A few are very close to the state $|\alpha\rangle$ and a few are very close to the state $|\beta\rangle$ but the vast majority are in superposition states that are intermediate between $|\alpha\rangle$ and $|\beta\rangle$. The proton spin polarization vectors are distributed almost uniformly, pointing in all possible directions of space:

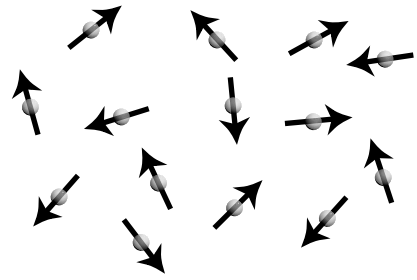

Figure 11.1
Ensemble of isolated spins-1/2.

Each proton spin behaves as described in Chapter 10. The total nuclear magnetization is the sum of innumerable small contributions from the individual spins. To calculate a macroscopic quantity, such as the magnetization, it is possible, at least in principle, to treat each spin individually and then to add the results together.

This calculation is impractical because there are so many spins. Fortunately, there is an elegant alternative, called the method of the *density operator*. The density operator describes the quantum state of the entire ensemble, without referring to the individual spin states. It is a tool of central importance in the theory of NMR.

Spin Dynamics: Basics of Nuclear Magnetic Resonance, Second Edition Malcolm H. Levitt

The density operator method is based on the properties of the expectation value of an observable (see Section 7.1.3). Consider a single spin in a general superposition state:

$$|\psi\rangle = \begin{pmatrix} c_\alpha \\ \\ c_\beta \end{pmatrix} \tag{11.1}$$

The expectation value of an operator $\widehat{Q}$ is given by

$$\begin{aligned} \langle \widehat{Q} \rangle &= \langle \psi | \widehat{Q} | \psi \rangle \\ &= ({c_\alpha}^* , \quad {c_\beta}^*) \begin{pmatrix} Q_{\alpha\alpha} & Q_{\alpha\beta} \\ \\ Q_{\beta\alpha} & Q_{\beta\beta} \end{pmatrix} \begin{pmatrix} c_\alpha \\ \\ c_\beta \end{pmatrix} \\ &= c_\alpha {c_\alpha}^* Q_{\alpha\alpha} + c_\alpha {c_\beta}^* Q_{\alpha\beta} + c_\beta {c_\alpha}^* Q_{\beta\alpha} + c_\beta {c_\beta}^* Q_{\beta\beta} \end{aligned} \tag{11.2}$$

The expression involves *quadratic products* of the superposition coefficients c_α and c_β. This suggests a way of representing the state of the spin by these quadratic products, rather than the coefficients themselves. A suitable construction is a matrix formed by multiplying the column vector $|\psi\rangle$ and the row vector $\langle\psi|$:

$$|\psi\rangle\langle\psi| = \begin{pmatrix} c_\alpha \\ \\ c_\beta \end{pmatrix} ({c_\alpha}^* , \quad {c_\beta}^*) = \begin{pmatrix} c_\alpha {c_\alpha}^* & c_\alpha {c_\beta}^* \\ \\ c_\beta {c_\alpha}^* & c_\beta {c_\beta}^* \end{pmatrix} \tag{11.3}$$

Note the order in which the bra and the ket are multiplied. If they were multiplied the other way round ($\langle\psi|\psi\rangle$), the result would be unity.

The expectation value of the operator $\widehat{Q}$ may be extracted from the object $|\psi\rangle\langle\psi|$ as follows:

$$\langle \widehat{Q} \rangle = \mathrm{Tr}\{ |\psi\rangle\langle\psi| \, \widehat{Q} \} \tag{11.4}$$

where the trace operation is described in Section 7.7.4. It may easily be verified that the expressions shown in Equations 11.2 and 11.4 are equivalent.

So far, this does not seem particularly helpful, since the state of the spin is represented in the matrix of Equation 11.3 by four complex numbers, instead of the two complex numbers required in the column vector of Equation 11.1.

However, now suppose there are two independent spins involved. Suppose the first spin has state $|\psi_1\rangle$ and the second spin has state $|\psi_2\rangle$. The result of measuring Q is still uncertain in general, because of quantum indeterminacy. However, the most likely outcome is the sum of the two expectation values:

$$Q_{\mathrm{obs}}(\text{most likely}) = \langle \psi_1 | \widehat{Q} | \psi_1 \rangle + \langle \psi_2 | \widehat{Q} | \psi_2 \rangle$$

which may be rewritten

$$Q_{\mathrm{obs}}(\text{most likely}) = \mathrm{Tr}\{ (|\psi_1\rangle\langle\psi_1| + |\psi_2\rangle\langle\psi_2|) \, \widehat{Q} \}$$

If there are a large number of spins involved, then repetition of this derivation gives

$$Q_{\mathrm{obs}}(\text{most likely}) = \mathrm{Tr}\{ (|\psi_1\rangle\langle\psi_1| + |\psi_2\rangle\langle\psi_2| + \ldots) \, \widehat{Q} \}$$

where the sum is taken over all spins in the ensemble.

Now suppose that an operator $\hat{\rho}$ is defined:

$$\hat{\rho} = \mathbb{N}^{-1} (|\psi_1\rangle\langle\psi_1| + |\psi_2\rangle\langle\psi_2| + \ldots)$$

where $\mathbb{N}$ is the number of members of the ensemble. For brevity, this expression may be written as

$$\hat{\rho} = \overline{|\psi\rangle\langle\psi|} \tag{11.5}$$

where the overbar indicates the *average* over all members of the ensemble. The *macroscopic* observation of Q for the entire ensemble of spins yields the result

$$Q_{\text{macro}} \cong \mathbb{N}\,\text{Tr}\{\hat{\rho}\widehat{Q}\}$$

which suddenly looks rather simple.

For the large numbers of spins involved in NMR, it may be shown that this equation is exact to within about $\mathbb{N}^{-1/2}$, which is smaller than 10^{-7} in the cases encountered in NMR.

If both sides are divided by $\mathbb{N}$, the equation becomes

$$\mathbb{N}^{-1}Q_{\text{macro}} = \text{Tr}\{\hat{\rho}\widehat{Q}\}$$

Normally this equation is written (rather loosely) as

$$\langle Q\rangle = \text{Tr}\{\hat{\rho}\widehat{Q}\} \tag{11.6}$$

Strictly, the left-hand side is not really the expectation value for a single system, but the average contribution of each ensemble member to the final macroscopic result, which is a slightly different thing. Nevertheless, I will not be pedantic and continue with the usual notation (Equation 11.6).

For historical reasons, the operator $\hat{\rho}$, defined in Equation 11.5, is known as the *spin density operator*.[2,3] The term is unfortunate. The operator $\hat{\rho}$ has no relationship with the physical density of the sample.

One should be aware of the very remarkable nature of this result. Equation 11.6 says that the result of *any* macroscopic observation may be deduced from two spin operators, with one representing the observable that is being measured and the other representing the state of *the entire spin ensemble*, independent of the number of spins it contains. This is an amazing simplification of the problem; instead of specifying the individual microscopic states of $\sim 10^{22}$ spins, one gets away with specifying the value of a single operator, i.e. the spin density operator $\hat{\rho}$.

11.2 Populations and Coherences

11.2.1 Density matrix

The matrix representation of the density operator, for an ensemble of non-interacting spins-1/2, is given by

$$\hat{\rho} = \begin{pmatrix} \rho_{\alpha\alpha} & \rho_{\alpha\beta} \\ \rho_{\beta\alpha} & \rho_{\beta\beta} \end{pmatrix} = \begin{pmatrix} \overline{c_\alpha {c_\alpha}^*} & \overline{c_\alpha {c_\beta}^*} \\ \overline{c_\beta {c_\alpha}^*} & \overline{c_\beta {c_\beta}^*} \end{pmatrix} \tag{11.7}$$

The overbars indicate an average over the ensemble. The right-hand-side in this equation is called the *density matrix*.

The *diagonal* elements of the spin density operator $\rho_{\alpha\alpha}$ and $\rho_{\beta\beta}$ are called the *populations*[4] of states $|\alpha\rangle$ and $|\beta\rangle$. The *off-diagonal* elements $\rho_{\alpha\beta}$ and $\rho_{\beta\alpha}$ are called the *coherences* between states $|\alpha\rangle$ and $|\beta\rangle$.

11.2.2 Box notation

In this book, I use a special *box notation* for the populations and coherences. The population of state $|\alpha\rangle$ is denoted $\rho_{\boxed{\alpha}}$, and is given by

$$\rho_{\boxed{\alpha}} = \langle\alpha|\hat{\rho}|\alpha\rangle = \overline{c_\alpha {c_\alpha}^*} \tag{11.8}$$

Similarly, the population of state $|\beta\rangle$ is denoted $\rho_{\boxed{\beta}}$, and is given by

$$\rho_{\boxed{\beta}} = \langle\beta|\hat{\rho}|\beta\rangle = \overline{c_\beta {c_\beta}^*} \tag{11.9}$$

The two coherences are denoted $\rho_{\boxed{+}}$ and $\rho_{\boxed{-}}$, and are given by

$$\begin{aligned} \rho_{\boxed{+}} &= \langle\alpha|\hat{\rho}|\beta\rangle = \overline{c_\alpha {c_\beta}^*} \\ \rho_{\boxed{-}} &= \langle\beta|\hat{\rho}|\alpha\rangle = \overline{c_\beta {c_\alpha}^*} \end{aligned} \tag{11.10}$$

Using this notation, the density matrix is

$$\hat{\rho} = \begin{pmatrix} \rho_{\boxed{\alpha}} & \rho_{\boxed{+}} \\ \rho_{\boxed{-}} & \rho_{\boxed{\beta}} \end{pmatrix}$$

The density operator may also be written as

$$\hat{\rho} = \rho_{\boxed{\alpha}} \hat{I}^\alpha + \rho_{\boxed{\beta}} \hat{I}^\beta + \rho_{\boxed{+}} \hat{I}^+ + \rho_{\boxed{-}} \hat{I}^-$$

using the shift operators $\hat{I}^+$ and $\hat{I}^-$, and the projection operators $\hat{I}^\alpha$ and $\hat{I}^\beta$. This can be seen from the matrix elements given in Sections 7.8.5 and 7.8.6.

The box notation is particularly useful for systems of many coupled spins, as will be seen later.

11.2.3 Balls and arrows

The state of the spin-1/2 ensemble is specified by the values of the populations $\rho_{\boxed{\alpha}}$ and $\rho_{\boxed{\beta}}$ and the coherences $\rho_{\boxed{+}}$ and $\rho_{\boxed{-}}$, which may be depicted by a diagram. The populations are drawn as 'little balls' sitting on the appropriate energy level, and the coherences are drawn as arrows 'connecting' the energy levels:

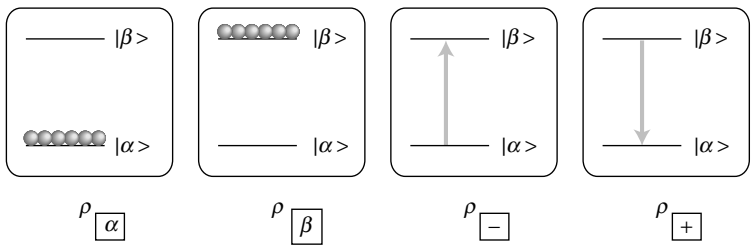

Figure 11.2
Pictorial representation of populations and coherences.

⚠The 'arrow' representation of coherences should not be misinterpreted: in particular, there is no 'flow' or 'transition' going on between the connected states. The arrow indicates only that there is a *coherence* between the states, defined mathematically in Equation 11.10. I will discuss in a moment what this means on a microscopic level.

11.2.4 Orders of coherence

It proves useful to classify the spin coherences on the basis of a quantum number called the *coherence order*.

Consider a coherence ρ_{rs} between two energy eigenstates $|r\rangle$ and $|s\rangle$, defined as

$$\rho_{rs} = \langle r|\hat{\rho}|s\rangle = \overline{\langle r|\psi\rangle\langle\psi|s\rangle}$$

In high magnetic field, the two energy eigenstates have well-defined values of the angular momentum in the magnetic field direction, by convention the z-axis:

$$\hat{I}_z|r\rangle = M_r|r\rangle$$
$$\hat{I}_z|s\rangle = M_s|s\rangle$$

The *order* p_{rs} of the coherence ρ_{rs} is defined as

$$p_{rs} = M_r - M_s \tag{11.11}$$

i.e. the difference in the z-angular momentum of the connected states.

For an ensemble of non-interacting spins-1/2, there are only two states, with z-angular momentum quantum numbers $\pm 1/2$. The two coherences, therefore, have order $+1$ and -1.

For the coherence $\rho_{\boxed{+}}$, the state $|r\rangle$ is equal to $|\alpha\rangle$, and the state $|s\rangle$ is equal to $|\beta\rangle$. The order of the coherence $\rho_{\boxed{+}}$ is

$$p_{\boxed{+}} = (+\tfrac{1}{2}) - (-\tfrac{1}{2}) = +1$$

The coherence $\rho_{\boxed{+}}$ is known as a $(+1)$-*quantum coherence*.

For the coherence $\rho_{\boxed{-}}$, the state $|r\rangle$ is equal to $|\beta\rangle$, and the state $|s\rangle$ is equal to $|\alpha\rangle$. The order of the coherence $\rho_{\boxed{-}}$ is

$$p_{\boxed{-}} = (-\tfrac{1}{2}) - (+\tfrac{1}{2}) = -1$$

The coherence $\rho_{\boxed{-}}$ is known as a (-1)-*quantum coherence*.

Since populations are diagonal elements, their coherence order is zero.

For non-interacting spins-1/2, there are three possible values for the coherence order: -1, 0 and $+1$.

⚠ The relationship between coherence order and the 'arrow diagrams' requires care. The coherence order corresponds to the z-angular momentum of the state at the arrow *head*, minus the z-angular momentum of the state at the arrow *tail*. For spins of positive γ, energy is proportional to negative z-angular momentum, so the arrows for $(+1)$-quantum coherences point *down*, whereas the arrows for (-1)-quantum coherence point *up*.

11.2.5 Relationships between populations and coherences

Coherences are *complex numbers*.

The (± 1)-quantum coherences are complex conjugates of each other:

$$\rho_{\boxed{+}} = \overline{c_\alpha c_\beta{}^*} = \left\{\overline{c_\beta c_\alpha{}^*}\right\}^* = \rho_{\boxed{-}}{}^* \tag{11.12}$$

It is impossible, therefore, to have a $(+1)$-quantum coherence without a (-1)-quantum coherence. *Coherences come in conjugate pairs*.

The populations are also interdependent. The state of each spin is normalized:

$$c_\alpha c_\alpha{}^* + c_\beta c_\beta{}^* = 1$$

Since this applies to all spins in the ensemble, it also applies to the ensemble average. The sum of the populations is therefore unity:

$$\rho_{\boxed{\alpha}} + \rho_{\boxed{\beta}} = 1 \tag{11.13}$$

In addition, the populations are by definition real and positive:

$$\rho_{\boxed{\alpha}}{}^{*} = \rho_{\boxed{\alpha}}; \qquad \rho_{\boxed{\beta}}{}^{*} = \rho_{\boxed{\beta}}$$

The population of any state lies between 0 and 1.

11.2.6 Physical interpretation of the populations

What is the physical interpretation of the components of the density operator, in terms of the microscopic states of the individual spins?

We start with the populations. Since the sum of the populations is always equal to one, only the *difference* in populations between the two states has any physical significance. The difference in spin state populations indicates net *longitudinal* spin polarization, i.e. magnetization of the sample in the direction of the field.

A state in which the population of state $|\alpha\rangle$ is *larger* than that of $|\beta\rangle$ indicates that there is a net polarization of the spins *along* the external field direction:

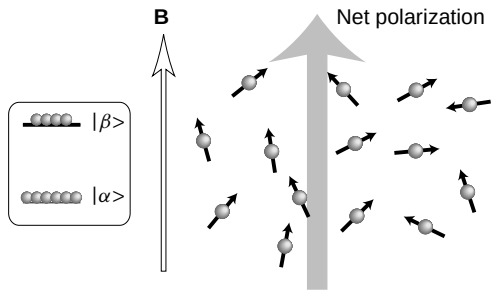

Figure 11.3
Net spin polarization along the field.

Similarly, a state in which the population of state $|\alpha\rangle$ is *less* than that of $|\beta\rangle$ indicates that there is a net polarization of the spins *against* the external field:

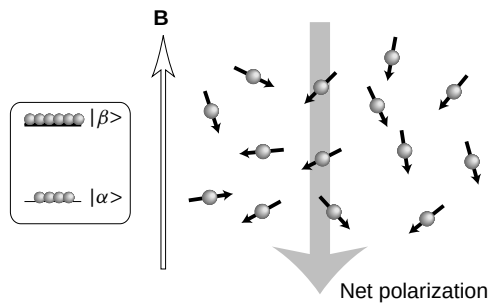

Figure 11.4
Net spin polarization against the field.

If the populations of the two states are equal ($\rho_{\boxed{\alpha}} = \rho_{\boxed{\beta}} = 1/2$), then there is no net polarization in the direction of the field. The number of spins pointing 'up' is equal, on the average, to the number of spins pointing 'down'.

⚠ The population of a state does *not* indicate the fraction of spins that are 'in' that state. In the drawings given above, there are no *individual* spins that are polarized exactly along or against the external field and, therefore, no spins which are exactly in the states $|\alpha\rangle$ and $|\beta\rangle$. Under ordinary circumstances, the majority of spins are always in superpositions of the two energy eigenstates, and point in an arbitrary direction.[5]

⚠ In the diagrams above, the degree of spin polarization is greatly exaggerated, for the sake of clarity. In reality, the net spin polarization in any particular direction is usually extremely small.

11.2.7 Physical interpretation of the coherences

The presence of coherences $\rho_{\boxed{+}}$ and $\rho_{\boxed{-}}$ indicates transverse spin magnetization, i.e. a net spin polarization *perpendicular* to the external field.

Suppose, for example, that the spin density operator has the following form:

$$\rho_{\boxed{\alpha}} = \rho_{\boxed{\beta}} = 1/2$$

$$\rho_{\boxed{-}} = \rho_{\boxed{+}}{}^{*} \neq 0$$

This state has the following physical interpretation:

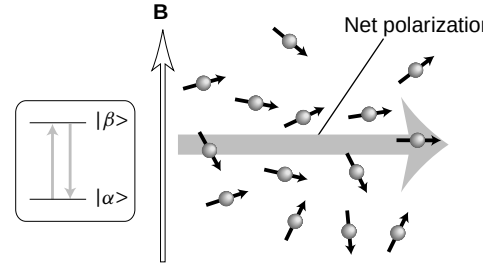

Figure 11.5
Net spin polarization perpendicular to the field.

The spins are equally likely to point either along or against the magnetic field. Nevertheless, there is net spin polarization *perpendicular* to the magnetic field.

Coherence, therefore, requires the existence of spins that have *transverse* polarization vectors, i.e. spins which are in superposition states. However, this is not sufficient. For coherence to exist, the transverse polarizations must also be partially aligned. Polarization vectors that are uniformly distributed in the *xy*-plane provide no coherence.[6] This idea is expressed in the following pictures of the *xy*-plane, perpendicular to the magnetic field:

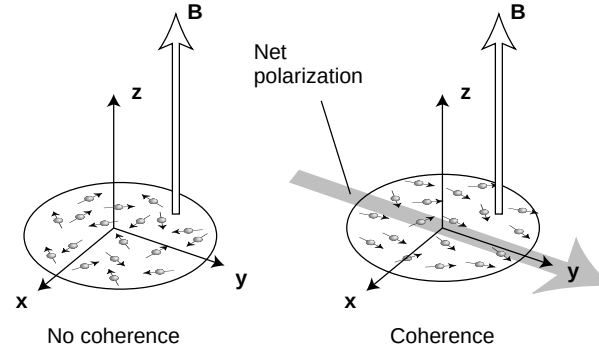

Figure 11.6
Partial alignment of spins in the transverse plane.

(The degree of alignment of the spins is greatly exaggerated.)

The coherences $\rho_{\boxed{+}}$ and $\rho_{\boxed{-}}$ are complex numbers. They have a phase and an amplitude. What is the physical significance of the phase of these complex numbers?

The phase of the coherences indicates the *direction* of the transverse spin polarization in the xy-plane. The phase of the (-1)-quantum coherence $\rho_{\boxed{-}}$ in the complex plane is the same as the angle of the transverse magnetization with respect to the x-axis:

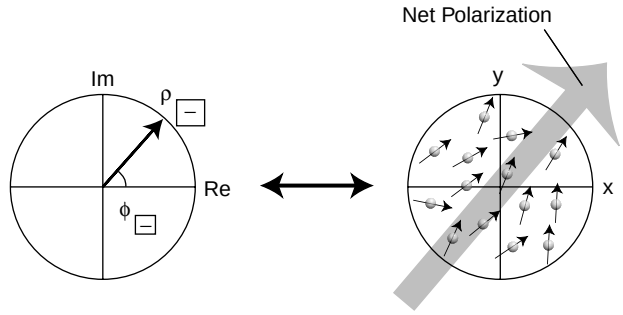

Figure 11.7
Phase of the (-1)-quantum coherence and the direction of the transverse polarization.

(The magnetic field points up, out of the paper.) If the (-1)-quantum coherence is written

$$\rho_{\boxed{-}} = |\rho_{\boxed{-}}| \exp\{i\phi_{\boxed{-}}\}$$

then the preferential polarization axis of the spins is

$$\mathbf{e}'_x \cos\phi_{\boxed{-}} + \mathbf{e}'_y \sin\phi_{\boxed{-}}$$

where $\mathbf{e}'_x$ and $\mathbf{e}'_y$ are the rotating frame axes (see Section 10.6). For example, when $\phi_{\boxed{-}} = 0$, the spins are preferentially polarized along the rotating-frame x-axis; when $\phi_{\boxed{-}} = \pi/2$, the spins are preferentially polarized along the rotating-frame y-axis, and so on.

What about the $(+1)$-quantum coherence?

This turns out to have no useful physical interpretation at all. It is simply a mirror image of the (-1)-quantum coherence. The $(+1)$-quantum coherence always accompanies the (-1)-quantum coherence, but carries no extra information. It is best to forget about it and concentrate on the (-1)-quantum coherence.[7]

11.3 Thermal Equilibrium

The density operator allows the state of the entire spin-1/2 ensemble to be specified using four numbers – an extraordinary simplification. Nevertheless, the method would not be very useful if there was no way of knowing what these numbers are.

If the state of the spin ensemble is known at one point in time, then it is possible to predict it at later times by applying the Schrödinger equation to each individual spin.

But how can one know the spin density operator at one point in time? The answer is that one can't know for certain, but it is possible to make a good guess. A spin system that has been left undisturbed for a long time, in contact with the molecular surroundings, is expected to reach a state of *thermal equilibrium* with those surroundings. Statistical arguments allow one to guess the values of the populations and the coherences in the thermal equilibrium state. For the numbers of spins involved in NMR, this guess is essentially foolproof.

Consider a general spin system with a set of energy eigenstates $|r\rangle$ with corresponding energies ω_r:

$$\widehat{\mathcal{H}}|r\rangle = \omega_r|r\rangle$$

Quantum statistical mechanics states that in thermal equilibrium at temperature T, the following properties hold:

1. The coherences between the states are all zero:

$$\rho_{rs}^{\text{eq}} = 0 \qquad (\text{for } r \neq s) \tag{11.14}$$

2. The populations of the energy states obey the *Boltzmann distribution*:

$$\rho_{rr}^{\text{eq}} = \frac{\exp\{-\hbar\omega_r / k_{\text{B}}T\}}{\sum_s \exp\{-\hbar\omega_s / k_{\text{B}}T\}} \tag{11.15}$$

where $k_{\text{B}} = 1.38066 \times 10^{-23}\,\text{J}\,\text{K}^{-1}$ is the *Boltzmann constant*, and the sum is over all eigenstates.

The Boltzmann distribution causes the lower energy eigenstates to be more populated than the higher energy eigenstates:

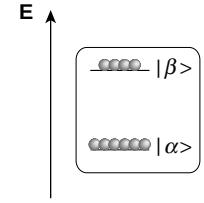

Figure 11.8
Boltzmann distribution of populations for spins with positive γ.

The difference in the population of two states at thermal equilibrium depends on their energy difference, compared with the available thermal energy at the temperature of the sample. At room temperature, the available thermal energy is $k_{\text{B}}T \cong 4.1 \times 10^{-21}\,\text{J}$.

For the case of the spin-1/2 ensemble, the energies of the states are

$$\omega_{\boxed{\alpha}} = \frac{1}{2}\omega^0 \qquad \omega_{\boxed{\beta}} = -\frac{1}{2}\omega^0$$

where $\omega^0 = -\gamma B^0$. The energy difference between the Zeeman states, for the case of protons in a field of 11.74 T, is $|\hbar\omega^0| \cong 3.3 \times 10^{-25}\,\text{J}$.

Since the difference in energy between the Zeeman eigenstates is four orders of magnitude smaller than the available thermal energy, the thermal equilibrium population difference between the states is very small. It is possible to simplify Equation 11.15 by using some approximations.

Define the *Boltzmann factor* $\mathbb{B}$ through the following:

$$\mathbb{B} = \frac{\hbar\gamma B^0}{k_{\text{B}}T} \tag{11.16}$$

The exponential factors in Equation 11.15 may be written as follows:

$$\exp\{-\frac{\hbar\omega_{\boxed{\alpha}}}{k_{\text{B}}T}\} = \exp\{\frac{1}{2}\mathbb{B}\} \qquad \exp\{-\frac{\hbar\omega_{\boxed{\beta}}}{k_{\text{B}}T}\} = \exp\{-\frac{1}{2}\mathbb{B}\}$$

In practice, $\mathbb{B}$ is a very small number. Therefore, it is possible to expand the exponentials as a power series and take only the first term:

$$\exp\{-\frac{\hbar\omega_{\boxed{\alpha}}}{k_B T}\} \cong 1 + \frac{1}{2}\mathbb{B} \qquad \exp\{-\frac{\hbar\omega_{\boxed{\beta}}}{k_B T}\} \cong 1 - \frac{1}{2}\mathbb{B}$$

The denominator of Equation 11.15 is given by

$$\exp\{-\hbar\omega_{\boxed{\alpha}}/k_B T\} + \exp\{-\hbar\omega_{\boxed{\beta}}/k_B T\} \cong 2$$

The thermal equilibrium populations of the two states are therefore:

$$\rho^{\text{eq}}_{\boxed{\alpha}} \cong \frac{1}{2}(1 + \frac{1}{2}\mathbb{B}) = \frac{1}{2} + \frac{1}{4}\mathbb{B}$$
$$\rho^{\text{eq}}_{\boxed{\beta}} \cong \frac{1}{2}(1 - \frac{1}{2}\mathbb{B}) = \frac{1}{2} - \frac{1}{4}\mathbb{B}$$

The above approximation is called the *high-temperature approximation*. This is a bit misleading, because it applies very well for any temperature warmer than a fraction of a degree kelvin.

For positive γ, the low-energy $|\alpha\rangle$ state is populated slightly more than the high-energy $|\beta\rangle$ state. The population difference is exceedingly small at ordinary temperatures and fields, only about 1 part in 10^5.

Physically, this means that, in thermal equilibrium, there is only a very slight polarization of the spin angular momentum vectors along the direction of the external magnetic field.

The *thermal equilibrium density matrix* for isolated spins-1/2 is therefore approximately given by

$$\hat{\rho}^{\text{eq}} = \begin{pmatrix} \frac{1}{2}+\frac{1}{4}\mathbb{B} & 0 \\ 0 & \frac{1}{2}-\frac{1}{4}\mathbb{B} \end{pmatrix} \tag{11.17}$$

In terms of angular momentum operators, this corresponds to:

$$\hat{\rho}^{\text{eq}} = \frac{1}{2}\hat{1} + \frac{1}{2}\mathbb{B}\hat{I}_z \tag{11.18}$$

This *thermal equilibrium density operator* forms the starting point for subsequent calculations.

11.4 Rotating-Frame Density Operator

We need the response of the spin ensemble to r.f. pulses. As discussed in Section 10.6, the calculation is best done by using the rotating frame. It is necessary, therefore, to transform the spin density operator into the rotating frame.

As shown in Section 10.6, the rotating-frame spin states are related to the fixed-frame states through the transformation

$$|\widetilde{\psi}\rangle = \widehat{R}_z(-\Phi(t))|\psi\rangle \tag{11.19}$$

where

$$\Phi(t) = \omega_{\text{ref}} t + \phi_{\text{ref}}$$

and ω_{ref} is the reference frequency of the spectrometer, equal to the frequency of the rotating frame. The operator $\widehat{R}_z(-\Phi)$ generates a rotation around the z-axis, through the angle $-\Phi$.

The *rotating-frame spin density operator* is defined through

$$\tilde{\hat{\rho}} = \overline{|\tilde{\psi}\rangle\langle\tilde{\psi}|} \tag{11.20}$$

and is related to the fixed-frame density operator by:

$$\tilde{\hat{\rho}} = \widehat{R}_z(-\Phi(t))\hat{\rho}\widehat{R}_z(+\Phi(t))$$

The matrix representations of the rotation operators (Appendix A.4) may be used to make the following correspondences between the rotating-frame and fixed-frame populations and coherences:

$$\begin{aligned} \tilde{\rho}_{\boxed{\alpha}} &= \rho_{\boxed{\alpha}} & \tilde{\rho}_{\boxed{\beta}} &= \rho_{\boxed{\beta}} \\ \tilde{\rho}_{\boxed{-}} &= \rho_{\boxed{-}} \exp\{-\mathrm{i}\Phi(t)\} & \tilde{\rho}_{\boxed{+}} &= \rho_{\boxed{+}} \exp\{+\mathrm{i}\Phi(t)\} \end{aligned} \tag{11.21}$$

The rotating-frame and fixed-frame populations are equal, and the rotating-frame and fixed-frame coherences are related by a time-dependent phase factor.

The thermal equilibrium density operator contains only populations, and is the same in both frames:

$$\tilde{\hat{\rho}}^{\mathrm{eq}} = \hat{\rho}^{\mathrm{eq}}$$

From Equation 11.18, the thermal equilibrium density operator in the rotating frame is given by

$$\tilde{\hat{\rho}}^{\mathrm{eq}} = \frac{1}{2}\widehat{1} + \frac{1}{2}\mathbb{B}\hat{I}_z \tag{11.22}$$

Since the description of r.f. pulses is much easier in the rotating frame, we will use the rotating frame consistently from now on.[8] *The tilde symbol is dropped*.

11.5 Magnetization Vector

In Chapter 10, the state of a single spin-1/2 was represented by an arrow, indicating the direction of well-defined spin angular momentum. The response of the spin to magnetic fields could be depicted by rotating this arrow around different axes in three-dimensional space.

A similar construction is possible for the *ensemble* of isolated spins-1/2. The spin density operator may be represented as a *magnetization vector* **M**, indicating the magnitude and direction of the net magnetization:

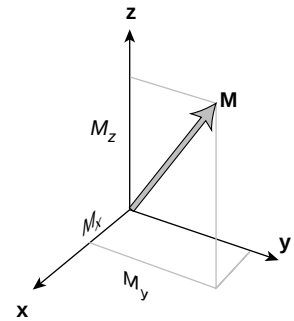

Figure 11.9
The magnetization vector.

The dynamics of the spin-1/2 ensemble correspond to the motion of the magnetization vector in three-dimensional space.

The magnetization vector has three Cartesian components:

$$\mathbf{M} = M_x \mathbf{e}'_x + M_y \mathbf{e}'_y + M_z \mathbf{e}'_z$$

The longitudinal component M_z is related to the *population difference* between the states:

$$M_z = 2\mathbb{B}^{-1}(\rho_{\boxed{\alpha}} - \rho_{\boxed{\beta}}) \tag{11.23}$$

The transverse components M_x and M_y are related to the (-1)-quantum coherence between the states:

$$\begin{aligned} M_x &= 4\mathbb{B}^{-1}\,\mathrm{Re}\{\rho_{\boxed{-}}\} \\ M_y &= 4\mathbb{B}^{-1}\,\mathrm{Im}\{\rho_{\boxed{-}}\} \end{aligned} \tag{11.24}$$

The numerical factors in Equations 11.23 and 11.24 are chosen so that the thermal equilibrium magnetization vector is equal to a unit vector along the z-axis:

$$\mathbf{M}^{\mathrm{eq}} = \mathbf{e}'_z \tag{11.25}$$

With these definitions, the spin density operator may always be written as

$$\begin{aligned} \hat{\rho} &= \frac{1}{2}\widehat{1} + \frac{1}{2}\mathbb{B}\mathbf{M}\cdot\hat{\mathbf{I}} \\ &= \frac{1}{2}\widehat{1} + \frac{1}{2}\mathbb{B}\left(M_x\hat{I}_x + M_y\hat{I}_y + M_z\hat{I}_z\right) \end{aligned} \tag{11.26}$$

The populations and coherences may be derived from the magnetization vector by using the definitions in Equations 11.23 and 11.24:

$$\begin{aligned} \rho_{\boxed{\alpha}} &= \frac{1}{2} + \frac{1}{4}\mathbb{B}M_z \qquad & \rho_{\boxed{\beta}} &= \frac{1}{2} - \frac{1}{4}\mathbb{B}M_z \\ \rho_{\boxed{+}} &= \frac{1}{4}\mathbb{B}(M_x - \mathrm{i}M_y) & \rho_{\boxed{-}} &= \frac{1}{4}\mathbb{B}(M_x + \mathrm{i}M_y) \end{aligned}$$

Note the direct relationship between the phase of the (-1)-quantum coherence and the transverse magnetization, as described in Section 11.2.7.

11.6 Strong Radio-Frequency Pulse

We are now ready to calculate the effect of a strong r.f. pulse on the spin-1/2 ensemble.

Consider a strong rectangular r.f. pulse of general phase ϕ_{p} and flip angle β_{p}, as described in Section 10.8:

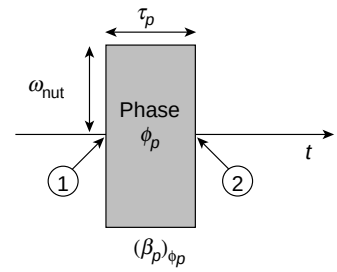

Figure 11.10
An r.f. pulse.

The flip angle of the pulse β_p is given by $\beta_\mathrm{p} = \omega_\mathrm{nut}\tau_\mathrm{p}$, where the nutation frequency ω_nut is a measure of the amplitude of the r.f. field and τ_p is the pulse duration. The time points ① and ② define the start and end of the pulse. The pulse is assumed to be strong enough that the off-resonance effects described in Section 10.8.5 may be ignored.[9]

For each spin in the ensemble, the rotating-frame state after the pulse is related to the rotating-frame state before the pulse through the following:

$$|\psi\rangle_② = \widehat{R}_{\phi_\mathrm{p}}(\beta_\mathrm{p})|\psi\rangle_①$$

The corresponding equation for the 'bra' states is

$$\langle\psi|_② = \langle\psi|_① \widehat{R}_{\phi_\mathrm{p}}(\beta_\mathrm{p})^\dagger$$

where the dagger symbol denotes the adjoint. Note that the adjoint reverses the order, as described in Section 6.2.6.

Since the rotation operators are unitary (see Section 7.6.2), this may be written as

$$\langle\psi|_② = \langle\psi|_① \widehat{R}_{\phi_\mathrm{p}}(-\beta_\mathrm{p})$$

The spin density operator after the pulse is therefore given by

$$\hat{\rho}_② = \overline{|\psi\rangle_②\langle\psi|_②} = \overline{\widehat{R}_{\phi_\mathrm{p}}(\beta_\mathrm{p})|\psi\rangle_①\langle\psi|_① \widehat{R}_{\phi_\mathrm{p}}(-\beta_\mathrm{p})}$$

The overbar in this equation means an average over all spins in the ensemble.

Now assume that all spins in the ensemble experience the same magnetic field. The ensemble average may be restricted to the central part of this expression, giving

$$\hat{\rho}_② = \widehat{R}_{\phi_\mathrm{p}}(\beta_\mathrm{p})\overline{|\psi\rangle_①\langle\psi|_①}\widehat{R}_{\phi_\mathrm{p}}(-\beta_\mathrm{p})$$

which is equal to

$$\hat{\rho}_② = \widehat{R}_{\phi_\mathrm{p}}(\beta_\mathrm{p})\hat{\rho}_① \widehat{R}_{\phi_\mathrm{p}}(-\beta_\mathrm{p}) \tag{11.27}$$

The pulse 'sandwiches' the density operator with two opposite rotation operators.

11.6.1 Excitation of coherence

We now use the sandwich equation to calculate the effect of a strong $(\pi/2)_x$ pulse on an ensemble of non-interacting spins-1/2 in a state of thermal equilibrium.

Before the pulse, the spin density operator is

$$\hat{\rho}_① = \hat{\rho}^\mathrm{eq} = \frac{1}{2}\widehat{1} + \frac{1}{2}\mathbb{B}\hat{I}_z$$

There are no coherences, and the populations are governed by the Boltzmann distribution, in the high-temperature limit.

After the pulse, the spin density operator is

$$\begin{aligned}\hat{\rho}_{②} &= \widehat{R}_x(\pi/2)\hat{\rho}_{①}\,\widehat{R}_x(-\pi/2) = \frac{1}{2}\widehat{R}_x(\pi/2)\widehat{1}\widehat{R}_x(-\pi/2) + \frac{1}{2}\mathbb{B}\,\widehat{R}_x(\pi/2)\hat{I}_z\widehat{R}_x(-\pi/2)\\ &= \frac{1}{2}\widehat{1} + \frac{1}{2}\mathbb{B}\,\widehat{R}_x(\pi/2)\hat{I}_z\widehat{R}_x(-\pi/2)\end{aligned}$$

since the unity operator $\widehat{1}$ commutes with all other operators.

The last term on the right-hand side may be calculated using the sandwich relationships given in Section 6.6.2:

$$\widehat{R}_x(\pi/2)\hat{I}_z\widehat{R}_x(-\pi/2) = -\hat{I}_y$$

The result is

$$\hat{\rho}_{②} = \frac{1}{2}\widehat{1} - \frac{1}{2}\mathbb{B}\hat{I}_y$$

If written in terms of the magnetization vector, this transformation is very simple:

$$\mathbf{M}_{①} = \mathbf{e}_z \quad \downarrow\ (\pi/2)_x \quad \mathbf{M}_{②} = -\mathbf{e}_y$$

The $(\pi/2)_x$ pulse rotates the magnetization vector from the z-axis to the $-y$-axis:

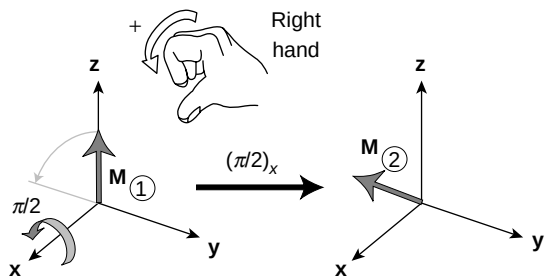

Figure 11.11
A $(\pi/2)_x$ pulse acting on a magnetization vector along the z-axis.

What happens to the populations and the coherences? In terms of the matrix representations, the action of the pulse is as follows:

$$\hat{\rho}_{①} = \begin{pmatrix} \frac{1}{2} + \frac{1}{4}\mathbb{B} & 0 \\ 0 & \frac{1}{2} - \frac{1}{4}\mathbb{B} \end{pmatrix} \xrightarrow{(\pi/2)_x} \hat{\rho}_{②} = \begin{pmatrix} \frac{1}{2} & -\frac{1}{4\mathrm{i}}\mathbb{B} \\ \frac{1}{4\mathrm{i}}\mathbb{B} & \frac{1}{2} \end{pmatrix}$$

The pulse, therefore, accomplishes two tasks:

1. The pulse *equalizes the populations* of the two states.
2. The pulse converts the *population difference* into *coherences*.

This process may be depicted as follows:

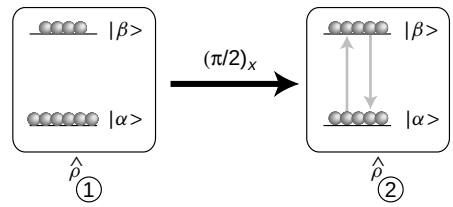

Figure 11.12
Excitation of coherence by a $(\pi/2)_x$ pulse.

11.6.2 Population inversion

Now calculate the action of a π_x pulse on the thermal equilibrium state. The calculation goes as follows:

$$\begin{aligned}\hat{\rho}_{②} &= \widehat{R}_x(\pi)\hat{\rho}_{①}\,\widehat{R}_x(-\pi) = \frac{1}{2}\widehat{1} + \frac{1}{2}\mathbb{B}\widehat{R}_x(\pi)\hat{I}_z\widehat{R}_x(-\pi) \\ &= \frac{1}{2}\widehat{1} - \frac{1}{2}\mathbb{B}\hat{I}_z\end{aligned}$$

In terms of the magnetization vector, this transformation may be written as

$$\begin{aligned}\mathbf{M}_{①} &= \mathbf{e}_z \\ &\downarrow\ \pi_x \\ \mathbf{M}_{②} &= -\mathbf{e}_z\end{aligned}$$

The π_x pulse accomplishes an *inversion* of the magnetization vector:

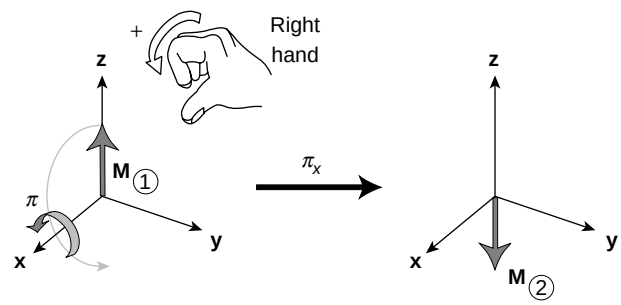

Figure 11.13
A π_x pulse acting on a magnetization vector along the z-axis.

In terms of the populations and coherences, the transformation reads as follows:

$$\hat{\rho}_{①} = \begin{pmatrix} \frac{1}{2} + \frac{1}{4}\mathbb{B} & 0 \\ 0 & \frac{1}{2} - \frac{1}{4}\mathbb{B} \end{pmatrix} \xrightarrow{\pi_x} \hat{\rho}_{②} = \begin{pmatrix} \frac{1}{2} - \frac{1}{4}\mathbb{B} & 0 \\ 0 & \frac{1}{2} + \frac{1}{4}\mathbb{B} \end{pmatrix}$$

The π_x pulse exchanges the populations of the two states, generating an *inverted population distribution*, in which the higher-energy state is more populated than the lower-energy state:

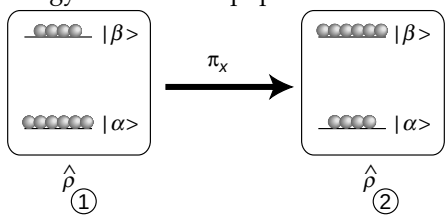

Figure 11.14
Population inversion by a π_x pulse.

11.6.3 Cycle of states

A π_x pulse is the same as two consecutive $(\pi/2)_x$ pulses. The calculations given above are readily continued for any number of consecutive $(\pi/2)_x$ pulses. Each $\pi/2$ pulse steps the spin system through the following cycle:

$$\begin{array}{ccc} \frac{1}{2}\hat{1} + \frac{1}{2}\mathbb{B}\hat{I}_z & \xrightarrow{(\pi/2)_x} & \frac{1}{2}\hat{1} - \frac{1}{2}\mathbb{B}\hat{I}_y \\ \uparrow{\scriptstyle (\pi/2)_x} & & \downarrow{\scriptstyle (\pi/2)_x} \\ \frac{1}{2}\hat{1} + \frac{1}{2}\mathbb{B}\hat{I}_y & \xleftarrow{(\pi/2)_x} & \frac{1}{2}\hat{1} - \frac{1}{2}\mathbb{B}\hat{I}_z \end{array}$$

In terms of the magnetization vector **M**, the cycle of states reads:

$$\begin{array}{ccc} +\mathbf{e}_z & \xrightarrow{(\pi/2)_x} & -\mathbf{e}_y \\ \uparrow{\scriptstyle (\pi/2)_x} & & \downarrow{\scriptstyle (\pi/2)_x} \\ +\mathbf{e}_y & \xleftarrow{(\pi/2)_x} & -\mathbf{e}_z \end{array}$$

Figure 11.15 shows the cycle of states using icons to represent the populations and coherences.

The first pulse equalizes the populations and generates coherences. The second pulse converts the coherences back into populations, generating an inverted population distribution. The third pulse equalizes the populations again and generates coherences once more (the 'icon' for the fourth state looks the same as that for the second state, but this is misleading, since the coherence *phases* are not shown). The fourth pulse destroys the coherences again and returns the system to equilibrium. The cycle may be continued with a fifth $(\pi/2)_x$ pulse, generating coherences again, and so on.

In principle, this cycle may be continued indefinitely. In practice, instrumental imperfections and relaxation cause losses. The spin system is not completely restored to equilibrium after every fourth $(\pi/2)_x$ pulse. Nevertheless, fairly accurate completion of four or five cycles is usually feasible in practice.

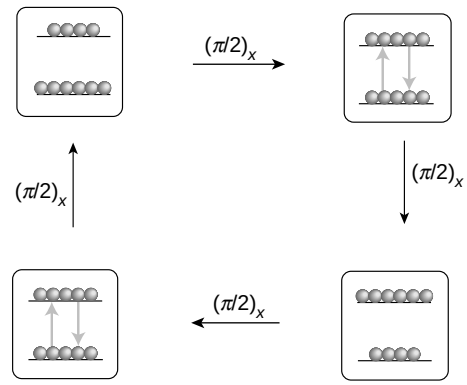

Figure 11.15
Cycle of states.

11.6.4 Stimulated absorption and emission

It is interesting to reflect on the excursions of the *energy* of the spin system during this cycle. In the initial state of thermal equilibrium, the energy of the spin system is low, since the low-energy state is more populated than the high-energy state. The first $(\pi/2)_x$ pulse raises the energy of the spin system, since the populations are equalized. The second $(\pi/2)_x$ pulse raises the energy still more, generating an inverted population distribution. The effect of the first two $(\pi/2)_x$ pulses is therefore to *raise* the energy of the spin system. The energy contained in the r.f. pulses is *absorbed* by the nuclear spins. This process corresponds to the *stimulated absorption* process in optical spectroscopy:

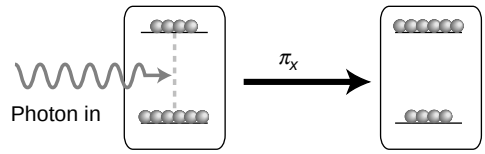

Figure 11.16
Stimulated absorption.

The behaviour of the energy during the next two $\pi/2$ pulses is more surprising. The third $\pi/2$ pulse equalizes the populations again, thereby *decreasing* the energy of the spin system. The fourth $\pi/2$ pulse decreases the energy of the spin system still more, thus regenerating the low-energy initial state.

At first sight, it is puzzling that the energetic r.f. pulses *decrease* the energy of the spin system. In fact, this phenomenon corresponds to *stimulated emission* in optical spectroscopy. If a system is not in equilibrium, then arrival of a photon may stimulate the emisson of a second photon by the spin system. The net effect is a release of energy by the molecular system back into the electromagnetic field:

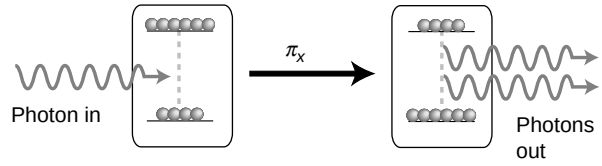

Figure 11.17
Stimulated emission.

Stimulated emission is the basis of the *laser*.

11.7 Free Precession Without Relaxation

Now consider the evolution of the density operator in the intervals between r.f. pulses. For example, suppose that, at the end of the pulse (time point $t_{②}$), the r.f. field is turned off and an interval τ is allowed to elapse:

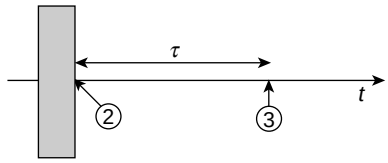

Figure 11.18
R.f. pulse and subsequent interval.

What is the spin density operator at time point $t_{③} = t_{②} + \tau$?

For the moment, ignore relaxation during the interval τ.

As described in Section 10.7, the rotating-frame state of a single spin evolves in the absence of r.f. fields according to

$$|\psi\rangle_{③} = \widehat{R}_z\left(\Omega^0\tau\right)|\psi\rangle_{②}$$

where Ω^0 is the resonance offset. The arguments given above may be repeated to obtain the following equation for the evolution of the spin density operator over an interval of free precession τ:

$$\hat{\rho}_{③} = \widehat{R}_z\left(\Omega^0\tau\right)\hat{\rho}_{②}\,\widehat{R}_z\left(-\Omega^0\tau\right) \qquad \text{(ignoring relaxation)} \tag{11.28}$$

This shows that the spin density operator gets sandwiched by two rotation operators around the z-axis, under an interval of free precession.

What does this mean for the populations and coherences?

If the matrix representations are multiplied out, we get the following equations for the populations:

$$\begin{aligned} \rho_{\boxed{\alpha}}③ &= \rho_{\boxed{\alpha}}② \\ \rho_{\boxed{\beta}}③ &= \rho_{\boxed{\beta}}② \qquad \text{(ignoring relaxation)} \end{aligned} \tag{11.29}$$

If relaxation is neglected, then *the populations of the states are constant during the intervals between r.f. pulses.*

For the (-1)-quantum coherence, we get

$$\rho_{\boxed{-}}③ = \exp\{+\mathrm{i}\Omega^0\tau\}\rho_{\boxed{-}}② \qquad \text{(ignoring relaxation)} \tag{11.30}$$

Between the pulses, the (-1)-quantum coherence revolves in the complex plane at the resonance offset frequency Ω^0:

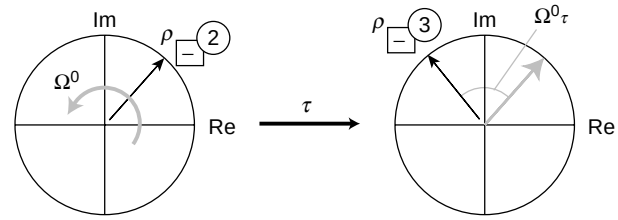

Figure 11.19
Precession of (−1)-quantum coherence.

The corresponding equation for the (+1)-quantum coherence is

$$\rho_{\boxed{+}}③ = \exp\{-i\Omega^0\tau\}\rho_{\boxed{+}}② \qquad \text{(ignoring relaxation)}$$

which shows that the (+1)-quantum coherence rotates in the opposite sense at the same frequency.

The free precession equations may also be written in terms of the magnetization vector. The magnetization vectors at the two time points are related by

$$\begin{aligned} M_x③ &= M_x② \cos\Omega^0 t - M_y② \sin\Omega^0 t \\ M_y③ &= M_x② \sin\Omega^0 t + M_y② \cos\Omega^0 t \\ M_z③ &= M_z② \end{aligned}$$

(ignoring relaxation) (11.31)

which represents a rotation of the magnetization vector around the z-axis at the frequency Ω^0:

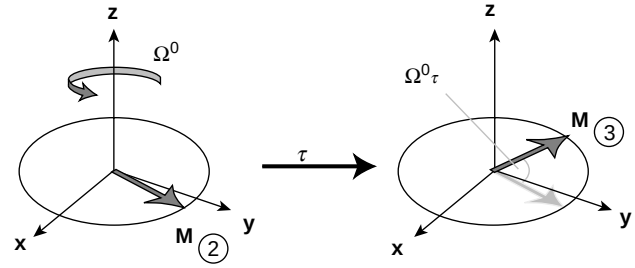

Figure 11.20
Precession of the magnetization vector.

For example, consider a $(\pi/2)_x$ pulse applied to a spin ensemble in thermal equilibrium, followed by an interval τ of free precession:

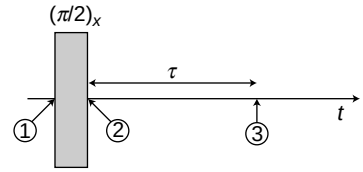

Figure 11.21
$(\pi/2)_x$ pulse, followed by a free precession interval.

The transformations of the spin density operator may be written as follows:

$$\begin{aligned}
\hat{\rho}_{①} = \hat{\rho}^{\mathrm{eq}} &= \tfrac{1}{2}\widehat{1} + \tfrac{1}{2}\mathbb{B}\hat{I}_z \\
&\Big\downarrow (\pi/2)_x \\
\hat{\rho}_{②} &= \tfrac{1}{2}\widehat{1} - \tfrac{1}{2}\mathbb{B}\hat{I}_y \\
&\Big\downarrow \tau \\
\hat{\rho}_{③} &= \tfrac{1}{2}\widehat{1} + \tfrac{1}{2}\mathbb{B}\left(-\hat{I}_y \cos\Omega^0\tau + \hat{I}_x \sin\Omega^0\tau\right)
\end{aligned} \tag{11.32}$$

For the magnetization vector, this reads as

$$\begin{aligned}
\mathbf{M}_{①} &= \mathbf{e}_z \\
&\Big\downarrow (\pi/2)_x \\
\mathbf{M}_{②} &= -\mathbf{e}_y \\
&\Big\downarrow \tau \\
\mathbf{M}_{③} &= \left(-\mathbf{e}_y \cos\Omega^0\tau + \mathbf{e}_x \sin\Omega^0\tau\right)
\end{aligned}$$

which may be depicted graphically as follows:

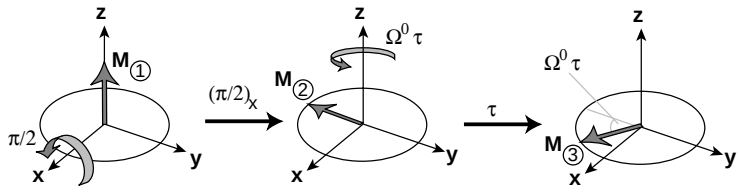

Figure 11.22
Motion of the magnetization vector during a pulse and the following interval.

If the equations in Equation 11.32 are compared, one may say loosely that the operator $\hat{I}_z$ is 'transformed' into $-\hat{I}_y$ by the $(\pi/2)_x$ pulse, and that the operator $-\hat{I}_y$ is 'transformed' into $-\hat{I}_y \cos\Omega^0\tau + \hat{I}_x \sin\Omega^0\tau$ by the interval of free precession. This is a convenient way of speaking, but should not be taken too literally. The operators themselves are not changed, of course. It is the state of the spin ensemble that changes – and this motion corresponds to the *substitution* of one angular momentum operator by another.

11.8 Operator Transformations

For convenience, the 'transformations' of the angular momentum operators under commonly-encountered pulses and precession intervals are now summarized. To calculate the effect of a pulse, or a precession interval, the angular momentum operators are substituted according to the rules given below.

11.8.1 Pulse of phase $\phi_{\mathrm{p}} = 0$

The effect of a pulse $(\beta_{\mathrm{p}})_x$ with flip angle β_{p} and phase $\phi_{\mathrm{p}} = 0$ may be calculated by the following operator substitutions:

pulse phase
$\phi_{\mathrm{p}} = 0$
'x-pulse'

$$\begin{cases} \hat{I}_x \rightarrow \hat{I}_x \\ \hat{I}_y \rightarrow \hat{I}_y \cos\beta_{\mathrm{p}} + \hat{I}_z \sin\beta_{\mathrm{p}} \\ \hat{I}_z \rightarrow \hat{I}_z \cos\beta_{\mathrm{p}} - \hat{I}_y \sin\beta_{\mathrm{p}} \end{cases} \tag{11.33}$$

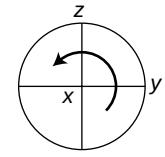

11.8.2 Pulse of phase $\phi_{\mathrm{p}} = \pi/2$

The effect of a pulse $(\beta_{\mathrm{p}})_y$ with flip angle β_{p} and phase $\phi_{\mathrm{p}} = \pi/2$ may be calculated by the following operator substitutions:

pulse phase
$\phi_{\mathrm{p}} = \pi/2$
'y-pulse'

$$\begin{cases} \hat{I}_x \rightarrow \hat{I}_x \cos\beta_{\mathrm{p}} - \hat{I}_z \sin\beta_{\mathrm{p}} \\ \hat{I}_y \rightarrow \hat{I}_y \\ \hat{I}_z \rightarrow \hat{I}_z \cos\beta_{\mathrm{p}} + \hat{I}_x \sin\beta_{\mathrm{p}} \end{cases} \tag{11.34}$$

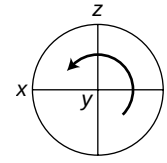

11.8.3 Pulse of phase $\phi_{\mathrm{p}} = \pi$

The effect of a pulse $(\beta_{\mathrm{p}})_{\bar{x}}$ with flip angle β_{p} and phase $\phi_{\mathrm{p}} = \pi$ may be calculated by the following substitutions:

pulse phase
$\phi_{\mathrm{p}} = \pi$
'$\bar{x}$-pulse'

$$\begin{cases} \hat{I}_x \rightarrow \hat{I}_x \\ \hat{I}_y \rightarrow \hat{I}_y \cos\beta_{\mathrm{p}} - \hat{I}_z \sin\beta_{\mathrm{p}} \\ \hat{I}_z \rightarrow \hat{I}_z \cos\beta_{\mathrm{p}} + \hat{I}_x \sin\beta_{\mathrm{p}} \end{cases} \tag{11.35}$$

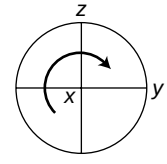

11.8.4 Pulse of phase $\phi_{\mathrm{p}} = 3\pi/2$

The effect of a pulse $(\beta_p)_{\bar{y}}$ with flip angle β_{p} and phase $\phi_{\mathrm{p}} = 3\pi/2$ may be calculated by the following substitutions:

pulse phase
$\phi_p = 3\pi/2$
"$\bar{y}$-pulse"

$$\begin{cases} \hat{I}_x \rightarrow \hat{I}_x \cos\beta_p + \hat{I}_z \sin\beta_p \\ \hat{I}_y \rightarrow \hat{I}_y \\ \hat{I}_z \rightarrow \hat{I}_z \cos\beta_p - \hat{I}_x \sin\beta_p \end{cases} \qquad (11.36)$$

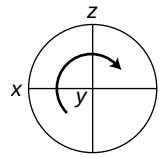

11.8.5 Pulse of general phase ϕ_p

From Equation 10.32, the effect of a pulse $(\beta_p)_{\phi_p}$ with flip angle β_p and general phase ϕ_p may be deduced by executing the following sequence of *three* transformations:

$$\xrightarrow{\hat{R}_z(-\phi_p)} \qquad \xrightarrow{\hat{R}_x(\beta_p)} \qquad \xrightarrow{\hat{R}_z(\phi_p)}$$

where the z-rotations transform the spin operators as follows:

z-rotation through the angle ϕ_p

$$\begin{cases} \hat{I}_x \rightarrow \hat{I}_x \cos\phi_p + \hat{I}_y \sin\phi_p \\ \hat{I}_y \rightarrow \hat{I}_y \cos\phi_p - \hat{I}_x \sin\phi_p \\ \hat{I}_z \rightarrow \hat{I}_z \end{cases} \qquad (11.37)$$

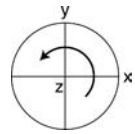

The effect of the central $\hat{R}_x(\beta_p)$ rotation is given in Equation 11.33.

11.8.6 Free precession for an interval τ

The effect of free precession for an interval τ may be calculated as follows:

free precession (no relaxation)

$$\begin{cases} \hat{I}_x \rightarrow \hat{I}_x \cos\Omega^0\tau + \hat{I}_y \sin\Omega^0\tau \\ \hat{I}_y \rightarrow \hat{I}_y \cos\Omega^0\tau - \hat{I}_x \sin\Omega^0\tau \\ \hat{I}_z \rightarrow \hat{I}_z \end{cases} \qquad (11.38)$$

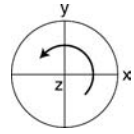

This neglects relaxation during the interval τ.

In all cases, the populations and coherences after a particular transformation may be calculated by writing the spin density operator as a matrix and identifying the appropriate matrix elements. Another method is to convert the angular momentum operators and the unity operator into shift and projection operators using the following relationships:

$$\frac{1}{2}\hat{1} = \frac{1}{2}\hat{I}^{\alpha} + \frac{1}{2}\hat{I}^{\beta} \qquad \hat{I}_z = \frac{1}{2}\hat{I}^{\alpha} - \frac{1}{2}\hat{I}^{\beta}$$

$$\hat{I}_x = \frac{1}{2}\hat{I}^{+} + \frac{1}{2}\hat{I}^{-} \qquad \hat{I}_y = \frac{1}{2\mathrm{i}}\hat{I}^{+} - \frac{1}{2\mathrm{i}}\hat{I}^{-}$$

The populations and coherences may be identified as the coefficients of the shift and projection operators in the expression for the density operator:

$$\hat{\rho} = \rho_{\boxed{\alpha}}\hat{I}^{\alpha} + \rho_{\boxed{\beta}}\hat{I}^{\beta} + \rho_{\boxed{+}}\hat{I}^{+} + \rho_{\boxed{-}}\hat{I}^{-}$$

11.9 Free Evolution with Relaxation

The above equations predict that, in the absence of an r.f. field, the populations do not change, and the coherences oscillate indefinitely at the frequency Ω^0 in the rotating frame.

Experimentally, one observes deviations from this ideal behaviour:

1. The populations are not time independent, but gradually drift towards their thermal equilibrium values.

2. The coherences do not last for ever, but gradually decay to zero.

These deviations are due to *relaxation*. The r.f. pulse causes the state of the spin system to depart from thermal equilibrium. Over a sufficiently long time, the fluctuating molecular surroundings cause the thermal equilibrium state to be gradually re-established.

This process corresponds to the 'wandering' motion of the precessing nuclear spins, introduced in Section 2.6. The fluctuations in the direction of the local magnetic fields, mentioned in that section, are due to the non-secular spin interactions discussed in Section 8.5.2.

In this section, I approach relaxation from a 'phenomenological' point of view, which is a polite way of saying that the equation of motion is simply faked so as to conform to the experimentally observed facts. The theory of relaxation is discussed more fully in Chapter 20.

In the phenomenological approach of Bloch, two relaxation time constants are introduced. The time constant T_1 (the *longitudinal relaxation time constant*, or *spin–lattice relaxation constant*) takes into account the drift of the populations towards their thermal equilibrium values. The time constant T_2 (the *transverse relaxation time constant*, or *spin–spin relaxation constant*) takes into account the decay of the coherences.[10]

11.9.1 Transverse relaxation

In practice, the coherences do not last for ever, but decay to zero. This behaviour is ensured in the equations by introducing an exponential decay term. The phenomenological equation for the rotating-frame coherences between time points ② and ③ is

$$\begin{aligned} \rho_{\boxed{-}}③ &= \rho_{\boxed{-}}② \exp\{\left(\mathrm{i}\Omega^0 - \lambda\right)\tau\} \\ \rho_{\boxed{+}}③ &= \rho_{\boxed{+}}② \exp\{\left(-\mathrm{i}\Omega^0 - \lambda\right)\tau\} \end{aligned} \tag{11.39}$$

where τ is the time interval between the two time points (compare this with Equation 11.30). The damping rate constant λ is given by the inverse of the *transverse relaxation time constant* T_2:

$$\lambda = {T_2}^{-1} \tag{11.40}$$

These equations for the coherences correspond to the following substitution rules for the transverse spin angular momentum operators:

free precession (with relaxation)

$$\begin{cases} \hat{I}_x \rightarrow \left(\hat{I}_x \cos\Omega^0\tau + \hat{I}_y \sin\Omega^0\tau\right) \mathrm{e}^{-\lambda\tau} \\ \hat{I}_y \rightarrow \left(\hat{I}_y \cos\Omega^0\tau - \hat{I}_x \sin\Omega^0\tau\right) \mathrm{e}^{-\lambda\tau} \end{cases} \tag{11.41}$$

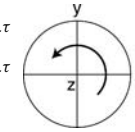

This is an 'improved' version of Equation 11.38.

For the transverse components of the magnetization vector, the appropriate equations are

$$M_x③ = \left(M_x② \cos \Omega^0 t - M_y② \sin \Omega^0 t\right) \mathrm{e}^{-\lambda\tau}$$
$$M_y③ = \left(M_x② \sin \Omega^0 t + M_y② \cos \Omega^0 t\right) \mathrm{e}^{-\lambda\tau}$$

which improves on Equation 11.31. The basic idea is that the transverse components of the magnetization vector *decay* at the same time as they precess:

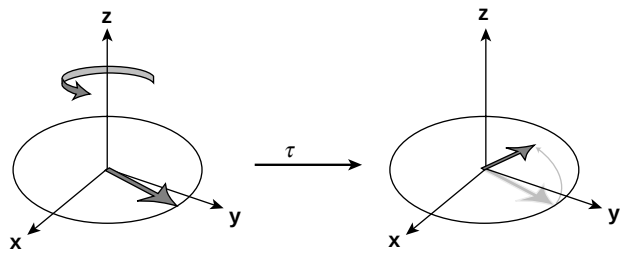

Figure 11.23
Precession of the magnetization vector, accompanied by T_2 decay.

(Note the shrinkage in the magnetization vector.)

Physically, it is easy to see why the coherences decay. Coherence requires a consistent polarization direction of the spin ensemble. Each spin precesses around the z-axis according to the strength of the local magnetic field. On the average, all spins experience the same field in a liquid, because of motional averaging, which creates identical conditions for all the spins, *on the average*. However, at any particular instant in time, the fields are slightly different on different spins, which causes a gradual loss of synchronization, like clocks in a clock shop, all started at the same time.

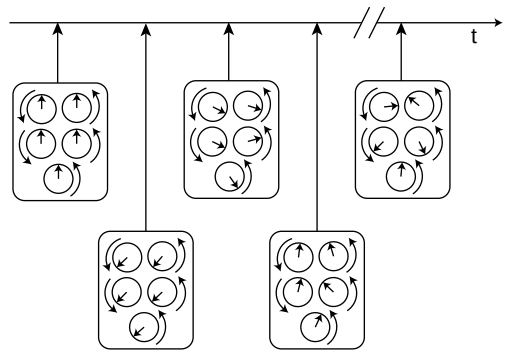

Figure 11.24
Microscopic mechanism of coherence decay.

For nuclear spins, the loss of synchronization can be remarkably slow. In many cases, the spins execute hundreds of millions of precession circuits before losing synchronization.

The decay of coherence does not necessarily involve any exchange of *energy* with the surroundings.[11] Coherence decay does, however, increase the *entropy* of the spin ensemble. The decay of coherence is therefore an *irreversible* process.

11.9.2 Longitudinal relaxation

The equation of motion for the populations is more complicated than for the coherences, in the presence of relaxation. The populations drift back to their thermal equilibrium values, while the coherences decay to zero.

The phenomological equation for the populations is

$$\begin{aligned} \rho_{\boxed{\alpha}}③ &= (\rho_{\boxed{\alpha}}② - \rho^{\text{eq}}_{\boxed{\alpha}})\mathrm{e}^{-\tau/T_1} + \rho^{\text{eq}}_{\boxed{\alpha}} \\ \rho_{\boxed{\beta}}③ &= \left(\rho_{\boxed{\beta}}② - \rho^{\text{eq}}_{\boxed{\beta}}\right)\mathrm{e}^{-\tau/T_1} + \rho^{\text{eq}}_{\boxed{\beta}} \end{aligned} \tag{11.42}$$

where the thermal equilibrium populations are

$$\rho^{\text{eq}}_{\boxed{\alpha}} = \frac{1}{2} + \frac{1}{4}\mathbb{B} \qquad \rho^{\text{eq}}_{\boxed{\beta}} = \frac{1}{2} - \frac{1}{4}\mathbb{B}$$

The time-constant T_1 is the *longitudinal* or *spin–lattice relaxation time*, and is typically in the range 100 ms–100 s. In exceptional cases, T_1 may be as long as hours or even months.

When the interval τ is equal to zero, Equation 11.42 gives the result $\rho_{\boxed{\alpha}}③ = \rho_{\boxed{\alpha}}②$, as it should. If τ is large, on the other hand, the population becomes equal to its thermal equilibrium value, $\rho_{\boxed{\alpha}}③ = \rho^{\text{eq}}_{\boxed{\alpha}}$. A similar property holds for the population of the $|\beta\rangle$ state.

For example, consider the motion of the populations after a π_x pulse, applied to a spin ensemble in thermal equilibrium. The populations immediately after the pulse are given by

$$\rho_{\boxed{\alpha}}② = \frac{1}{2} - \frac{1}{4}\mathbb{B} \qquad \rho_{\boxed{\beta}}② = \frac{1}{2} + \frac{1}{4}\mathbb{B}$$

as described in Section 11.6.2. The equation of motion of the populations after the pulse, as given by Equation 11.42, is therefore

$$\begin{aligned} \rho_{\boxed{\alpha}}③ &= \frac{1}{2} + \frac{1}{4}\mathbb{B}\left(1 - 2\mathrm{e}^{-\tau/T_1}\right) \\ \rho_{\boxed{\beta}}③ &= \frac{1}{2} - \frac{1}{4}\mathbb{B}\left(1 - 2\mathrm{e}^{-\tau/T_1}\right) \end{aligned}$$

The motion of the populations during and after the pulse is as follows:

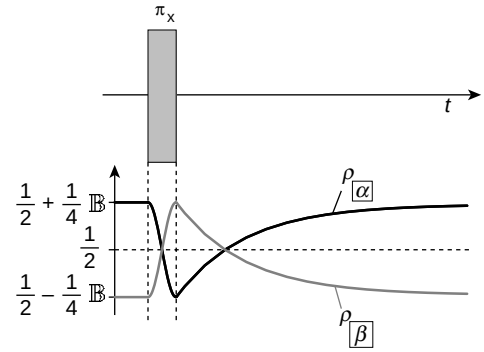

Figure 11.25
Motion of the populations during and after a π_x pulse.

The populations are inverted by the pulse and then slowly relax back to their equilibrium values. (The duration of the pulse is exaggerated for clarity; in practice, the duration of the pulse is around five orders of magnitude shorter than the time constant T_1.)

As a second example, consider a $(\pi/2)_x$ pulse. In this case, the populations are equalized by the pulse

$$\rho_{\boxed{\alpha}②} = \frac{1}{2} \qquad \rho_{\boxed{\beta}②} = \frac{1}{2}$$

The equation of motion of the populations after the pulse is as follows:

$$\rho_{\boxed{\alpha}③} = \frac{1}{2} + \frac{1}{4}\mathbb{B}\left(1 - \mathrm{e}^{-\tau/T_1}\right)$$

$$\rho_{\boxed{\beta}③} = \frac{1}{2} - \frac{1}{4}\mathbb{B}\left(1 - \mathrm{e}^{-\tau/T_1}\right)$$

which corresponds to the following motion:

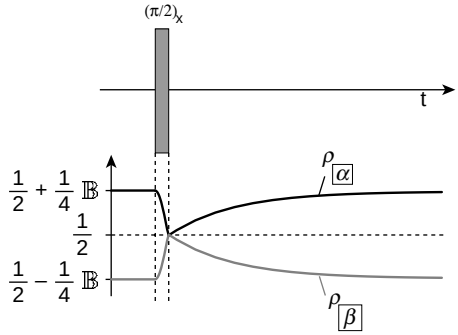

Figure 11.26
Motion of the populations during and after a $(\pi/2)_x$ pulse.

The populations are equalized by the pulse and then drift back to their different equilibrium values.

Longitudinal relaxation involves an exchange of energy between the spin system and the molecular surroundings. The energy transport in a pulse experiment may be depicted as follows:

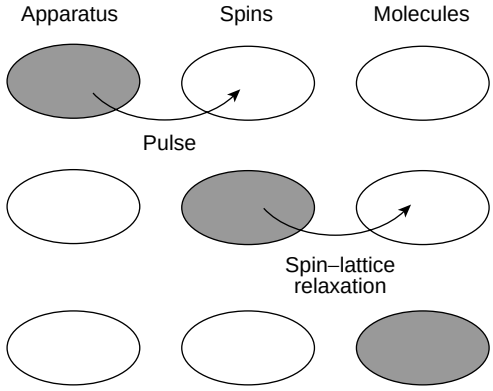

Figure 11.27
Energy transport in a pulsed NMR experiment.

The value of T_1 sets a theoretical upper limit on the possible value of T_2. This is because the fluctuating molecular fields cannot rotate the individual spin polarizations towards the z-axis while maintaining coherence of the transverse spin polarizations in the xy-plane. The following relationship holds absolutely:[12]

$$T_2 \leq 2T_1 \qquad \text{(theoretical limit)} \tag{11.43}$$

In most cases, however, it is usually found that T_2 is less than, or equal to, T_1:

$$T_2 \leq T_1 \qquad \text{(usual practical limit)} \tag{11.44}$$

The case $2T_1 > T_2 > T_1$ is possible, but is rarely encountered.[13]

It is also possible to visualize longitudinal relaxation in terms of the z-component of the magnetization vector. From Equations 11.23 and 11.42, the motion of the longitudinal component of the magnetization vector is

$$M_z③ = (M_z② - 1)\,\mathrm{e}^{-\tau/T_1} + 1 \tag{11.45}$$

where thermal equilibrium is represented by a unit magnetization vector along the z-axis.

Consider again a π_x pulse. The trajectory of the z-component of the magnetization vector looks as follows:

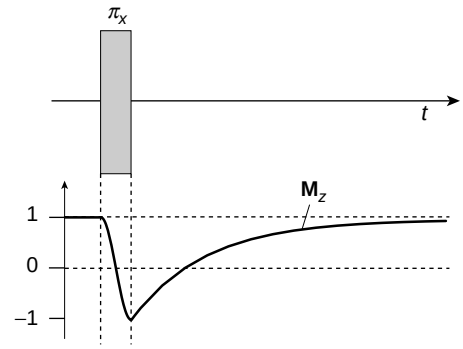

Figure 11.28
Motion of the z-component of the magnetization vector during and after a π_x pulse.

The magnetization vector is inverted and then relaxes back to its initial position.

In the case of a $(\pi/2)_x$ pulse, the z-component of the magnetization vector is destroyed by the pulse and then recovers:

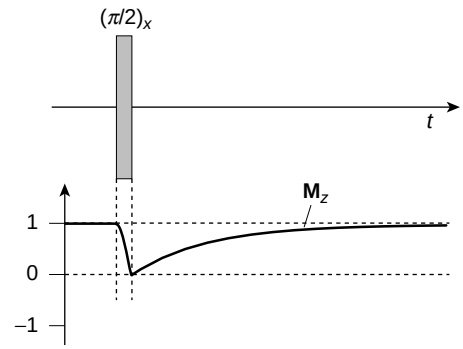

Figure 11.29
Motion of the z-component of the magnetization vector during and after a $(\pi/2)_x$ pulse.

11.10 Magnetization Vector Trajectories

In general, the populations and coherences change at the same time. The magnetization vector tracks out a trajectory in three-dimensional space.

For example, consider a single $(\pi/2)_x$ pulse, applied to a thermal equilibrium system:

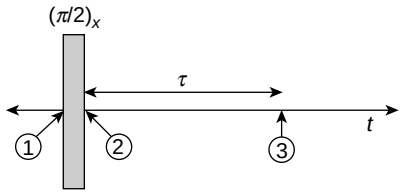

Figure 11.30
A $(\pi/2)_x$ pulse, followed by a free precession interval.

If the results in the previous sections are combined, we get the following evolution of the spin density operator:

$$\hat{\rho}_{①} = \hat{\rho}^{\mathrm{eq}} = \tfrac{1}{2}\widehat{1} + \tfrac{1}{2}\mathbb{B}\hat{I}_z$$

$$\downarrow \; (\pi/2)_x$$

$$\hat{\rho}_{②} = \tfrac{1}{2}\widehat{1} - \tfrac{1}{2}\mathbb{B}\hat{I}_y$$

$$\downarrow \; \tau$$

$$\hat{\rho}_{③} = \tfrac{1}{2}\widehat{1} + \tfrac{1}{2}\mathbb{B}\left(1 - \mathrm{e}^{-\tau/T_1}\right)\hat{I}_z + \tfrac{1}{2}\mathbb{B}\left(-\hat{I}_y \cos\Omega^0\tau + \hat{I}_x \sin\Omega^0\tau\right)\mathrm{e}^{-\tau/T_2}$$

This corresponds to the following motion of the magnetization vector in the interval after the pulse:

$$M_x(\tau) = \sin\Omega^0\tau\ \mathrm{e}^{-\tau/T_2}$$
$$M_y(\tau) = -\cos\Omega^0\tau\ \mathrm{e}^{-\tau/T_2}$$
$$M_z(\tau) = 1 - \mathrm{e}^{-\tau/T_1}$$

In order to visualize this motion, it is useful to follow the track left by the *tip* of the magnetization vector. The following plots show the track traced out by the tip of the magnetization vector after a $\pi/2$ pulse, for various parameters:

$\Omega^0/2\pi = 1$ Hz
$T_1 = T_2 = 2$s

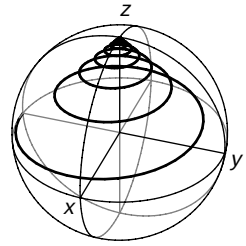

Figure 11.31
The trajectory taken by the tip of the magnetization vector, after a $(\pi/2)_x$ pulse (case 1).

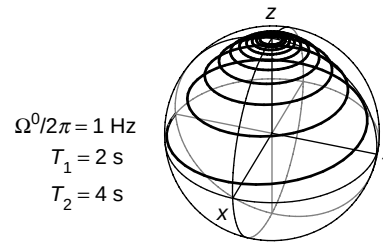

Figure 11.32
The trajectory taken by the tip of the magnetization vector, after a $(\pi/2)_x$ pulse (case 2).

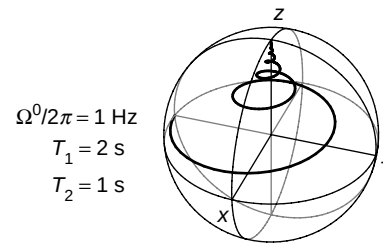

Figure 11.33
The trajectory taken by the tip of the magnetization vector, after a $(\pi/2)_x$ pulse (case 3).

Figure 11.32 corresponds to the rare case[13] in which T_2 is equal to $2T_1$.

Note how the transverse magnetization oscillates and dies out, at the same time as the longitudinal magnetization relaxes back towards the z-axis.

11.11 NMR Signal and NMR Spectrum

The precessing transverse nuclear magnetization induces an electric current in the coil surrounding the sample.[11] As discussed in Chapter 4, the current is amplified and subjected to quadrature detection. The two outputs of the quadrature detector are digitized and stored in the computer as a set of complex numbers. The NMR signal is Fourier transformed to obtain the NMR spectrum.

In Appendix A.5, it is shown that the complex NMR signal has the following relationship with the rotating-frame (−1)-quantum coherence:

$$s(t) \sim 2\mathrm{i}\rho_{\boxed{-}}(t)\,\exp\{-\mathrm{i}\phi_{\mathrm{rec}}\} \tag{11.46}$$

where ϕ_{rec} is the receiver phase shift, as discussed in Section 4.5.4.

Equation 11.46 states that only the rotating-frame (−1)-quantum coherence is detected in the quadrature receiver.[14] The populations and the (+1)-quantum coherence are both invisible. Only the (−1)-quantum coherence gives rise to an NMR signal, and hence to the peak in the NMR spectrum:

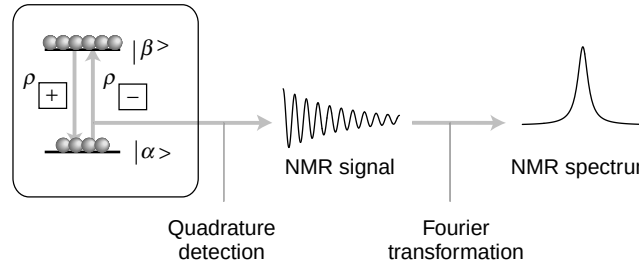

Figure 11.34
The relationship between the (−1)-quantum coherence and the spectral peak.

Let's get more quantitative. Suppose that the r.f. pulse sequence generates a (-1)-quantum coherence with amplitude $\rho_{\boxed{-}}(0)$ at the time point $t = 0$, which is defined as the start of signal acquisition.[15] From Equation 11.39, the amplitude of the coherence at a later time $t \geq 0$ is given by

$$\rho_{\boxed{-}}(t) = \rho_{\boxed{-}}(0) \exp\{\left(\mathrm{i}\Omega^0 - \lambda\right)t\right)\}$$

where $\lambda = {T_2}^{-1}$. These equations may be put together to obtain

$$s(t) = 2\mathrm{i}\rho_{\boxed{-}}(0) \exp\{-\mathrm{i}\phi_{\mathrm{rec}} + (\mathrm{i}\Omega^0 - \lambda)t\}$$

which may be written as

$$s(t) = a \ \exp\{\left(\mathrm{i}\Omega^0 - \lambda\right)t\right)\} \tag{11.47}$$

The *signal amplitude* a is given by

$$a = 2\mathrm{i}\rho_{\boxed{-}}(0) \exp\{-\mathrm{i}\phi_{\mathrm{rec}}\} \tag{11.48}$$

The amplitude of the NMR signal is therefore equal to the value of the (-1)-quantum coherence at the beginning of signal detection multiplied by some phase factors.

The expression for the NMR signal in Equation 11.47 has the same form as that assumed in Section 5.7.

The discussion in Section 5.8.1 may now be followed to obtain the NMR *spectrum* after Fourier transformation. The result is as follows:

$$S(\Omega) = a\mathcal{L}(\Omega; \Omega^0, \lambda) \tag{11.49}$$

where $\mathcal{L}$ is the complex Lorentzian function defined in Equation 5.12. For an ensemble of isolated spins-1/2, the NMR spectrum consists of a single Lorentzian peak at the resonance offset Ω^0. The width at half-height of the absorption peak is given in units of radians per second by 2λ, where λ is the coherence decay constant $\lambda = {T_2}^{-1}$. In units of hertz, the width at half-height is equal to $2\lambda/2\pi = 1/(\pi T_2)$. The complex amplitude of the peak is given by Equation 11.48, and is proportional to the (-1)-quantum coherence at the time point $t = 0$, i.e. the start of the signal acquisition.

To summarize, for a system of isolated spins-1/2, the NMR spectrum for a sequence of pulses may be calculated through the following steps:

1. Determine the resonance offset Ω^0, based on the known chemical shift of the spins and the position of the spectrometer reference frequency (Equation 10.21).

2. Set the spin density operator to the thermal equilibrium value (Equation 11.18).

3. Transform the spin density operator by the r.f. pulses according to Equations 11.33–11.36. For free precession, use Equations 11.29 and 11.38 if the intervals are short, so that relaxation may be neglected. For long intervals, use Equations 11.41 and 11.42.

4. Stop the calculation at the beginning of signal acquisition, time point $t = 0$. Determine the (-1)-quantum coherence $\rho_{\boxed{-}}$ at this point.

5. The spectrum is given by Equation 11.49. This describes a Lorentzian peak centred at frequency Ω^0, and with width at half-height 2λ, where λ is the inverse of T_2.

6. The complex amplitude of the peak is given by Equation 11.48, which involves the (-1)-quantum coherence at time point $t = 0$, as well as the signal phase shift parameters.

7. Normally only the real part of the spectrum is plotted. Consult Section 5.8.4 to determine the appearance of the spectrum in the case that the amplitude a is a complex number.

11.12 Single-Pulse Spectra

These results are now applied to some simple situations.

1. *Single* $(\pi/2)_x$ *pulse.* Suppose that a strong $(\pi/2)_x$ pulse is used for excitation and that the receiver phase ϕ_{rec} is set to zero during the acquisition of the NMR signal. The signal acquisition is started immediately after the pulse.

The density operator at the end of the pulse is calculated in the usual way starting from the thermal equilibrium state:

$$\begin{aligned} \hat{\rho}^{\text{eq}} &= \tfrac{1}{2}\widehat{1} + \tfrac{1}{2}\mathbb{B}\hat{I}_z \\ &\Big\downarrow (\pi/2)_x \\ \hat{\rho}(0) &= \tfrac{1}{2}\widehat{1} - \tfrac{1}{2}\mathbb{B}\hat{I}_y \end{aligned}$$

The result may be written in terms of the shift and projection operators:

$$\hat{\rho}(0) = \frac{1}{2}\hat{I}^{\alpha} + \frac{1}{2}\hat{I}^{\beta} - \frac{1}{4\text{i}}\mathbb{B}\hat{I}^{+} + \frac{1}{4\text{i}}\mathbb{B}\hat{I}^{-}$$

The (-1)-quantum coherence is equal to the coefficient of the $\hat{I}^{-}$ operator:

$$\rho_{\boxed{-}}(0) = \frac{1}{4\text{i}}\mathbb{B}$$

The signal amplitude a is therefore

$$a = 2\text{i}\frac{1}{4\text{i}}\mathbb{B} = \frac{1}{2}\mathbb{B}$$

assuming that there is no receiver phase shift ($\phi_{\text{rec}} = 0$).

The amplitude a is a real positive number, indicating that the real part of the NMR spectrum is an absorption Lorentzian and that the imaginary part of the spectrum is a dispersion Lorentzian:

$$\text{Re}\{S(\Omega)\} = \frac{1}{2}\mathbb{B}\mathcal{A}(\Omega; \Omega^0, \lambda)$$

$$\text{Im}\{S(\Omega)\} = \frac{1}{2}\mathbb{B}\mathcal{D}(\Omega; \Omega^0, \lambda)$$

as shown below:

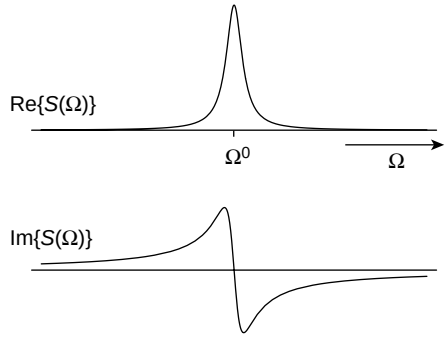

Figure 11.35
Real and imaginary parts of the spectrum generated by a $(\pi/2)_x$ pulse with $\phi_{\text{rec}} = 0$.

2. *Single* $(\pi/2)_y$ *pulse.* If a strong $(\pi/2)_y$ pulse is used instead, the calculation of the spin density operator runs as follows:

$$\begin{aligned}\hat{\rho}^{\text{eq}} &= \tfrac{1}{2}\widehat{1} + \tfrac{1}{2}\mathbb{B}\hat{I}_z \\ &\Big\downarrow (\pi/2)_y \\ \hat{\rho}(0) &= \tfrac{1}{2}\widehat{1} + \tfrac{1}{2}\mathbb{B}\hat{I}_x \\ &= \tfrac{1}{2}\hat{I}^{\alpha} + \tfrac{1}{2}\hat{I}^{\beta} + \tfrac{1}{4}\mathbb{B}\hat{I}^{+} + \tfrac{1}{4}\mathbb{B}\hat{I}^{-}\end{aligned}$$

The amplitude of the (-1)-quantum coherence at the start of the detection is

$$\rho_{\boxed{-}}(0) = \frac{1}{4}\mathbb{B}$$

The signal amplitude a is therefore

$$a = 2\mathrm{i}\frac{1}{4}\mathbb{B} = \mathrm{i}\frac{1}{2}\mathbb{B} \tag{11.50}$$

assuming no receiver phase shift ($\phi_{\text{rec}} = 0$).

In this case, the amplitude a is imaginary. The real part of the NMR spectrum is a negative dispersion Lorentzian and the imaginary part of the spectrum is in absorption:

$$\text{Re}\{S(\Omega)\} = -\frac{1}{2}\mathbb{B}\mathcal{D}(\Omega;\Omega^0,\lambda) \qquad \text{Im}\{S(\Omega)\} = \frac{1}{2}\mathbb{B}\mathcal{A}(\Omega;\Omega^0,\lambda)$$

as shown below:

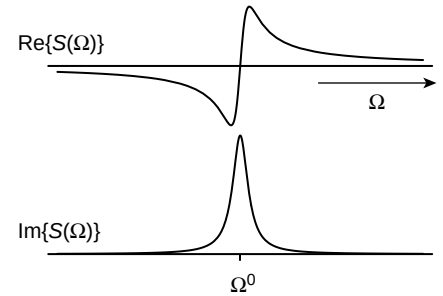

Figure 11.36
Real and imaginary parts of the spectrum generated by a $(\pi/2)_y$ pulse with $\phi_{\text{rec}} = 0$.

Similar calculations may be performed for pulses of any desired phase. It is easy to verify that the real part of the spectrum is in negative absorption for a $(\pi/2)_{\bar{x}}$ pulse, and that the real part of the spectrum is in negative dispersion for a $(\pi/2)_{\bar{y}}$ pulse.

Normally, these calculations are not performed in such detail. With experience, the form of the spectrum is determined simply *by inspection* of the density operator at the beginning of the detection period. The simple rules in the case $\phi_{\text{rec}} = 0$ are:

1. If the spin density operator $\hat{\rho}(0)$ contains a term proportional to $-\hat{I}_y$ (and no $\hat{I}_x$ terms), then the real part of the spectrum is in *positive absorption*.

2. If the spin density operator $\hat{\rho}(0)$ contains a term proportional to $\hat{I}_x$ (and no $\hat{I}_y$ terms), then the real part of the spectrum is in *negative dispersion*.

3. If the spin density operator $\hat{\rho}(0)$ contains a term proportional to $+\hat{I}_y$ (and no $\hat{I}_x$ terms), then the real part of the spectrum is in *negative absorption*.

4. If the spin density operator $\hat{\rho}(0)$ contains a term proportional to $-\hat{I}_x$ (and no $\hat{I}_y$ terms), then the real part of the spectrum is in *positive dispersion*.

Even more concisely:

$$\begin{aligned}
\hat{\rho}(0) &\sim -\hat{I}_y \xrightarrow{\phi_{\text{rec}} = 0} \text{positive absorption} \\
\hat{\rho}(0) &\sim +\hat{I}_x \longrightarrow \text{negative dispersion} \\
\hat{\rho}(0) &\sim +\hat{I}_y \longrightarrow \text{negative absorption} \\
\hat{\rho}(0) &\sim -\hat{I}_x \longrightarrow \text{positive dispersion}
\end{aligned} \tag{11.51}$$

If the receiver phase is shifted, then the correspondences between the spin density operator and the spectrum are different. For example, the rules for the case $\phi_{\text{rec}} = \pi/2$ are as follows:

$$\begin{aligned}
\hat{\rho}(0) &\sim -\hat{I}_y \xrightarrow{\phi_{\text{rec}} = \pi/2} \text{positive dispersion} \\
\hat{\rho}(0) &\sim +\hat{I}_x \longrightarrow \text{positive absorption} \\
\hat{\rho}(0) &\sim +\hat{I}_y \longrightarrow \text{negative dispersion} \\
\hat{\rho}(0) &\sim -\hat{I}_x \longrightarrow \text{negative absorption}
\end{aligned}$$

Notes

1. The protons in water behave independently of each other if one ignores (i) the *intra*molecular coupling between the protons in each water molecule and also (ii) the *inter*molecular couplings between protons on different water molecules. As shown in Chapter 14, the *intra*molecular coupling may be neglected (except for relaxation effects) if the two chemical shifts are the same and the sample is an isotropic liquid. Both conditions are satisfied for the protons in water. The *inter*molecular couplings in water are purely long range (see Section 8.6.4) and may also be neglected, in most circumstances (see *Further Reading* to Chapter 8).

2. The much better term *statistical operator* is sometimes encountered.

3. The symbol $\hat{\sigma}$ is sometimes used in the NMR literature instead of $\hat{\rho}$.

4. The sum of the diagonal elements is equal to one, so they are best understood as the *fractional populations* of the states. However, the term *population* has become standard.

5. The density operator does not specify a *unique* microscopic situation. The density operator only provides sufficient information for predicting the results of macroscopic observations, which are ensemble averages. For example, a hypothetical situation in which half the spins really are precisely in the state $|\alpha\rangle$ and half are precisely in the state $|\beta\rangle$ would have a density operator with equal populations $\rho_{\boxed{\alpha}} = \rho_{\boxed{\beta}} = \frac{1}{2}$. This state would give the same value for all macroscopic observables as a more general state, in which the spins are in superposition states and point in all possible directions. However, the situation in which most of the spins are in superposition states is much more *likely* to be correct.

6. In systems of spins $I > 1/2$, and coupled spin systems, there may arise additional types of coherence that cannot be represented as the alignment of spin polarizations with an external axis. This subject is explored in Chapters 13 and 15.

7. The (+1)-quantum coherence may make its presence felt if the quadrature receiver is not correctly adjusted, in which case it gives rise to *quadrature image peaks* at the frequency $-\Omega^0$ (see Appendix A.5). Such image peaks have been rendered negligible by advances in receiver technology.

8. Although almost all NMR calculations are performed in the rotating frame, there is one important exception. The estimation of the thermal equilibrium state through the Boltzmann distribution (Equation 11.15) must be performed using the fixed-frame Hamiltonian. For example, it is incorrect to use the eigenvalues of the rotating-frame Hamiltonian $\hat{\tilde{\mathcal{H}}}$ in the Boltzmann distribution.

9. The treatment of r.f. pulses in Section 11.8 ignores off-resonance effects and relaxation during the pulses. A more complete treatment is given by the *Bloch equations*, which are discussed in Appendix A.13.

10. In practice, the relaxation behaviour of spin systems is often quite complicated and cannot be described by single exponential functions. One example is analysed more fully in Chapter 20.

11. The coupling of the spins to the receiver coil withdraws a small amount of energy from the spin system, and acts in some respects like an additional relaxation mechanism. The generation of the NMR signal itself tends to pull the magnetization vector towards its thermal equilibrium value. This effect is called *radiation damping* or *coil reaction*. The real situation is complicated because of the 'feedback' between the nuclear spin system and the tuned circuit in the probe: the nuclear spins induce an NMR signal in the coil, which is amplified by electromagnetic resonance in the tuned circuit, which generates a magnetic field in the sample, which acts back on the spins again, and so on. The evolution of the signal can get quite complicated, with marked deviations from the simple form of Equation 11.47. It is even possible for the signal to *grow*, rather than decay! See A. Vlassenbroek, J. Jeener and P. Broekaert, *J. Chem. Phys.*, **103**, 5886 (1995). Such feedback effects are only dramatic in special circumstances, and I ignore them in this book.

12. The relationship between T_1 and T_2 given in Equation 11.43 may be understood using relaxation theory, as sketched in Chapter 20. In that chapter, it is shown that, for isolated spins-1/2, the longitudinal relaxation rate constant ${T_1}^{-1}$ is equal to $2W$, where W is the transition probability per unit time between the states. In general, the transverse relaxation rate constant has two contributions, i.e. an *adiabatic* contribution, which is due to the fluctuations of the energy levels, and a *non-adiabatic* contribution due

to the limited lifetime of the energy eigenstates, as a result of transitions. The transverse relaxation rate constant ${T_2}^{-1}$ cannot be smaller than the non-adiabatic contribution, which is equal to the transition probability per unit time, W. Hence, we have ${T_2}^{-1} \geq W$ and ${T_1}^{-1} = 2W$, which leads to Equation 11.43. In most common cases, there is also an adiabatic contribution to the transverse relaxation rate constant, so that ${T_2}^{-1}$ is either approximately the same as or larger than the longitudinal relaxation rate constant ${T_1}^{-1}$.

13. The case where $T_2 > T_1$ is encountered when the spin relaxation is caused by fluctuating microscopic fields that are predominantly transverse rather than longitudinal. One mechanism which gives rise to fields of this form involves the *antisymmetric component of the chemical shift tensor* (not to be confused with the CSA). In the notation of Section 9.1, this mechanism involves differences in non-secular chemical shift tensor components of the form $\delta^j_{xz} - \delta^j_{zx}$ and $\delta^j_{yz} - \delta^j_{zy}$. Molecular systems in which this mechanism is dominant are exceedingly rare (see F. A. L. Anet, D. J. O'Leary, C. G. Wade and R. D. Johnson, *Chem. Phys. Lett.*, **171**, 401 (1990)).

14. The fact that only the (-1)-quantum coherence is observable often causes confusion. As shown in Appendix A.5, this is not a fundamental property of the detection process, but rather derives from the particular representation of the quadrature receiver outputs as the two components of a complex signal.

15. The choice of time origin $t = 0$ as the start of signal acquisition is consistent with the definition of Fourier transformation, given in Section 5.8.1. Much NMR literature defines $t = 0$ to be the starting point of the pulse sequence, but this is strictly incorrect. The distinction becomes important for experiments on rotating samples, as is common in solid-state NMR.

Further Reading

- For further pedagogical discussion on the meaning of the spin density operator, see J. C. Paniagua, *Concepts Magn. Reson. A* **28**, 384–409 (2006).
- For a more thorough introduction to the spin density operator, see M. Goldman, *Quantum Description of High-Resolution NMR in Liquids*, Clarendon Press, Oxford, 1988 and R. R. Ernst, G. Bodenhausen and A. Wokaun, *Principles of Nuclear Magnetic Resonance in One and Two Dimensions*, Clarendon Press, Oxford, 1987.
- For the connection between NMR and coherent optics, see E. Lippert and J. D. Macomber, *Dynamics During Spectroscopic Transitions*, Springer, Berlin, 1995, and D. Suter, *The Physics of Laser–Atom Interactions*, Cambridge University Press, Cambridge, 1997.

Exercises

11.1 An ensemble of isolated protons is in thermal equilibrium at a temperature of 300 K.
(i) At what magnetic field is the population difference between the $|\alpha\rangle$ and $|\beta\rangle$ spin states equal to 5×10^{-5}?
(ii) What is the proton Larmor frequency in this field?
(iii) What is the thermal equilibrium population difference between the $|\alpha\rangle$ and $|\beta\rangle$ states of ^{13}C spins at the same temperature and in the same field?

11.2 In real experiments, the r.f. field created by the coil is not precisely uniform over the volume of the sample. This imperfection is called *r.f. inhomogeneity*. This exercise examines one strategy for rendering experiments less sensitive to r.f. inhomogeneity.

(i) An NMR experiment is performed on isolated proton spins. Suppose that the peak r.f. field in the *centre* of the sample is $B_{\mathrm{RF}} = 4.697\,\mathrm{mT}$, and that a pulse of duration $\tau_{\mathrm{p}} = 5\,\mu\mathrm{s}$ and phase $\phi_{\mathrm{p}} = 0$ is applied. What is the flip angle of the pulse in the centre of the sample? If the magnetization vector before the pulse is $\mathbf{M} = \mathbf{e}_z$, what is the magnetization vector after the pulse? Ignore off-resonance effects.

(ii) At the *edge* of the sample, the peak r.f. field is only $B_{\mathrm{RF}} = 4.228\,\mathrm{mT}$. If the magnetization vector at the edge of the sample before the pulse is $\mathbf{M} = \mathbf{e}_z$, what is the magnetization vector at the edge of the sample after the pulse? What is the angle between the magnetization vectors at the edge of the sample and at the centre of the sample, after the pulse?

(iii) Now suppose that the single r.f. pulse is replaced by a sequence of three pulses of durations $2.5\,\mu\mathrm{s}$, $5.0\,\mu\mathrm{s}$ and $2.5\,\mu\mathrm{s}$, with phases 0, $\pi/2$ and 0, respectively. This three-pulse sequence is an example of a *composite pulse*. If the magnetization vector before the pulse is $\mathbf{M} = \mathbf{e}_z$, what is the magnetization vector at the *centre* of the sample after the pulse?

(iv) Calculate the magnetization vector at the *edge* of the sample after the composite pulse. What is the angle between the magnetization vector at the edge of the sample and the magnetization vector at the centre of the sample, after the pulse?

(v) Explain the operation of the composite pulse geometrically.

12 Experiments on Non-Interacting Spins-1/2

In this chapter I discuss some common NMR experiments that may be understood using the density operator theory.

12.1 Inversion Recovery: Measurement of T_1

The first experiment is a method for measuring the longitudinal relaxation time constant of the spins, T_1. The value of T_1 provides valuable information as to the motion and dynamics of the molecules (see Chapter 20). Here, we are only concerned with the measurement procedure itself.

The usual technique for measuring T_1 is called *inversion recovery*. The pulse sequence is given by:

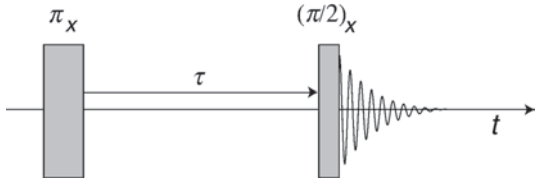

Figure 12.1 Inversion-recovery pulse sequence.

and consists of two r.f. pulses separated by an interval τ. The use of a single-headed arrow indicates that the experiment is performed in an *arrayed* fashion, as described in Section 5.6. This means that the pulse sequence is repeated, with different values of the interval τ, and the results compiled in a two-dimensional data matrix. If the time variable during the signal acquisition interval is denoted t, then the two-dimensional data matrix may be denoted $s(\tau, t)$.

The iconic pulse sequence given above conceals a number of details. First, for each value of τ, the pulse sequence and data acquisition are normally repeated many times, adding the signals together in order to enhance the signal at the expense of the noise, as described in Section 5.2. Second, each repetition of the pulse sequence is separated by a long interval τ_{wait}, during which the spins return to a reproducible thermal equilibrium state. For this to be satisfied, the waiting interval τ_{wait}, plus the signal acquisition period τ_{acq}, must be several times the relaxation time constant T_1 (which implies that one should already have a good guess as to the value of T_1 before determining it this way). Third, a phase cycle of the pulses is normally

Spin Dynamics: Basics of Nuclear Magnetic Resonance, Second Edition Malcolm H. Levitt

performed to reduce the sensitivity of the experiment to imperfections. In the following discussion, I ignore the phase cycle and assume that the r.f. pulses are perfect.

The first pulse in the sequence is a π_x pulse and generates an inverted population distribution. The populations relax back towards thermal equilibrium during the interval τ: their progress is monitored by the second pulse, which converts the population difference into coherences, including the observable (-1)-quantum coherence, which induces an NMR signal:

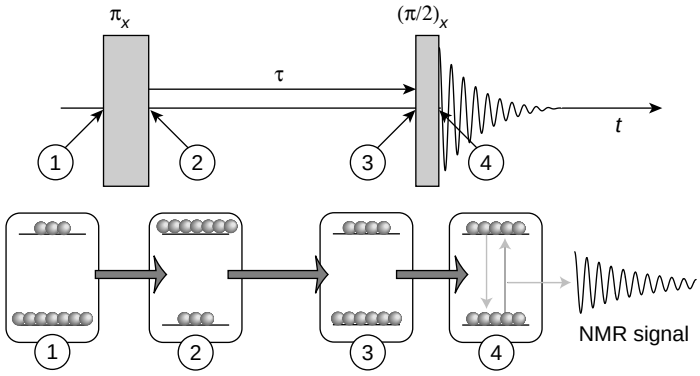

Figure 12.2
Populations and coherences during the inversion-recovery pulse sequence.

The spin density operator goes through the following transformations:

$$\hat{\rho}_{①} = \hat{\rho}^{\mathrm{eq}} = \tfrac{1}{2}\widehat{1} + \tfrac{1}{2}\mathbb{B}\hat{I}_z$$

$$\downarrow \pi_x$$

$$\hat{\rho}_{②} = \widehat{R}_x(\pi)\hat{\rho}_{①}\widehat{R}_x(-\pi) = \tfrac{1}{2}\widehat{1} - \tfrac{1}{2}\mathbb{B}\hat{I}_z$$

$$\downarrow \tau$$

$$\hat{\rho}_{③} = \tfrac{1}{2}\widehat{1} + \tfrac{1}{2}\mathbb{B}\left(1 - 2\mathrm{e}^{-\tau/T_1}\right)\hat{I}_z$$

$$\downarrow (\pi/2)_x$$

$$\hat{\rho}_{④} = \widehat{R}_x(\pi/2)\hat{\rho}_{③}\widehat{R}_x(-\pi/2) = \tfrac{1}{2}\widehat{1} - \tfrac{1}{2}\mathbb{B}\left(1 - 2\mathrm{e}^{-\tau/T_1}\right)\hat{I}_y$$

The observable spin coherence is therefore a function of the interval between the pulses τ and the time t after the last pulse. If the resonance offset of the spins is Ω^0, then the NMR signal is

$$s(\tau, t) = a(\tau)\,\exp\{\left(\mathrm{i}\Omega^0 - \lambda\right)t\}$$

where the amplitude $a(\tau)$ reflects the history of the longitudinal magnetization:

$$a(\tau) = \frac{1}{2}\mathbb{B}\left(1 - 2\mathrm{e}^{-\tau/T_1}\right)$$

The spectral peak amplitude is negative for small values of τ, but goes through zero and becomes positive for large values of τ:

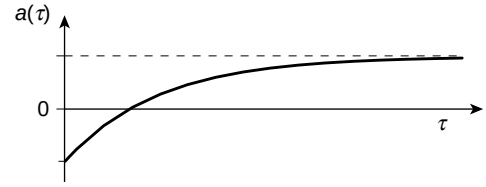

Figure 12.3
Trajectory of the peak amplitude a as a function of τ in the inversion-recovery experiment.

Now suppose that there are several different spin ensembles in the sample. Each different spin ensemble might belong to a different chemical compound, or to different isotopomers of the same compound. Different regions of the sample may also constitute individual ensembles, if, for example, the magnetic field is different at different points of space. In all cases, the total signal is simply a superposition of contributions from each ensemble:

$$s(\tau, t) = \sum_j a_j(\tau) \exp\{\left(\mathrm{i}\Omega_j^0 - \lambda_j\right) t\}$$

Here, Ω_j^0 is the resonance offset of spins in ensemble j and λ_j is a peakwidth parameter for ensemble j. The amplitude a_j of each signal component reflects the spin–lattice relaxation history of spins in each ensemble:

$$a_j(\tau) = \frac{1}{2}\mathbb{B}\left(1 - 2\mathrm{e}^{-\tau/T_1^j}\right)$$

where T_1^j is the spin–lattice relaxation time constant of spins belonging to ensemble j.

The data matrix $s(\tau, t)$ is Fourier transformed with respect to t according to

$$S(\tau, \Omega) = \int_0^\infty s(\tau, t) \exp\{-\mathrm{i}\Omega t\}\, \mathrm{d}t$$

The result is

$$S(\tau, \Omega) = \sum_j a_j(\tau)\mathfrak{L}\left(\Omega; \Omega_j^0, \lambda_j\right)$$

We get a superposition of Lorentzian peaks, one for spins in each ensemble. Each peak amplitude depends on τ according to the spin–lattice relaxation time constant for the corresponding ensemble j:

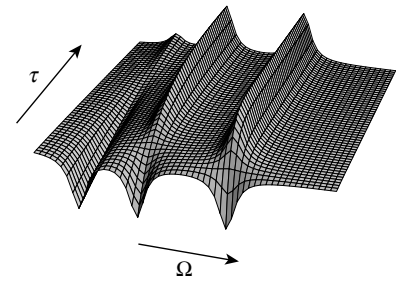

Figure 12.4
Real part of a signal data matrix $s(\tau, t)$ obtained from an inversion-recovery experiment.

In the surface above, note that the three peaks relax back to equilibrium at different rates. The value of T_1^j for each ensemble may be deduced by tracking the individual amplitudes $a_j(\tau)$.

An experimental data matrix $S(\tau, \Omega)$ for a sample with four different chemical sites is shown in Figure 12.5. In this case, each peak in the spectrum comes from a different isotopomer.

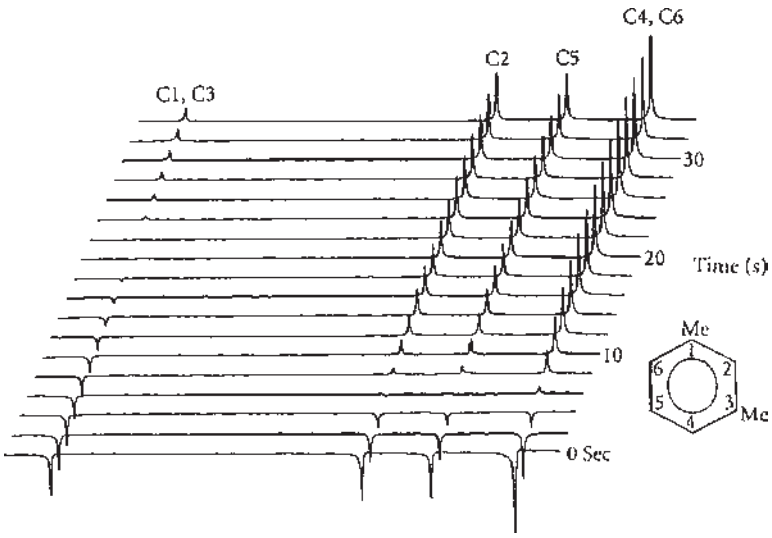

Figure 12.5
Set of experimental inversion-recovery spectra. From R. Freeman, *Spin Choreography*, Spektrum, Oxford, 1997, p. 47. (Copyright Spektrum Academic Publishers).

The value of T_1 may be extracted from the experimental peak amplitudes $a(\tau)$ by standard methods. For example, the values $\log(a(\infty) - a(\tau))$ may be plotted against τ and fitted to a straight line. The slope of the best-fit line is the estimated value of $-{T_1}^{-1}$.

12.2 Spin Echoes: Measurement of T_2

12.2.1 Homogenous and inhomogenenous broadening

The relaxation time constant T_2 conveys information about the dynamics of the molecules (see Chapters 19 and 20).

According to the theory given in Chapter 11, the width-at-half-height of the spectral peak (in hertz) is given by $1/(\pi T_2)$, where T_2 is the transverse relaxation time constant. This suggests that T_2 may be estimated simply by measuring the width of the spectral peak.

Unfortunately, this rarely gives a reliable estimate of T_2. The width of the NMR peaks tends to be larger than $1/(\pi T_2)$, because of *inhomogeneous broadening*, as discussed in Section 3.6. The magnetic field varies from place to place in the sample, which spreads the peaks out, thus giving a larger overall linewidth.

Therefore, there are (at least) two mechanisms of peak broadening in NMR spectra:

1. *Homogeneous broadening*. This is due to fluctuating *microscopic* magnetic fields, and is quantified by the transverse relaxation time constant T_2.

2. *Inhomogeneous broadening*. This is due to the variation of the *macroscopic* magnetic field over the volume of the sample, due to instrumental imperfections, or susceptibility effects.

The full peakwidth in the spectrum is a superposition of these two effects.[1]

The *spin echo method* allows the homogeneous decay to be distinguished from the inhomogeneous decay, so that T_2 may be measured even when the magnetic field is inhomogeneous.

12.2.2 Inhomogenenous broadening in the time domain

The mechanism of inhomogeneous broadening may be visualized in the frequency domain, as was done in Section 3.6. The magnetic field causes the Larmor frequency to vary from place to place in the sample. The spectrum consists of many overlapping peaks at slightly different positions, which gives rise to additional line broadening.

It is also instructive to view the effect of inhomogeneous broadening in the time domain. The FID from the whole sample is a superposition of many FID components, each with a slightly different frequency, and decaying with the natural decay time constant T_2. The many different frequency components get out of phase with each other and destructively interfere at long times, giving rise to an artificially rapid decay of the total signal:[1]

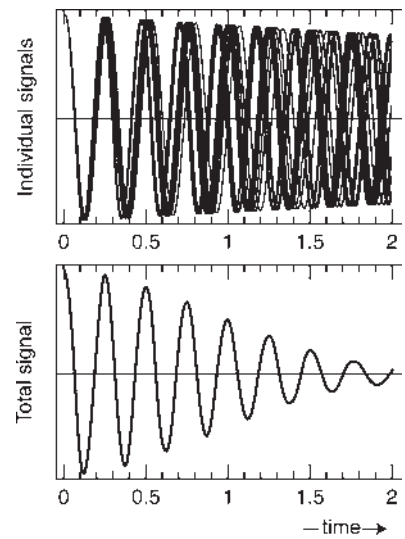

Figure 12.6
Inhomogeneous broadening gives rise to a superposition of signals with different frequencies. These interfere to give an enhanced signal decay.

Since the total signal decays faster, FT gives a spectrum with an increased peakwidth.

In the *spin echo* experiment, the *inhomogeneous* part of the signal decay is reversed by the application of a second r.f. pulse. This allows the *homogeneous* decay constant T_2 to be measured even in a non-uniform magnetic field.

12.2.3 Spin echo pulse sequence

The spin echo pulse sequence is as follows:

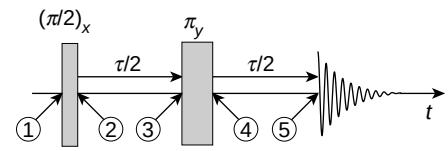

Figure 12.7
Spin echo pulse sequence.

The interval between the first pulse and the second pulse is equal to $\frac{1}{2}\tau$. The same interval is left after the second pulse before signal acquisition starts. As denoted by the single-headed arrows, an arrayed

experiment is performed in which the experiment is repeated with different values of τ (the two delays marked $\frac{1}{2}\tau$ are always kept the same as each other). The data matrix $s(\tau, t)$ is Fourier transformed with respect to t to give a spectrum $S(\tau, \Omega)$, containing peaks whose amplitudes varies as a function of τ:

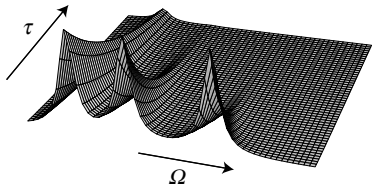

Figure 12.8
Spectral data matrix $S(\tau, \Omega)$ from the spin echo experiment.

The τ-dependence of each peak amplitude may be analysed to obtain the value of T_2 for each spin ensemble, independent of the inhomogeneous broadening.

I first give a mathematical description of the experiment, returning afterwards to a more 'physical' explanation.

For simplicity, consider first the case of just one spin ensemble. The transformation of the spin density operator by the first pulse should be familiar by now:

$$\begin{aligned} \hat{\rho}_{①} &= \hat{\rho}^{\mathrm{eq}} = \tfrac{1}{2}\widehat{1} + \tfrac{1}{2}\mathbb{B}\hat{I}_z \\ &\Big\downarrow (\pi/2)_x \\ \hat{\rho}_{②} &= \tfrac{1}{2}\widehat{1} - \tfrac{1}{2}\mathbb{B}\hat{I}_y \end{aligned}$$

From now on, the 'population parts' of the density operator (terms proportional to $\widehat{1}$ and $\hat{I}_z$) will be dropped. The subsequent evolution, including the second r.f. pulse, does not convert them into coherences, so they do not contribute to the final NMR signal.

The evolution during the first $\frac{1}{2}\tau$ period runs as follows:

$$\begin{aligned} \hat{\rho}_{②} &= -\tfrac{1}{2}\mathbb{B}\hat{I}_y + \ldots \\ &\Big\downarrow \tfrac{1}{2}\tau \\ \hat{\rho}_{③} &= \tfrac{1}{2}\mathbb{B}\left(-\hat{I}_y \cos \Omega^0 \tfrac{1}{2}\tau + \hat{I}_x \sin \Omega^0 \tfrac{1}{2}\tau\right) \mathrm{e}^{-\lambda \frac{1}{2}\tau} + \ldots \end{aligned}$$

This describes a rotation of the magnetization vector around the z-axis at the offset frequency Ω^0:

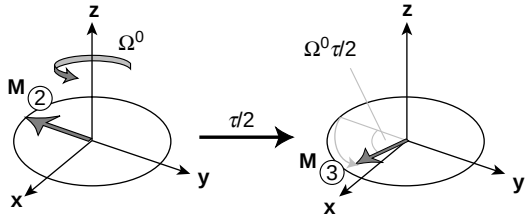

Figure 12.9
Precession of the magnetization during the first $\frac{1}{2}\tau$ interval.

The homogeneous decay of the transverse magnetization is taken into account by the $\exp\{-\lambda\frac{1}{2}\tau\}$ term (note the 'shrinkage' of the magnetization vector in the diagram above).

The second π_y pulse has the effect of reversing the $\hat{I}_x$ component, leaving the $\hat{I}_y$ component unchanged:

$$\hat{\rho}_{③} = \tfrac{1}{2}\mathbb{B}\left(-\hat{I}_y \cos\Omega^0\tfrac{1}{2}\tau + \hat{I}_x \sin\Omega^0\tfrac{1}{2}\tau\right)\mathrm{e}^{-\lambda\frac{1}{2}\tau} + \ldots$$

$$\Big\downarrow \pi_y$$

$$\hat{\rho}_{④} = \tfrac{1}{2}\mathbb{B}\left(-\hat{I}_y \cos\Omega^0\tfrac{1}{2}\tau - \hat{I}_x \sin\Omega^0\tfrac{1}{2}\tau\right)\mathrm{e}^{-\lambda\frac{1}{2}\tau} + \ldots$$

This is shown below:

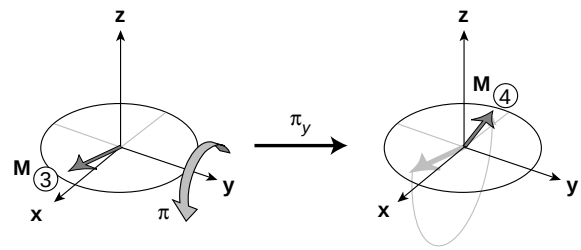

Figure 12.10
Rotation of the magnetization by the $(\pi/2)_y$ pulse.

There now follows another $\frac{1}{2}\tau$ interval, before the signal is detected. During this period, the magnetization vector rotates through an angle $\Omega^0\frac{1}{2}\tau$ again. This rotation exactly compensates the precession between the two pulses, leading to a magnetization vector exactly along the negative y-axis at time $t = 0$:

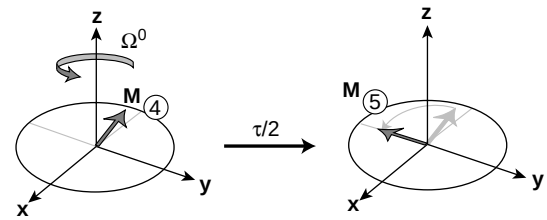

Figure 12.11
Precession of the magnetization during the second $\frac{1}{2}\tau$ interval.

It may be verified from the explicit transformation rules in Section 11.8, or from simple geometrical arguments, that the result is

$$\hat{\rho}_{⑤} = -\frac{1}{2}\mathbb{B}\hat{I}_y\mathrm{e}^{-\lambda\tau} + \ldots \tag{12.1}$$

The peak amplitudes in the NMR spectra $S(\tau, \Omega)$ are therefore given by

$$a(\tau) = \frac{1}{2}\mathbb{B}\mathrm{e}^{-\tau/T_2}$$

The exponential decay may readily be analysed to obtain an estimate for the value of T_2.

The key point here is that the final density operator $\hat{\rho}_{⑤}$, as given in Equation 12.1, is independent of the value of the resonant offset Ω^0. This implies that the signal at this time point is independent of the value of the magnetic field. By analysing the peak heights as a function of τ, an estimate of T_2 is obtained, independent of the inhomogeneous broadening.

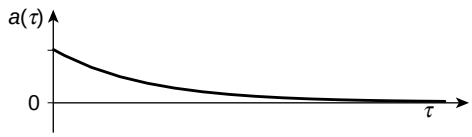

Figure 12.12
Trajectory of the peak amplitude a as a function of τ in the spin echo experiment.

12.2.4 Refocusing

Physically, the evolution under the second half of the pulse sequence corresponds to a reversal of the inhomogeneous part of the signal decay. The π_y pulse causes the magnetization vectors to be set up in such a way that the signal grows bigger rather than smaller:

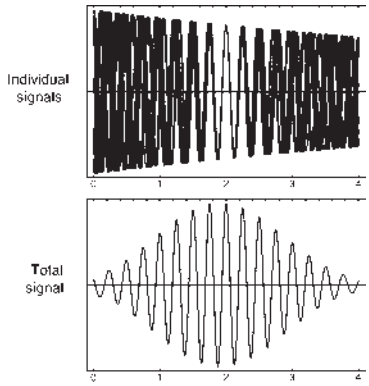

Figure 12.13
Constructive interference of the inhomogeneous signal components produces a spin echo.

The effect can be dramatic. It is quite feasible for the NMR signal to die out completely at the end of the first $\frac{1}{2}\tau$ interval, only to be resurrected, seemingly from nowhere, at the end of the second $\frac{1}{2}\tau$ interval. The term 'spin echo' is descriptive of this mysterious appearance of the signal from a state of silence.

The discovery of the spin echo by Erwin Hahn in 1950 may be regarded as the birth of modern pulsed NMR.[2]

The geometrical mechanism of the spin echo is seen clearly by associating a magnetization vector with many small sample regions, located at different points in space. If the field is inhomogeneous, then the precession frequencies of the magnetization vectors are all different. The pictures below show the trajectories of many magnetization vectors, with darker shading for those belonging to sample regions in relatively strong magnetic fields.

The magnetization vectors from different spatial regions fan out after the first pulse, as shown by the following snapshots during the first $\tau/2$ interval:

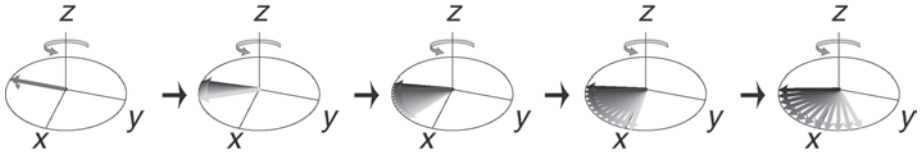

Figure 12.14
Spreading of magnetization vectors during the first $\tau/2$ interval.

This is called *dephasing*, and leads to a loss in the total signal during the first $\tau/2$ interval.

The second pulse rotates all vectors by π around the y-axis. Figure 12.15 shows the trajectories traced out by the tips of the magnetization vectors as they are rotated by their pulse, and their final positions after the π rotation:

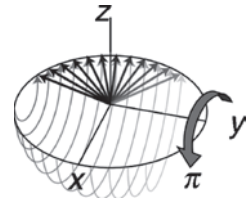

Figure 12.15
Rotation of magnetization vectors during the π_y pulse.

After the pulse, each vector rotates around the z-axis, at the frequency corresponding to its local magnetic field. Since the π pulse inverts the relative positions of the magnetization vectors belonging to strong and weak magnetic fields, they all *refocus* simultaneously at the $-y$-axis after the second $\tau/2$ interval, forming the echo:

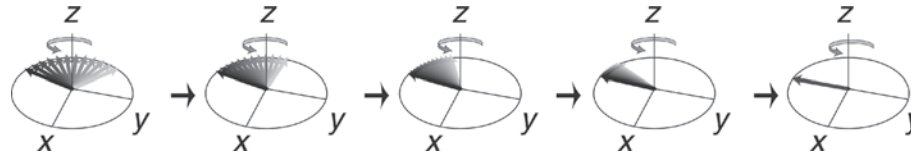

Figure 12.16
Refocusing of magnetization vectors during the second $\tau/2$ interval.

An experimental spin echo signal is shown in Figure 12.17.

Perfect refocusing requires that the inhomogeneous magnetic fields do not change while the pulse sequence is going on, so that the precession angle during the second $\tau/2$ interval is exactly the same as the precession angle during the first $\tau/2$ interval. The echo formation is disturbed if there is any sort of motion of the spins into different field regions, or if the fields themselves vary in time. If the fields change, or if the spins move into a region with a different magnetic field, then the precession after the π_y pulse no longer cancels exactly the precession before the pulse, thus leading to a reduction in signal at the echo maximum. This property can be very useful, because it allows the spin echo to detect *molecular motion*. Spin echo experiments are often used to quantify *diffusion* and *flow* processes (see Exercise 12.2 and Section 19.8).

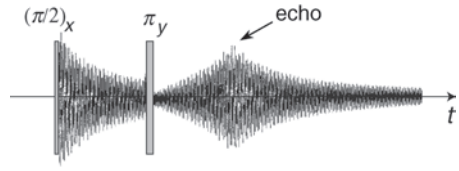

Figure 12.17 Experimental echo signal. Adapted from A. E. Derome, *Modern NMR Techniques for Chemistry Research*, Pergamon Press, Oxford, 1987, p. 91. Copyright, Elsevier Science.

12.2.5 Coherence interpretation

An equivalent interpretation of spin echo formation follows the histories of individual spin *coherences* during the echo sequence, rather than the magnetization vector trajectories. The coherence interpretation is more abstract than the magnetization vector interpretation, but proves to be easier to generalize to higher spin quantum numbers and coupled spin systems.

As discussed in Section 11.11, the quadrature-detected NMR signal is generated by (-1)-quantum coherences existing during the detection interval. However, the π pulse *inverts* the coherence order, as one can see from the following transformation properties:

$$\widehat{R}_y(\pi)\hat{I}^+\widehat{R}_y(\pi)^\dagger = -\hat{I}^-$$
$$\widehat{R}_y(\pi)\hat{I}^-\widehat{R}_y(\pi)^\dagger = -\hat{I}^+ \tag{12.2}$$

It follows that the echo signal derives from (+1)-quantum coherences existing *before* the π pulse (time point ③), which are transformed by the pulse into observable (−1)-quantum coherences.

The following coherence transfer processes, therefore, give rise to the echo signal:

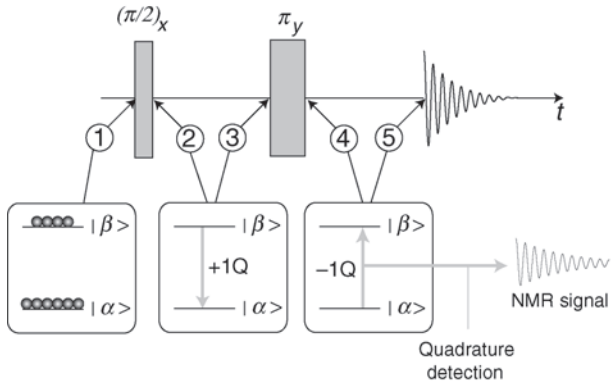

Figure 12.18
Coherence transfer processes leading to the spin echo signal.

The thermal equilibrium population difference is transformed by the $\pi/2$ pulse into a (+1)-quantum coherences, which evolves during the first $\tau/2$ interval (a (−1)-quantum coherence is also generated, but this does not give rise to a final NMR signal, and may therefore be ignored). The (+1)-quantum coherence is transformed by the π_y pulse into a (−1)-quantum coherence, which, after evolving for a further interval $\tau/2$, generates the quadrature NMR signal.

In the coherence interpretation, it is the *sign inversion of coherence order* induced by the π pulse that gives rise to the spin echo formation. As discussed in Section 11.7, the (+1)-quantum coherences evolve in the complex plane at the *negative* resonance offset under free precession, and hence

$$\rho_{\boxed{+}}③ = \rho_{\boxed{+}}② \exp\{(-i\Omega - \lambda)\tau/2\} \tag{12.3}$$

As shown in Equation 12.2, the π_y pulse converts the (+1)-quantum coherence into a (−1)-quantum coherence:

$$\rho_{\boxed{-}}④ = -\rho_{\boxed{+}}③ \tag{12.4}$$

The (−1)-quantum coherence evolves in the complex plane at the *positive* resonance offset under free precession, and hence

$$\rho_{\boxed{-}}⑤ = \rho_{\boxed{-}}④ \exp\{(+i\Omega - \lambda)\tau/2\} \tag{12.5}$$

These equations may be combined to get

$$\begin{aligned}\rho_{\boxed{-}}⑤ &= -\rho_{\boxed{+}}② \exp\{(-i\Omega - \lambda)\tau/2\} \exp\{(+i\Omega - \lambda)\tau/2\} \\ &= -\rho_{\boxed{+}}② \exp\{-\lambda\tau\}\end{aligned} \tag{12.6}$$

The observable (−1)-quantum coherence at the peak of the echo is therefore independent of the resonance offset, and hence of the local magnetic field strength.

This is an example of an important principle: whenever the sign of the coherence order is inverted by a pulse and the magnetic field is inhomogeneous, a spin echo may be formed.

12.2.6 Coherence transfer pathway

The sequence of coherence transfer events leading to a spin echo may be summarized by drawing a *coherence transfer pathway diagram*. The history of coherence orders leading to the observable signal is denoted as follows:

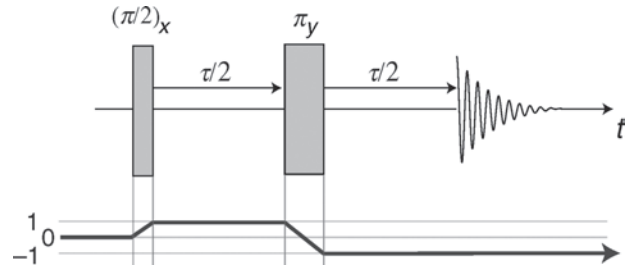

Figure 12.19
Coherence transfer pathway diagram for a spin echo.

In the lower part of the diagram, the accessible coherence orders are depicted as horizontal lines. For an ensemble of isolated spins-1/2, the only accessible orders are -1, 0 and $+1$. The coherence transfer pathway leading to the observable signal is represented by the bold line with an arrowhead. The initial thermal equilibrium state has order 0, since the corresponding density operator contains only populations. The first $\pi/2$ pulse converts the population difference into (± 1)-quantum coherence. Only the $(+1)$-quantum coherence is shown on the coherence transfer pathway diagram, since only this coherence gives rise to the observable signal at the end of the pulse sequence. The sign of the coherence order is inverted by the π pulse; as discussed above, it is this sign change that gives rise to a spin echo in an inhomogeneous magnetic field. The coherence transfer pathway terminates with order -1, since only (-1)-quantum coherences are observable under quadrature detection of the NMR signal. Note that the pathway diagram always shows horizontal lines during the intervals of free precession, to indicate that no changes in coherence order take place in the absence of r.f. pulses.

Coherence transfer pathway diagrams are very useful tools for portraying the essential features of complex NMR experiments, without going into details. They are particularly useful for constructing phase cycles (see Appendix A.11).

12.3 Spin Locking: Measurement of $T_{1\rho}$

In the Carr–Purcell echo, transverse magnetization is allowed to precess freely before reversing its evolution using a π pulse. In contrast, the *spin-locking* method employs a resonant r.f. field to *suppress* the free evolution of transverse magnetization, locking it to a particular direction in the rotating frame.

A typical spin-locking pulse sequence is as follows:

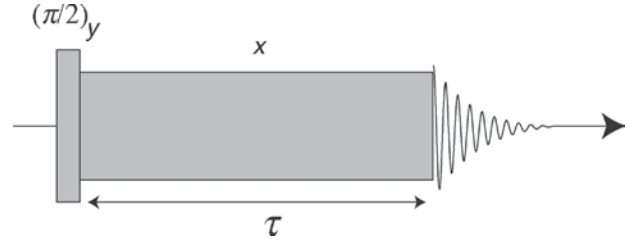

Figure 12.20
Pulse sequence for a spin-locking experiment.

The operation of this pulse sequence is as follows:

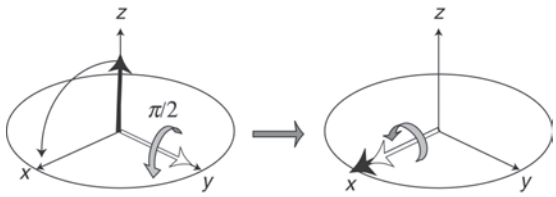

Figure 12.21
Spin magnetization (black arrow) is rotated from the z-axis to the x-axis by a $(\pi/2)_y$ pulse, where it is locked by an r.f. field along the x-axis (white arrow).

The initial $(\pi/2)_y$ pulse converts the initial longitudinal magnetization into transverse magnetization along the rotating-frame x-axis. The phase of the r.f. field is then suddenly changed to $\phi = 0$, so that the rotating-frame r.f. field is also along the x-axis, i.e. in the same direction as the transverse magnetization. If the r.f. field is large enough, then the transverse magnetization is unable to precess away from the x-axis – it is said to be *spin locked*. After a time τ, the locking field is turned off, releasing the transverse magnetization and allowing it to generate an NMR signal.

In most cases, the spin-locked magnetization decays roughly exponentially to zero.[3] The decay process may be followed by conducting a series of experiments with several values of the locking time τ. The time constant of the exponential decay is usually denoted $T_{1\rho}$, and is usually called the *spin–lattice relaxation time constant in the rotating frame*.[4]

The study of the time constant $T_{1\rho}$ can reveal details of slow molecular dynamics. The procedure is often used for the study of motions in polymers.

12.4 Gradient Echoes

R.f. pulses are not the only way to induce spin echoes. A different type of spin echo arises when an applied field gradient (see Section 4.7) is reversed in sign. This is called a *gradient echo*. Consider the following pulse sequence:

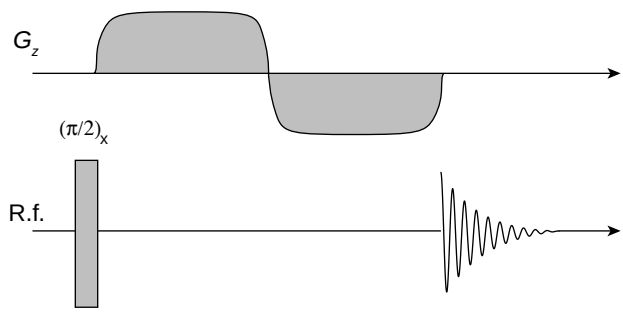

Figure 12.22
Pulse sequence for inducing a gradient echo.

After transverse magnetization is excited by the first $\pi/2$ pulse, a magnetic field gradient is switched on along the z-axis. After a certain time interval the gradient is reversed in sign for the same interval. The gradient echo forms when the integral of the field gradient over time is equal to zero.

The gradient echo may be visualized by imagining the transverse magnetization vectors of a series of small volume elements displaced along the direction of the field gradient, i.e. along the z-axis in the case of a G_z gradient. In the presence of the gradient, spins at different positions z experience different local magnetic fields, so that the transverse magnetization components precess at different frequencies. As the evolution proceeds in the presence of the gradient, a *magnetization helix* is wound around the z-axis:

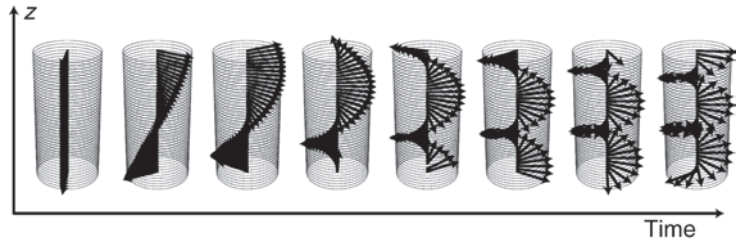

Figure 12.23
The evolution of transverse magnetization vectors at different points along the z-axis, in the presence of a field gradient G_z.

The pitch of the helix is inversely proportional to the magnitude of the gradient, and the time for which it is applied. Large gradients applied for long times lead to a short pitch. When the gradient is applied for a long enough time, the pitch of the helix becomes much smaller than the sample dimensions and the signal vanishes, since the individual magnetization components cancel out.

The magnetization helix is unwound by reversing the sign of the gradient:

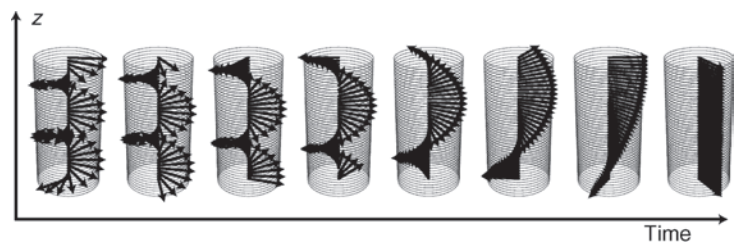

Figure 12.24
Reversal of the sign of G_z causes the magnetization helix to unwind, forming a field gradient echo.

The right-hand frame in Figure 12.24 represents the gradient echo: all transverse magnetization components are restored with the same phase, so the bulk transverse magnetization reappears.

Note that the phase of the gradient echo (right-hand frame in Figure 12.24) is different from that of the initial state after the $\pi/2$ pulse (left-hand frame in Figure 12.23).This is due to the chemical shift evolution during the gradient periods. Chemical shift precession occurs in parallel with the evolution under the field gradient, and is not influenced by the sign of the gradient. Unlike pulsed spin echoes, gradient echoes do not refocus the evolution due to chemical shifts or other local field deviations.

Gradient echoes are a common motif in NMR imaging experiments. They are also used to measure the physical diffusion of molecules along the gradient axis (see Section 19.8).

12.5 Slice Selection

If a weak r.f. pulse is applied at the same time as a field gradient, NMR signals are selected from a set of volume elements that lie in a plane, perpendicular to the gradient axis. This is called *slice selection*.

Consider, for example, the following pulse sequence:

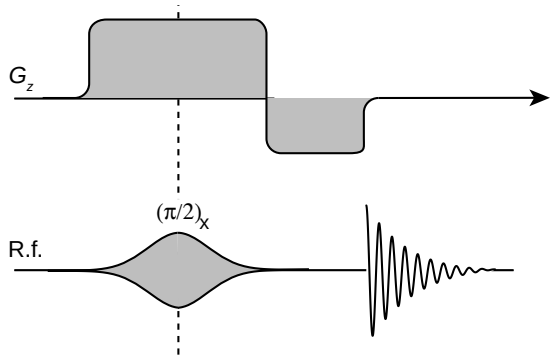

Figure 12.25
Pulse sequence for selecting NMR signals from a plane perpendicular to the z-axis.

The pulse sequence is similar to the gradient echo sequence in Figure 12.22, but there are three differences. First, the field gradient G_z is turned on *before* the r.f. pulse is applied, so that the centre of the r.f. pulse coincides with the centre of the positive gradient pulse (dashed line). Second, the r.f. pulse is not rectangular, but has a smooth amplitude profile. Third, the negative gradient pulse is only half the duration of the positive gradient pulse.

When the field gradient G_z is applied, the Larmor frequencies of the nuclei become dispersed along the z-axis. As a result, the r.f. pulse is only exactly resonant with nuclei at one position along the z-axis. At this position, the r.f. frequency is the same as the gradient-shifted Larmor frequency. For nuclei located at this value of z, the on-resonance $(\pi/2)_x$ pulse excites transverse magnetization along the rotating-frame $-y$-axis.

Now consider nuclei a short distance δz above the position of exact resonance. Spins at this point experience a resonance offset in the presence of the field gradient, given by

$$\Omega^0(\delta z) = -\gamma G_z \delta z$$

The effect of an off-resonance pulse is discussed in Section 10.8.5. Transverse magnetization will still be excited by the pulse, providing that the resonance offset is not too large compared with the nutation frequency ω_{nut}, which depends on the strength of the r.f. field. The width of the excited slice is therefore approximately equal to $2|\omega_{\text{nut}}/\gamma G_z|$. Strong r.f. fields and weak gradients excite a thick slice. Weak r.f. fields and strong gradients excite a thin slice. The smooth shaping of the r.f. pulse profile in Figure 12.25 optimizes the selectivity, giving rise to insignificant excitation of transverse magnetization outside the selected slice.

We must also consider the phase of the excited transverse magnetization. For nuclei that are exactly on-resonance with the pulse, the transverse magnetization is generated along the rotating frame $-y$-axis, as usual. But for nuclei that are slightly above or below the plane of exact resonance, the transverse magnetization is generated with a phase shift, as discussed in Section 10.8.5. This phase shift depends on the resonance offset, and hence on position along the z-axis. It may be shown that the phase shift is the same as that which would have arisen if the transverse magnetization had been generated instantaneously at the exact centre of the pulse (dashed line in Figure 12.25), and then allowed to precess in the presence of the field gradient. In order to obtain a significant NMR signal, the phase shift across the selected slice must be refocused by reversing the sign of the gradient. The gradient echo forms when the integral of the positive gradient, *measured from the centre of the pulse onwards*, is equal to the integral of the negative gradient. This is the configuration shown in Figure 12.25.

Figure 12.26 shows the evolution of the magnetization helix during the interval when a negative field gradient is applied. Note that the final transverse magnetization components come into phase at the end

of the negative gradient pulse, and that the excited transverse magnetization originates in a region with a narrow range of z-coordinates.

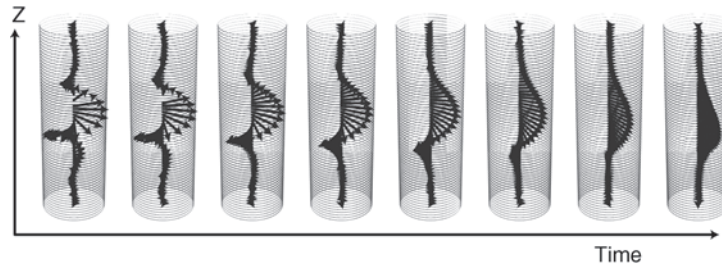

Figure 12.26
Formation of a gradient echo in the second half of a slice selection sequence.

12.6 NMR Imaging

NMR imaging is certainly the most visible form of NMR to the general public. Generally known as *magnetic resonance imaging* (MRI), it has reached most regions of the planet:

Figure 12.27
NMR imaging has become routine (a scene from southern India).

MRI is particularly useful in medicine, where it has become a routine diagnostic tool, especially for conditions of the brain, nervous system, and soft tissues of the body. Peter Mansfield and Paul Lauterbur were awarded the Nobel Prize in 2003 for their role in the early development of NMR imaging.

NMR imaging is based on a very simple insight: in the presence of a field gradient, the NMR spectrum maps the density of nuclear spins along the gradient axis. To see what this means, suppose that the sample is a long thin rod, oriented along the x-axis, perpendicular to the main magnetic field. Suppose also that the rod is made of some material that absorbs water, but that the distribution of water in the material is not uniform. The water is concentrated in two regions:

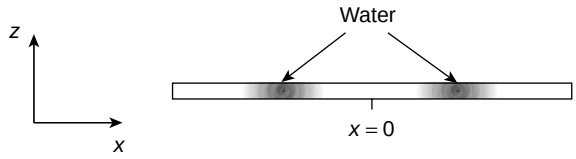

Figure 12.28
A thin rod containing two regions of high water density.

The density of the water may be described by a function $d(x)$, which in the case above has the following form:

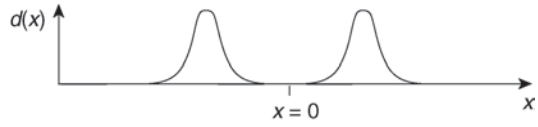

Figure 12.29
The water density in the rod.

The centre of the rod is assumed to be the point $x = 0$.

Suppose now that a field gradient G_x is applied along the x-axis, using the coils and drivers described in Section 4.7. In the presence of the gradient, nuclear spins in the rod experience a total field that is given by the sum of the main magnetic field and the gradient field:

$$\mathbf{B} = (B^0 + G_x x)\,\mathbf{e}_z$$

(ignoring chemical shifts). Note that the gradient field and the main field are *both* along the z-axis. As described in Section 4.7, a gradient G_x does not describe a field along the x-axis, but instead a field along the z-axis that depends on the x-coordinate.[5]

In the presence of the gradient, the Larmor frequency of a spin is dependent on its position in space x, and is given by

$$\omega^0(x) = -\gamma(B^0 + G_x x) = \omega^0(0) - \gamma G_x x$$

where $\omega^0(0)$ is the Larmor frequency in the exact centre of the rod.

Suppose now that an NMR experiment is performed using a spectrometer reference frequency ω_{ref} equal to the Larmor frequency at the centre of the rod $\omega^0(0)$. The offset frequency of the spins is spatially dependent:

$$\Omega^0(x) = \omega^0(x) - \omega_{\text{ref}} = -\gamma G_x x$$

The important point is that the Larmor frequency depends in a very simple way on spatial position. Each part of the sample gives an NMR peak at a frequency that is directly proportional to the spatial coordinate of the precessing spins:

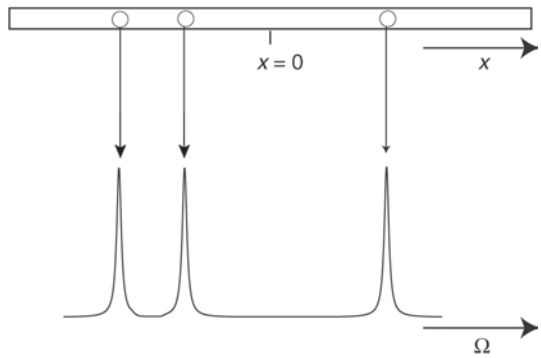

Figure 12.30
Mapping of spatial position on to spectral coordinate, for a field gradient along the x-axis.

(This is drawn for a negative gradient.)

This simple relationship between the frequency of a peak and the position in space works the other way round as well. If one obtains a peak at a frequency Ω, then this signal must originate from a point in space x_Ω, given by

$$\Omega = -\gamma G_x x_\Omega$$

and hence

$$x_\Omega = -\frac{\Omega}{\gamma G_x} \tag{12.7}$$

If the field gradient G_x is known, then one can work out from which part of the sample a given NMR signal comes from.

Now consider the NMR spectrum from the entire sample. All the peaks add up, and the more spins there are in a particular place, the more peaks add up at a particular point in the spectrum. As a result, the *total* spectral amplitude at a particular spectral coordinate Ω is directly proportional to the total spin density at the corresponding spatial coordinate x:

$$S(\Omega) \sim d(x_\Omega)$$

Here $d(x)$ is the spin density function, and x_Ω is the spatial coordinate corresponding to the offset frequency Ω, in the presence of the field gradient G_x.

The NMR spectrum is therefore a *map* of the spin density function $d(x)$:

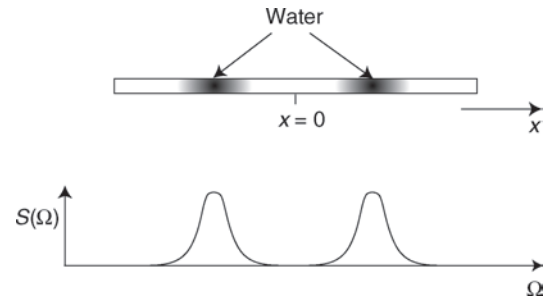

Figure 12.31
Mapping of spin density onto the NMR spectrum, for a field gradient along the x-axis.

The NMR spectrum in the presence of the gradient reveals directly the distribution of water in the rod.

In practice, most samples are not long thin rods. The above technique does not work very well for a sample of general shape, because there are many positions in the sample that have the same x-coordinate, and which give NMR peaks at the same place in the spectrum. The one-dimensional spectrum of the form gives the *projection* of the spin density along the x-axis, as illustrated below:

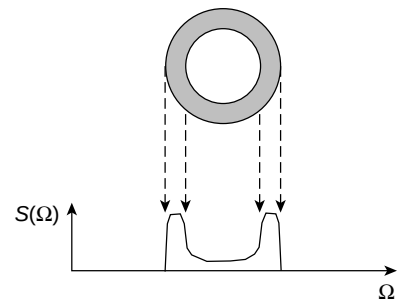

Figure 12.32
Projection of spin density on to the x-axis, for a ring-shaped sample.

The projection gives some clues about the spatial distribution of nuclear spins, but not the whole answer. Two objects may have very different spatial spin distributions, but still give the same projection along the *x*-axis:

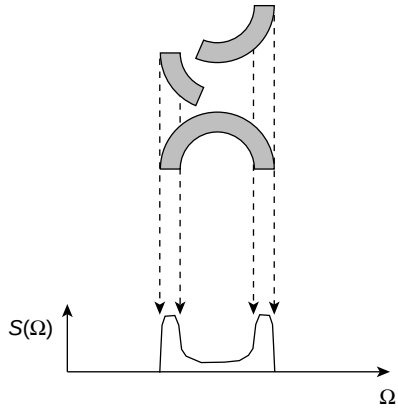

Figure 12.33
A different sample geometry that gives the same projection onto the *x*-axis.

To get more spatial information, the method has to be extended further, using the concept of two-dimensional spectroscopy (Section 5.9). Suppose that the sample is a flat pancake, oriented in the *xy*-plane:

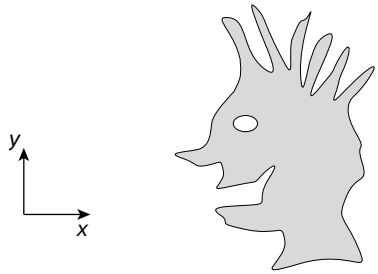

Figure 12.34
A pancake-shaped object in the *xy*-plane.

We wish to make an image of this flat object by NMR.
Consider the following pulse sequence:

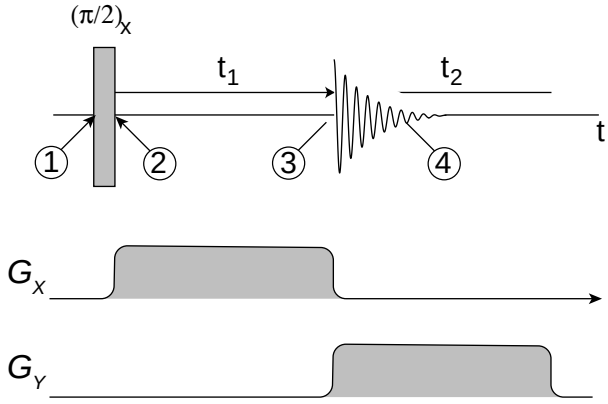

Figure 12.35
A two-dimensional NMR imaging pulse sequence.

After the initial $\pi/2$ pulse for exciting the spin coherences, there follows a variable evolution interval t_1 during which the gradient G_x is applied, and the magnetic field has the following form:

$$\mathbf{B} = (B^0 + G_x x)\,\mathbf{e}_z \qquad (\text{during } t_1)$$

At time point ③, the magnetic field gradient G_x is turned off, and the gradient G_y is turned on. The magnetic field has the following form during the signal acquisition interval t_2:

$$\mathbf{B} = (B^0 + G_y y)\,\mathbf{e}_z \qquad (\text{during } t_2)$$

The experiment is conducted in an arrayed fashion, with the interval t_1 taking a large set of values, so that a data matrix $s(t_1, t_2)$ is built up, in the fashion described in Section 5.6.

Consider first the NMR signal from just one point in the sample, with spatial coordinate (x, y):

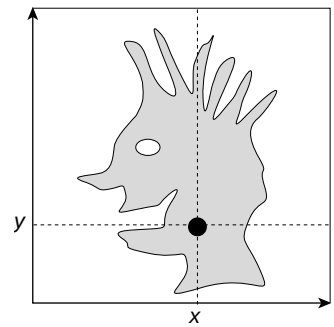

Figure 12.36
One point in the pancake-shaped object, with coordinates x and y.

The Larmor frequency of the spins is different in the two parts of the pulse sequence, because the external magnetic field is different. During the t_1 interval, the magnetic field gradient is along the x-axis, so the offset frequency during t_1 is given by

$$\Omega^0(1) = -\gamma G_x x \tag{12.8}$$

During the t_2 interval, the magnetic field gradient is along the z-axis, so the offset frequency during t_2 is given instead by

$$\Omega^0(2) = -\gamma G_y y \tag{12.9}$$

After the first $\pi/2$ pulse, the spin density operator at the point (x, y) is given as usual by

$$\hat{\rho}_{②} = \frac{1}{2}\widehat{1} - \frac{1}{2}\mathbb{B}\hat{I}_y$$

The observable (-1)-quantum coherence at this point is therefore

$$\rho_{\boxed{-}②} = \frac{1}{4\mathrm{i}}\mathbb{B}$$

During the subsequent t_1 period, this coherence precesses at the frequency $\Omega^0(1)$, so that at time point ③ the coherence amplitude is

$$\rho_{\boxed{-}③} = \frac{1}{4\mathrm{i}}\mathbb{B}\exp\{\left(\mathrm{i}\Omega^0(1) - \lambda\right)t_1\}$$

where λ is the inverse of T_2. The precession continues during the t_2 period, so that at time point ④ the coherence amplitude is

$$\rho_{\boxed{-}④} = \frac{1}{4\mathrm{i}}\mathbb{B}\exp\{\left(\mathrm{i}\Omega^0(1) - \lambda\right)t_1 + \left(\mathrm{i}\Omega^0(2) - \lambda\right)t_2\}$$

The NMR signal is proportional to the amplitude of the (−1)-quantum coherence. The component of the two-dimensional NMR signal originating from a volume element at point (x, y) is therefore

$$s(t_1, t_2; x, y) \sim \exp\{\left(\mathrm{i}\Omega^0(1) - \lambda\right) t_1 + \left(\mathrm{i}\Omega^0(2) - \lambda\right) t_2\} \tag{12.10}$$

Now suppose that a two-dimensional FT is performed, as described in Section 5.9. The two-dimensional spectrum contains a peak at the frequency coordinates $(\Omega^0(1), \Omega^0(2))$:

$$S(\Omega_1, \Omega_2; x, y) \sim \mathfrak{L}\,(\Omega_1, \Omega_2; \Omega^0(1), \lambda, \Omega^0(2), \lambda)$$

using the two-dimensional complex Lorentzian function defined in Equation 5.20.

Now from Equations 12.8 and 12.9, the frequency coordinates $\Omega^0(1)$ and $\Omega^0(2)$ are directly proportional to the spatial coordinates x and y. The position of the peak in the two-dimensional spectrum, therefore, maps directly onto the position of the spins in the spatial (x, y) plane:

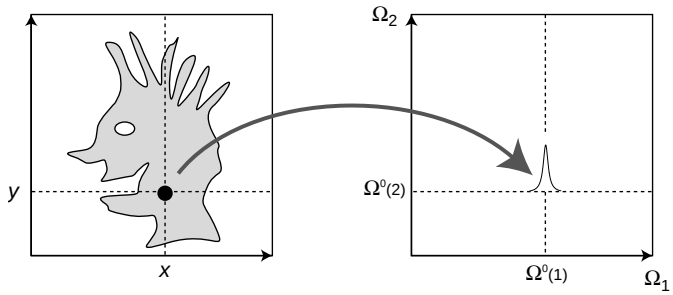

Figure 12.37
A point in the object gives a peak at the corresponding position in the two-dimensional spectrum.

A different point in the object generates a peak at a different position in the two-dimensional spectrum:

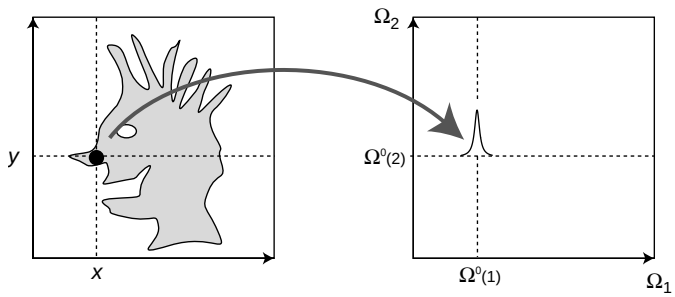

Figure 12.38
A different point in the object gives a peak at a different position in the two-dimensional spectrum.

(These sketches are for negative gradients G_x and G_y.)

In practice, all regions in the sample contribute simultaneously. The two-dimensional spectrum is a superposition of many two-dimensional peaks. The *total* amplitude at a certain point in the two-dimensional spectrum depends on how many spins are found at the corresponding point in real space, according to

$$S(\Omega_1, \Omega_2) \sim d(x_{\Omega_1}, y_{\Omega_2})$$

where $d(x, y)$ is the density of spins at point (x, y), and the coordinates x_{Ω_1} and y_{Ω_2} are given by

$$x_{\Omega_1} = -\frac{\Omega_1}{\gamma G_x} \qquad y_{\Omega_2} = -\frac{\Omega_2}{\gamma G_y}$$

by analogy to Equation 12.7.

The two-dimensional spectrum is therefore an *image* of the two-dimensional spin density:

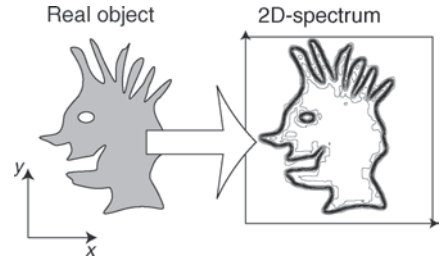

Figure 12.39
Mapping of a two-dimensional object onto a two-dimensional NMR spectrum (shown as a contour plot).

An image of a three-dimensional object may be constructed by performing a three-dimensional NMR experiment, using gradients along all three axes, followed by three-dimensional FT of the data matrix, as described in Section 5.10. Alternatively, a two-dimensional image of a slice through the object may be generated by the following pulse sequence:

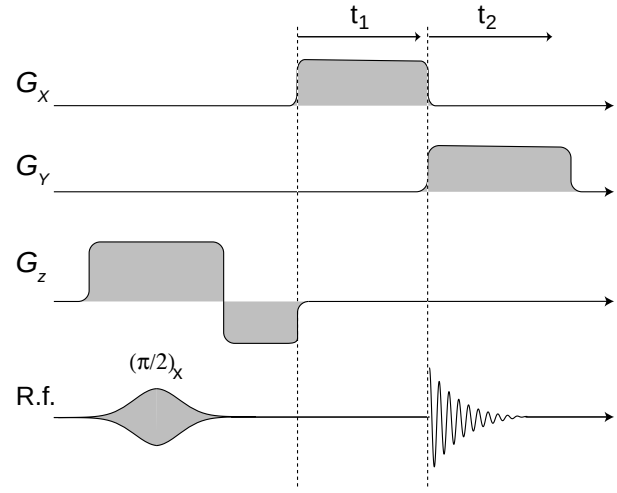

Figure 12.40
Pulse sequence for NMR imaging of a slice through a three-dimensional object, perpendicular to the z-axis.

This combines the two-dimensional pulse sequence of Figure 12.35 with the slice selection technique of Figure 12.25. The position and thickness of the slice along the z-axis is set by adjusting the r.f. pulse frequency and the amplitude of the G_z gradient.

Whereas an ordinary photograph (or an X-ray image) counts *photons*, an NMR image counts *protons*.

This discussion only scratches the surface of a very rich subject. The simple pulse sequences described above give relatively poor resolution and are susceptible to various instrumental imperfections. In practice, a whole array of more sophisticated procedures is available that gives better, faster, and more reliable performance (see *Further Reading*). Contrast is often enhanced by using pulse sequences that are sensitive to T_1 or T_2, as well as the spin density. It is also possible to produce images that contain signals only from spins in a *flowing* liquid, such as blood. One may also combine imaging with the other techniques described in this book to produce NMR spectra at certain points in the body, and hence follow the concentration of metabolites.

Three-dimensional NMR images are shown in Plate 3 and Plate 4.

An even more remarkable development is *functional NMR imaging* (fMRI), in which small differences in the brain NMR image are detected when mental processes are underway (see *Further Reading*). An example of fMRI is given in Plate 1. The mechanism of functional contrast in NMR imaging is believed to involve changes in blood flow, and the different magnetic susceptibilities of oxygenated and deoxygenated blood.

Notes

1. The effects of T_2 decay and inhomogeneous broadening are sometimes combined by using an 'effective T_2' parameter, usually denoted T_2^*, where $T_2^* \leq T_2$ (the asterisk does not indicate the complex conjugate in this case). The inhomogeneously broadened linewidth is given by $1/(\pi T_2^*)$ in units of hertz. Unlike T_2, the effective time constant T_2^* has no fundamental significance and depends on the magnetic field homogeneity. Only the inhomogeneous contribution to T_2^* is refocused by using a spin echo.

2. The spin echoes originally described by Hahn involved two $\pi/2$ pulses (see E. L. Hahn, *Phys. Rev.*, **80,** 580(1950)). However, this type of spin echo is relatively weak and difficult to use. The 'modern' type of spin echo, induced by a π pulse, was developed by Carr and Purcell (see H. Y. Carr, E. M. Purcell, *Phys. Rev.* **94,** 630(1954)). Despite this, π-pulse echoes are commonly called 'Hahn echoes'.

3. One occasionally finds a statement that the spin-locked magnetization does not decay to zero, but to a position of thermal equilibrium state along the spin-locking field, i.e. a value proportional to $\gamma B^{\mathrm{RF}}/k_B T$, where B^{RF} is the locking field and T is the temperature. This is not correct. The final state of the spin system is unrelated to thermal equilibrium, since the spin Hamiltonian is time dependent. The correct final value of the transverse magnetization is zero, assuming that the nutation frequency is large compared with the relaxation time constants.

4. The notation $T_{1\rho}$, and the term 'spin-lattice relaxation in the rotating frame' are unfortunate for the following reasons. First, exchange of energy with the lattice is *not* required for the $T_{1\rho}$ process. Second, the decay of spin-locked transverse magnetization is more closely related to T_2 than to T_1. Third, the use of a rotating reference frame is obviously irrelevant to a physical phenomenon such as the decay of magnetization. A more accurate term would be 'decay time constant for transverse magnetization in the presence of an r.f. field', with the suggested notation $T_2{}^{\mathrm{RF}}$.

5. The fields created by the gradient coils also have components in the x- and y-directions. These transverse field components are unimportant in practice, because of the dominating effect of the main magnetic field (compare Section 9.1.7).

Further Reading

- For more on spin echoes, see R. Freeman, *Spin Choreography. Basic Steps in High Resolution NMR*, Spektrum, Oxford, 1997, and J. Keeler, *Understanding NMR Spectroscopy*, Wiley, Chichester, 2005.
- For the theory of $T_{1\rho}$, see T. E. Bull, *Prog. NMR Spectrosc.* **24**, 377–410 (1992).
- NMR imaging is an enormous field. For an early review, see P. Mansfield and P. G. Morris, 'NMR imaging in biomedicine', *Adv. Magn. Reson. Suppl. 2*, (1982).
  For later material, see the many entries in D. M. Grant and R. K. Harris (eds), *Encyclopedia of Nuclear Magnetic Resonance*, Wiley, 1996.
- For the applications of imaging to small objects, see P. T. Callaghan, *Principles of Nuclear Magnetic Resonance Microscopy*, Clarendon Press, Oxford, 1991.
- For a theoretical treatment of selected imaging methodologies, see the appropriate chapter of R. R. Ernst, G. Bodenhausen, A. Wokaun, *Principles of Nuclear Magnetic Resonance in One and Two Dimensions*, Clarendon Press, Oxford, 1987.
- For the mechanism and examples of functional NMR imaging, see S. A. Huettel, A. W. Song and G. McCarthy, *Functional Magnetic Resonance Imaging*, Sinauer, Sunderland, USA, 2004.

Exercises

12.1 The amplitudes of two peaks in an inversion-recovery experiment depend on the interval τ as shown in the following table:

τ/s	Amplitude of peak 1	Amplitude of peak 2
0	−0.96	−0.96
1	−0.18	−0.67
2	0.30	−0.37
3	0.60	−0.11
4	0.69	0.10
5	0.84	0.27
6	0.88	0.41
7	0.92	0.55
8	1.00	0.61
9	1.00	0.72
10	0.98	0.78

Estimate the value of T_1 for each peak.

12.2 This exercise illustrates the measurement of *flow* by NMR. An NMR probe is equipped with special field coils, which slightly enhance the magnetic field along the z-axis for spatial positions $x < 0$, and which slightly decrease the magnetic field along the z-axis for spatial positions $x > 0$. A pipe containing a flowing liquid is mounted in the probe, with the liquid flowing along the x-axis:

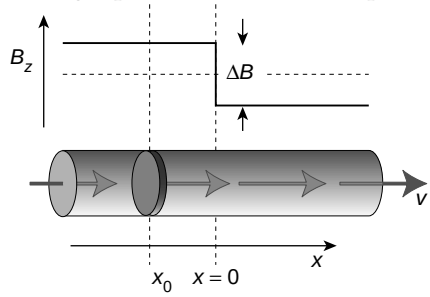

The flow velocity is $v\,\mathrm{m\,s^{-1}}$. We follow the proton NMR signals from a plug of liquid, positioned initially at x_0. One may imagine that only the plug of liquid contains protons, the rest of the fluid being non-protonated. Suppose that the difference in magnetic field for positive and negative values of x is equal to ΔB.

A spin echo sequence $(\pi/2)_x - \tau/2 - \pi_y - \tau/2 -$ (acquire signal) is applied to the flowing sample. The plug of liquid has position x_0 at the beginning of the pulse sequence (the diagram shows a negative value of x_0).

Calculate the *phase* of the NMR signals at the end of the pulse sequence in the following cases:

(i) x_0 is positive, so that the plug of liquid does not cross the line $x = 0$ during the pulse sequence.
(ii) x_0 satisfies $-v\tau/2 < x_0 < 0$, so that the plug crosses the line $x = 0$ before the π pulse arrives.
(iii) x_0 satisfies $-v\tau < x_0 < -v\tau/2$, so that the plug crosses the line $x = 0$ after the π pulse arrives.
(iv) x_0 satisfies $x_0 < -v\tau$, so that the plug of liquid does not cross the line $x = 0$ before signal acquisition.

13 Quadrupolar Nuclei

Nuclei with spin $I > 1/2$ have an electric quadrupole moment. Quadrupolar nuclear isotopes are widely distributed throughout the periodic table, and include many important elements that lack spin-1/2 isotopes, such as the alkali metals. The NMR of quadrupolar nuclei offers many theoretical and practical challenges, due to the strong interactions between the nuclear electric quadrupole moments and the local electric field gradients that are present in many substances. This chapter only scratches the surface of a very rich subject.

13.1 Spin $I = 1$

The only natural spin $I = 1$ nuclei are ^{2}H, ^{14}N and ^{6}Li (see Plate B).

Although nitrogen is a very important element, and ^{14}N is 99.6% abundant, NMR experiments on ^{14}N nuclei are seldom performed. This is because ^{14}N often experiences considerable electric field gradients, giving rise to coupling constants C_Q of many megahertz. The large quadrupolar interactions and relatively low gyromagnetic ratio makes ^{14}N a difficult NMR nucleus in most circumstances.[1]

Deuterium (^{2}H), in contrast, has a very low natural abundance (0.012%), but a low electric quadrupolar moment. Since it is often relatively easy and inexpensive to enrich materials in ^{2}H, and the low value of Q leads to rather small nuclear quadrupolar interactions, deuterium NMR is very popular, especially in the NMR of solids and liquid crystals.

The quadrupolar coupling constant C_Q for ^{2}H depends strongly on the local electronic environment and on internal molecular motion. For ^{2}H nuclei in CD groups, attached to rigid parts of the molecule, the quadrupolar coupling constant is typically around $C_Q = 130\,\text{kHz}$. The quadrupole coupling can be considerably reduced in the presence of internal molecular motions. For example, ^{2}H nuclei in rapidly rotating ND_3^+ groups have a typical quadrupolar coupling constant of around 50 kHz. The quadrupole coupling tensor may become strongly biaxial ($\eta_Q \neq 0$) if the local molecular motion lacks symmetry. The sensitivity of ^{2}H spectra to the symmetry and time-scale of molecular motion is one of the informative and useful features of solid-state ^{2}H NMR.

NMR experiments on ^{6}Li are uncommon, since the spin-3/2 isotope ^{7}Li is more abundant and has a larger gyromagnetic ratio.

13.1.1 Spin-1 states

A spin-1 nucleus I has three eigenstates of angular momentum along the z-axis, denoted by the kets $|1, M\rangle$ where the quantum number M is equal to $+1$, 0, or -1. These Zeeman eigenstates have the properties given in Section 7.9:

$$\begin{aligned} \hat{I}_z|1, M\rangle &= M|1, M\rangle \\ \hat{I}^2|1, M\rangle &= I(I+1)|1, M\rangle = 2|1, M\rangle \end{aligned} \tag{13.1}$$

Spin Dynamics: Basics of Nuclear Magnetic Resonance, Second Edition Malcolm H. Levitt

where $\hat{I}^2 = \hat{I}_x^2 + \hat{I}_y^2 + \hat{I}_z^2$.

In general, the quantum state of a spin-1 nucleus is a *superposition* of all three Zeeman eigenstates, as follows:

$$|\psi\rangle = c_1|1,+1\rangle + c_0|1,0\rangle + c_{-1}|1,-1\rangle$$

where the coefficients $\{c_1, c_0, c_{-1}\}$ are complex numbers.[2] The same state may be written in column vector form:

$$|\psi\rangle = \begin{pmatrix} c_1 \\ c_0 \\ c_{-1} \end{pmatrix}$$

The 'bra' state is the adjoint of the 'ket' state:

$$\langle\psi| = (\,{c_1}^*, \quad {c_0}^*, \quad {c_{-1}}^*\,)$$

The normalization condition is as follows:

$$\langle\psi|\psi\rangle = |c_1|^2 + |c_0|^2 + |c_{-1}|^2 = 1$$

13.1.2 Spin-1 energy levels

In the presence of a strong external magnetic field B^0 along the z-axis, a spin-1 nucleus experiences a Zeeman Hamiltonian of the usual form:

$$\hat{\mathcal{H}}^0 = \omega^0 \hat{I}_z \tag{13.2}$$

where the nuclear Larmor frequency is given by

$$\omega^0 = -\gamma B^0(1+\delta)$$

and δ is the chemical shift. The states $|1, M\rangle$ are energy eigenstates in the presence of the field B^0:

$$\hat{\mathcal{H}}^0|1, M\rangle = M\omega^0|1, M\rangle$$

The energy-level diagram for a spin-1 nucleus I, therefore, has three energy levels, spaced evenly by ω^0 in natural units, if the quadrupole interaction is ignored:

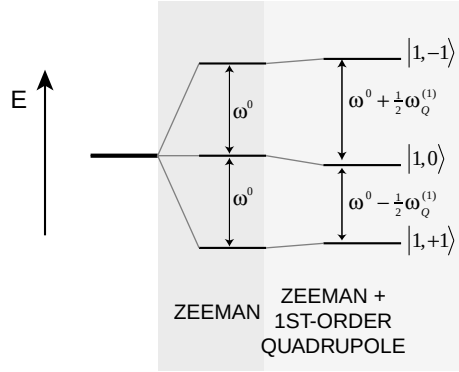

Figure 13.1
Energy levels of a spin-1 nucleus.

If the nuclear environment is anisotropic after motional averaging, the spin Hamiltonian is equal to the sum of the Zeeman and quadrupole coupling terms:

$$\widehat{\mathcal{H}} = \widehat{\mathcal{H}}^0 + \widehat{\mathcal{H}}_{\mathrm{Q}}^{(1)} + \widehat{\mathcal{H}}_{\mathrm{Q}}^{(2)} + \ldots \tag{13.3}$$

where the first-order quadrupolar Hamiltonian is given by

$$\begin{aligned}\widehat{\mathcal{H}}_{\mathrm{Q}}^{(1)} &= \omega_{\mathrm{Q}}^{(1)} \times \frac{1}{6}\left(3\hat{I}_z^2 - I(I+1)\widehat{1}\right) \\ &= \omega_{\mathrm{Q}}^{(1)} \times \frac{1}{6}\left(3\hat{I}_z^2 - 2 \times \widehat{1}\right) \qquad \text{(for spin } I = 1\text{)}\end{aligned} \tag{13.4}$$

and the first-order quadrupolar coupling $\omega_{\mathrm{Q}}^{(1)}$ is given in the general case by Equation 9.23. The first-order quadrupolar coupling $\omega_{\mathrm{Q}}^{(1)}$ depends on the nuclear quadrupole moment, the electronic environment of the nucleus, the phase of matter, and the molecular orientation, as described in Section 9.2.

The series in Equation 13.3 may be truncated after the first term, if the quadrupolar coupling constant $C_{\mathrm{Q}} = e^2qQ/h$ is much smaller in magnitude than the Larmor frequency ω^0. This is usually a good approximation for ^{2}H.

In solids, the first-order quadrupolar coupling is given in terms of the quadrupolar coupling constant C_{Q} by

$$\begin{aligned}\omega_{\mathrm{Q}}^{(1)}(\theta_{\mathrm{Q}}) &= \frac{3\pi C_{\mathrm{Q}}}{2I(2I-1)} \times \left(3\cos^2\theta_{\mathrm{Q}} - 1\right) \\ &= 3\pi C_{\mathrm{Q}} \times \frac{1}{2}\left(3\cos^2\theta_{\mathrm{Q}} - 1\right) \qquad \text{(for spin } I = 1\text{)}\end{aligned} \tag{13.5}$$

assuming a uniaxial electric field gradient tensor ($\eta_{\mathrm{Q}} = 0$). Here, θ_{Q} is the angle between the major principal axis of the electric field gradient tensor and the magnetic field.

The Zeeman eigenstates are eigenstates of the first-order quadrupolar Hamiltonian:

$$\begin{aligned}\widehat{\mathcal{H}}_{\mathrm{Q}}^{(1)}|1,+1\rangle &= +\frac{1}{6}\omega_{\mathrm{Q}}^{(1)}|1,+1\rangle \\ \widehat{\mathcal{H}}_{\mathrm{Q}}^{(1)}|1,0\rangle &= -\frac{1}{3}\omega_{\mathrm{Q}}^{(1)}|1,0\rangle \\ \widehat{\mathcal{H}}_{\mathrm{Q}}^{(1)}|1,-1\rangle &= +\frac{1}{6}\omega_{\mathrm{Q}}^{(1)}|1,-1\rangle\end{aligned}$$

A positive quadrupolar coupling $\omega_{\mathrm{Q}}^{(1)}$ shifts the states $|1,\pm1\rangle$ up in energy, whereas the central state $|1,0\rangle$ shifts down in energy by twice as much. All shifts are in the opposite direction if $\omega_{\mathrm{Q}}^{(1)}$ is negative.

13.1.3 Spin-1 density matrix

Suppose now that the sample contains an ensemble of isolated spins-1. The *density operator* technique introduced in Chapter 11 may be used to describe the quantum state of the entire spin-1 ensemble. The density operator contains enough information to calculate the expectation values of all spin observables.

The density operator of the spin-1 ensemble may be written as follows:

$$\hat{\rho} = \overline{|\psi\rangle\langle\psi|}$$

where the overbar denotes an ensemble average. For a spin-1 ensemble, the matrix representation of the density operator (the *density matrix*) is a 3×3 complex matrix of the following form:

$$\hat{\rho} = \begin{pmatrix} \overline{c_1{}^* c_1} & \overline{c_1{}^* c_0} & \overline{c_1{}^* c_{-1}} \\ \overline{c_0{}^* c_1} & \overline{c_0{}^* c_0} & \overline{c_0{}^* c_{-1}} \\ \overline{c_{-1}{}^* c_1} & \overline{c_{-1}{}^* c_0} & \overline{c_{-1}{}^* c_{-1}} \end{pmatrix}$$

Each element of the density matrix is given by a product of superposition coefficients for a pair of spin states, averaged over the ensemble.

Populations appear on the diagonal of the density operator, and are denoted in this book by the following symbols:

$$\rho_{|+1\rangle} = \overline{c_1{}^* c_1}$$
$$\rho_{|0\rangle} = \overline{c_0{}^* c_0}$$
$$\rho_{|-1\rangle} = \overline{c_{-1}{}^* c_{-1}}$$

The populations are often represented by 'little balls' sitting on the energy levels:

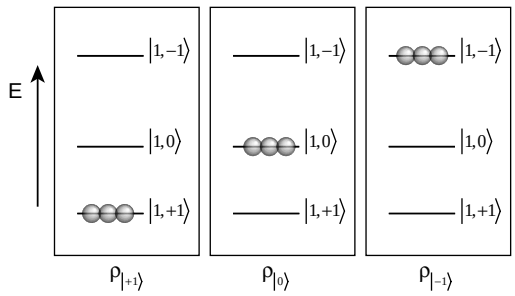

Figure 13.2
State populations for an ensemble of spins-1.

The three populations $\rho_{|+1\rangle}$, $\rho_{|0\rangle}$ and $\rho_{|-1\rangle}$ of the spin-1 ensemble are analogous to the two populations $\rho_{\boxed{\alpha}}$ and $\rho_{\boxed{\beta}}$ of the spin-1/2 ensemble. The three spin-1 populations sum to unity:

$$\rho_{|+1\rangle} + \rho_{|0\rangle} + \rho_{|-1\rangle} = 1$$

The off-diagonal density matrix elements are called *coherences*. The spin-1 ensemble supports six coherences, instead of two for the spin-1/2 ensemble. The coherences are represented by arrows linking a pair of energy levels:

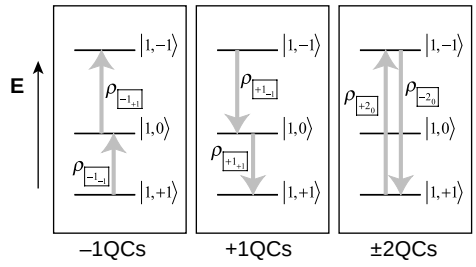

Figure 13.3
Coherences for an ensemble of spins-1.

In this book, the coherences of quadrupolar nuclei are denoted as follows:

$$\langle I, M_r|\hat{\rho}|I, M_s\rangle = \rho_{\boxed{p_{rs\,qrs}}} \tag{13.6}$$

The subscript p_{rs} denotes the *coherence order*, which is equal to the *difference* in Zeeman quantum numbers M for the connected states (see Section 11.2.4). The sub-subscript q_{rs} is called the *satellite order*, and is equal to the difference in the *squares* of the Zeeman quantum numbers M for the connected states:[3]

$$\begin{aligned} p_{rs} &= M_r - M_s \\ q_{rs} &= M_r^2 - M_s^2 \end{aligned} \tag{13.7}$$

The spin-1 ensemble supports two (-1)-quantum coherences, which connect states differing in angular momentum by -1 unit:

$$\begin{aligned} \rho_{\boxed{-1_{-1}}} &= \overline{c_0{}^* c_1} \\ \rho_{\boxed{-1_{+1}}} &= \overline{c_{-1}{}^* c_0} \end{aligned} \tag{13.8}$$

These are analogous to the (-1)-quantum coherence $\rho_{\boxed{-}}$ of the spin-1/2 ensemble.

Similarly, there are two $(+1)$-quantum coherences, which connect states differing in angular momentum by $+1$ unit:

$$\begin{aligned} \rho_{\boxed{+1_{+1}}} &= \overline{c_1{}^* c_0} \\ \rho_{\boxed{+1_{-1}}} &= \overline{c_0{}^* c_{-1}} \end{aligned} \tag{13.9}$$

These are analogous to the $(+1)$-quantum coherence $\rho_{\boxed{+}}$ of the spin-1/2 ensemble.

The spin-1 density matrix may also contain *double-quantum coherences*, which have quantum order $p = \pm 2$ and satellite order $q = 0$:

$$\begin{aligned} \rho_{\boxed{-2_0}} &= \overline{c_{-1}{}^* c_1} \\ \rho_{\boxed{+2_0}} &= \overline{c_1{}^* c_{-1}} \end{aligned} \tag{13.10}$$

These double-quantum coherences have no direct analogy in the ensemble of isolated spins-1/2.

The density matrix may be written, using the notation above:

$$\hat{\rho} = \begin{pmatrix} \rho_{|+1\rangle} & \rho_{\boxed{+1_{+1}}} & \rho_{\boxed{+2_0}} \\ \rho_{\boxed{-1_{-1}}} & \rho_{|0\rangle} & \rho_{\boxed{+1_{-1}}} \\ \rho_{\boxed{-2_0}} & \rho_{\boxed{-1_{+1}}} & \rho_{|-1\rangle} \end{pmatrix}$$

13.1.4 Coherence evolution

Suppose that a particular spin-1 density operator exists at a time point t_a. We wish to predict the spin density operator at a later time $t_b = t_a + \tau$, where the two time points are separated by an interval τ of free evolution, in the absence of applied r.f. fields:

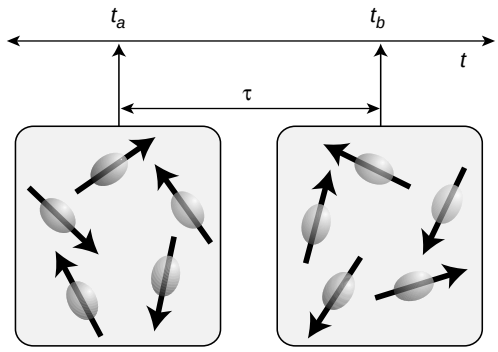

Figure 13.4
Free evolution of a spin-1 ensemble over an interval τ.

If spin–lattice relaxation is ignored, and no r.f. field is applied, then the populations do not change:

$$\rho_{|+1\rangle}(t_\mathrm{b}) \cong \rho_{|+1\rangle}(t_\mathrm{a})$$
$$\rho_{|0\rangle}(t_\mathrm{b}) \cong \rho_{|0\rangle}(t_\mathrm{a})$$
$$\rho_{|-1\rangle}(t_\mathrm{b}) \cong \rho_{|-1\rangle}(t_\mathrm{a})$$

The coherences, on the other hand, oscillate at the energy level differences of the connected states, as described in Section 11.7. The rotating-frame frequencies of all six coherences in the spin-1 ensemble are as follows:

$$\begin{aligned}
\Omega_{\boxed{-1_{-1}}} &= \Omega^0 + \frac{1}{2}\omega_\mathrm{Q}^{(1)} \\
\Omega_{\boxed{-1_{+1}}} &= \Omega^0 - \frac{1}{2}\omega_\mathrm{Q}^{(1)} \\
\Omega_{\boxed{+1_{+1}}} &= -\Omega^0 - \frac{1}{2}\omega_\mathrm{Q}^{(1)} \\
\Omega_{\boxed{+1_{-1}}} &= -\Omega^0 + \frac{1}{2}\omega_\mathrm{Q}^{(1)} \\
\Omega_{\boxed{-2_0}} &= 2\Omega^0 \\
\Omega_{\boxed{+2_0}} &= -2\Omega^0
\end{aligned} \tag{13.11}$$

where the chemical shift offset frequency is given by

$$\Omega^0 = -\gamma B^0(\delta - \delta_\mathrm{ref}) \tag{13.12}$$

as in the spin-1/2 case. Here, δ is the chemical shift and δ_ref is the chemical shift corresponding to the spectrometer reference frequency.

For example, the (-1)-quantum coherences evolve as follows:

$$\rho_{\boxed{-1_{-1}}}(t_\mathrm{b}) = \rho_{\boxed{-1_{-1}}}(t_\mathrm{a})\exp\{(\mathrm{i}\Omega_{\boxed{-1_{-1}}} - \lambda)\tau\}$$
$$\rho_{\boxed{-1_{+1}}}(t_\mathrm{b}) = \rho_{\boxed{-1_{+1}}}(t_\mathrm{a})\exp\{(\mathrm{i}\Omega_{\boxed{-1_{+1}}} - \lambda)\tau\}$$

where the decay constant $\lambda = T_2{}^{-1}$ takes into account the homogeneous decay. From Equation 13.11, the evolution frequencies of the two (-1)-quantum coherences differ by the first-order quadrupolar interaction $\omega_{\mathrm{Q}}^{(1)}$.

Note that the double-quantum frequencies $\rho_{\boxed{-2_0}}$ and $\rho_{\boxed{+2_0}}$ are independent of the first-order quadrupolar interaction. This is because the first-order quadrupolar interaction shifts the energies of the $|1, \pm 1\rangle$ states by the same amount in the same direction (see Figure 13.1).

13.1.5 Observable coherences and NMR spectrum

As described in Appendix A.5, quadrature detection provides a complex NMR signal given by

$$s(t) \sim 2\mathrm{i}\langle \hat{I}^+ \rangle \exp\{-\mathrm{i}\phi_{\mathrm{rec}}\} \tag{13.13}$$

where ϕ_{rec} is the receiver phase. The spin-1 matrix representation of the shift operator $\hat{I}^+$ is given in Section 7.9, as follows:

$$\hat{I}^+ = \begin{pmatrix} 0 & \sqrt{2} & 0 \\ 0 & 0 & \sqrt{2} \\ 0 & 0 & 0 \end{pmatrix}$$

The NMR signal may be evaluated in terms of the coherence amplitudes by using $\langle \hat{I}^+ \rangle = \mathrm{Tr}\{\hat{I}^+ \hat{\rho}\}$. This gives the following expression:

$$s(t) \sim 2\mathrm{i}\sqrt{2} \exp\{-\mathrm{i}\phi_{\mathrm{rec}}\} \left(\rho_{\boxed{-1_{-1}}}(t) + \rho_{\boxed{-1_{+1}}}(t) \right) \qquad \text{(for spin } I = 1\text{)} \tag{13.14}$$

From this we see that the two (-1)-quantum coherences contribute equally to the spin-1 NMR signal, providing that they have the same amplitude.

The populations, the $(+1)$-quantum coherences, and the (± 2)-quantum coherences do not give rise to detectable NMR signals.[4] This does not imply, of course, that these density matrix elements are unimportant. They may give rise to NMR signals later on, if they are transformed into detectable (-1)-quantum coherences by subsequent pulses.

If the NMR signal from a spin-1 ensemble is collected as a function of time variable t, and Fourier transformed, the result is an NMR spectrum containing two Lorentzian peaks:

$$\begin{aligned} S(\Omega) &= a_{\boxed{-1_{-1}}} \mathcal{L}(\Omega; \Omega_{\boxed{-1_{-1}}}, \lambda) + a_{\boxed{-1_{+1}}} \mathcal{L}(\Omega; \Omega_{\boxed{-1_{+1}}}, \lambda) \\ &= a_{\boxed{-1_{-1}}} \mathcal{L}(\Omega; \Omega^0 + \frac{1}{2}\omega_{\mathrm{Q}}^{(1)}, \lambda) + a_{\boxed{-1_{+1}}} \mathcal{L}(\Omega; \Omega^0 - \frac{1}{2}\omega_{\mathrm{Q}}^{(1)}, \lambda) \end{aligned} \tag{13.15}$$

where the Lorentzian functions are defined in Equation 5.12. The peak amplitudes are proportional to the (-1)-quantum coherences existing at the beginning of the detection interval:

$$\begin{aligned} a_{\boxed{-1_{-1}}} &= 2\mathrm{i}\sqrt{2} \exp\{-\mathrm{i}\phi_{\mathrm{rec}}\} \rho_{\boxed{-1_{-1}}}(0) \\ a_{\boxed{-1_{+1}}} &= 2\mathrm{i}\sqrt{2} \exp\{-\mathrm{i}\phi_{\mathrm{rec}}\} \rho_{\boxed{-1_{+1}}}(0) \end{aligned} \tag{13.16}$$

The NMR spectrum generated by a spin-1 ensemble is therefore a *doublet* with a splitting of $\omega_{\mathrm{Q}}^{(1)}$, with each peak corresponding to one of the (-1)-quantum coherences. If the amplitudes $a_{\boxed{-1_{\pm 1}}}$ are real numbers, then the two peaks are in the absorption phase, as illustrated below:

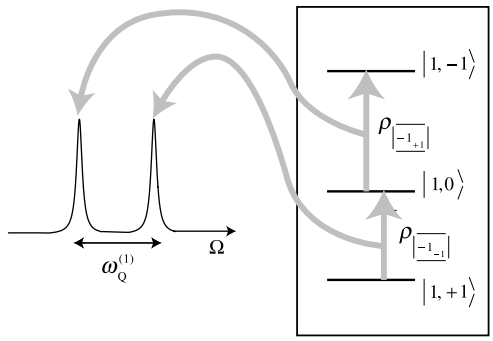

Figure 13.5
Each (−1)-quantum coherence in a spin-1 ensemble gives rise to a spectral peak.

13.1.6 Thermal equilibrium

In thermal equilibrium, the density matrix contains populations given by the Boltzmann distribution, and no coherences. If the temperature is high compared with the Zeeman splitting and the Zeeman splitting is much larger than the quadrupolar interaction, then the thermal equilibrium populations may be calculated according to the technique in Section 11.3. This leads to the following equilibrium spin-1 populations:

$$\rho_{|+1\rangle} \cong \frac{1}{3}(1+\mathbb{B}) \qquad \rho_{|0\rangle} \cong \frac{1}{3} \qquad \rho_{|-1\rangle} \cong \frac{1}{3}(1-\mathbb{B})$$

where the Boltzmann factor $\mathbb{B}$ is given in Equation 11.16. Since $\mathbb{B}$ is very small, this represents a tiny excess of population in the lower $|1,+1\rangle$ state and a tiny deficit of population in the upper $|1,-1\rangle$ state:

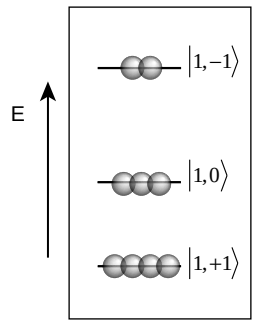

Figure 13.6
Thermal equilibrium state for an ensemble of spins-1 (the population differences are greatly exaggerated).

The thermal equilibrium spin density operator is therefore given by

$$\hat{\rho}^{\text{eq}} = \frac{1}{3}\hat{1} + \frac{1}{3}\mathbb{B}\hat{I}_z \tag{13.17}$$

13.1.7 Strong radio-frequency pulse

Suppose that a strong r.f. pulse of phase ϕ_p and duration τ_p is applied to an ensemble of spins-1. We wish to calculate the spin density operator at time point ② after the pulse, if it is known at time point ① before the pulse:

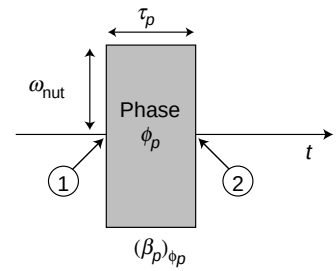

Figure 13.7
R.f. pulse applied to a spin-1 ensemble.

The rotating-frame spin Hamiltonian during the pulse is given by

$$\widehat{\mathcal{H}}_{\mathrm{p}} = \widehat{\mathcal{H}}_{\mathrm{int}} + \omega_{\mathrm{nut}}(\hat{I}_x \cos\phi_{\mathrm{p}} + \hat{I}_y \sin\phi_{\mathrm{p}}) \tag{13.18}$$

where the nutation frequency ω_{nut} is proportional to the strength of the resonant r.f. field component, as in Equation 10.25:

$$\omega_{\mathrm{nut}} = |\tfrac{1}{2}\gamma B^{\mathrm{RF}} \sin\theta_{\mathrm{RF}}| \tag{13.19}$$

$\widehat{\mathcal{H}}_{\mathrm{int}}$ is the internal spin Hamiltonian in the rotating reference frame:

$$\widehat{\mathcal{H}}_{\mathrm{int}} = \Omega^0 \hat{I}_z + \widehat{\mathcal{H}}_{\mathrm{Q}}$$

It can be difficult to treat the evolution of the spin system under the Hamiltonian in Equation 13.18, since the internal and external parts of the Hamiltonian may have similar magnitudes and do not commute with each other. However, the problem becomes much simpler to handle in the *strong pulse limit*. This requires that the interaction with the r.f. field is much stronger than the chemical shifts and the first-order quadrupolar interaction:

$$|\omega_{\mathrm{nut}}| >> |\Omega^0|, |\omega_{\mathrm{Q}}^{(1)}| \tag{13.20}$$

The 'strong pulse' condition in Equation 13.20 requires either a small quadrupolar interaction, or a very strong r.f. field.

The strong pulse condition is usually difficult to satisfy for ^{14}N, due to the very large quadrupole interaction. The rest of this section, therefore, mainly concerns ^{2}H NMR, where the strong pulse condition is often satisfied to a good approximation.

In the strong pulse limit, the internal spin Hamiltonian may be ignored during the r.f. pulse, so the rotating-frame spin Hamiltonian during the pulse is given by

$$\widehat{\mathcal{H}}_{\mathrm{p}} \cong \omega_{\mathrm{nut}}(\hat{I}_x \cos\phi_{\mathrm{p}} + \hat{I}_y \sin\phi_{\mathrm{p}})$$

The nuclear spin states, therefore, are transformed by the pulse as follows:

$$|\psi\rangle_{②} = \widehat{R}_{\phi_{\mathrm{p}}}(\beta_{\mathrm{p}})|\psi\rangle_{①}$$

where $|\psi\rangle_{①}$ is the spin state before the pulse, $|\psi\rangle_{②}$ is the spin state after the pulse, and the *flip angle* is given by

$$\beta_{\mathrm{p}} = \omega_{\mathrm{nut}}\tau_{\mathrm{p}} \tag{13.21}$$

where τ_{p} is the pulse duration, and $\widehat{R}_{\phi_{\mathrm{p}}}(\beta_{\mathrm{p}})$ is a rotation operator, as described in Section 10.8.

The spin density operator, which describes the state of the entire spin-1 ensemble, is transformed according to the sandwich equation (see Section 11.6).

$$\hat{\rho}_{②} = \widehat{R}_{\phi_p}(\beta_p)\hat{\rho}_{①}\widehat{R}_{\phi_p}(\beta_p)^{\dagger}$$

Here, $\hat{\rho}_{①}$ is the density operator before the pulse and $\hat{\rho}_{②}$ is the density operator after the pulse. The action of a sufficiently strong r.f. pulse on a spin-1 ensemble has exactly the same mathematical form as for spins-1/2.

13.1.8 Excitation of coherence

We can now calculate what happens if a pulse with flip angle $\beta_p = \pi/2$ and phase $\phi_p = 0$ is applied to a spin-1 ensemble in thermal equilibrium. From Equation 13.17, the density operator after the pulse is given by

$$\hat{\rho}_{②} = \frac{1}{3}\widehat{1} + \frac{1}{3}\mathbb{B}\widehat{R}_x(\pi/2)\hat{I}_z\widehat{R}_x(\pi/2)^{\dagger} = \frac{1}{3}\widehat{1} - \frac{1}{3}\mathbb{B}\hat{I}_y$$

The operator matrix representations in Section 7.9 may be used to write this in the following form:

$$\hat{\rho}_{②} = \frac{1}{3}\begin{pmatrix} 1 & \mathrm{i}\frac{1}{\sqrt{2}}\mathbb{B} & 0 \\ -\mathrm{i}\frac{1}{\sqrt{2}}\mathbb{B} & 1 & \mathrm{i}\frac{1}{\sqrt{2}}\mathbb{B} \\ 0 & -\mathrm{i}\frac{1}{\sqrt{2}}\mathbb{B} & 1 \end{pmatrix} \tag{13.22}$$

This shows that the $\pi/2$ pulse transforms the thermal population difference between the Zeeman states into (± 1)-quantum coherences:

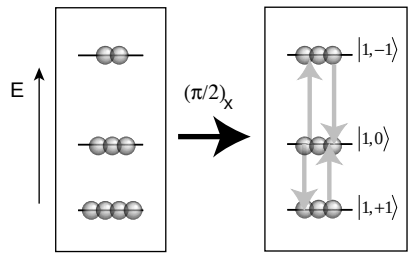

Figure 13.8
Excitation of (± 1)-quantum coherences in a spin-1 ensemble by a $\pi/2$ pulse applied to a thermal equilibrium state.

Spins-1 behave in much the same way as spins-1/2. The main difference is that *two* pairs of (± 1)-quantum coherences are excited by the pulse, instead of one in the spin-1/2 case. The amplitudes of the two (-1)-quantum coherences at the end of the pulse are given by

$$\rho_{\boxed{-1_{-1}}}② = \rho_{\boxed{-1_{+1}}}② = -\mathrm{i}\frac{1}{3\sqrt{2}}\mathbb{B} \tag{13.23}$$

Note that only (± 1)-quantum coherences are excited by the strong pulse applied to a thermal equilibrium spin-1 ensemble. Double-quantum coherences are not excited:

$$\rho_{\boxed{-2_0}}② = \rho_{\boxed{+2_0}}② = 0$$

13.1.9 NMR spectrum

Suppose that the NMR signal is acquired immediately after the pulse, using receiver phase $\phi_{rec} = 0$.

FT of the NMR signal provides the NMR spectrum, which consists of two Lorentzian peaks, at frequencies $\Omega^0 \pm \frac{1}{2}\omega_Q^{(1)}$, as described in Equation 13.15. The amplitudes of the peaks may be calculated by combining Equations 13.16 and 13.23, in the case $\phi_{rec} = 0$:

$$a_{\boxed{-1_{-1}}} = a_{\boxed{-1_{+1}}} = 2i\sqrt{2} \times \{-i\frac{1}{3\sqrt{2}}\mathbb{B}\} = \frac{2}{3}\mathbb{B}$$

Since the amplitudes are real, the real part of the NMR spectrum consists of two absorption-mode Lorentzian peaks, with equal amplitudes (see Section 11.11):

$$S(\Omega) = \frac{2}{3}\mathbb{B}\left(\mathcal{A}(\Omega; \Omega^0 + \frac{1}{2}\omega_Q^{(1)}, \lambda) + \mathcal{A}(\Omega; \Omega^0 - \frac{1}{2}\omega_Q^{(1)}, \lambda)\right)$$

The form of the NMR spectrum depends strongly on the phase of matter, since this determines the size of the motionally averaged first-order quadrupolar coupling $\omega_Q^{(1)}$:

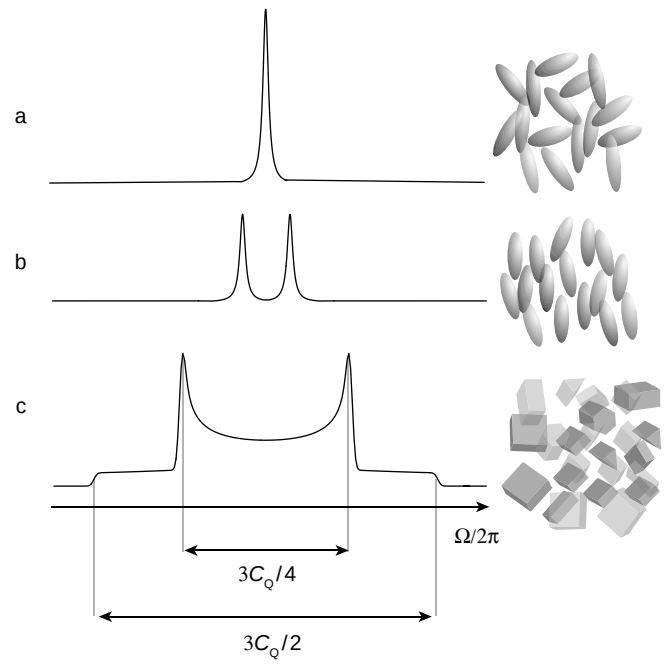

Figure 13.9
Typical appearance of spin-1 spectra for: (a) an isotropic liquid; (b) a nematic liquid crystal oriented along the magnetic field; (c) a solid powder.

Isotropic liquids. The first-order quadrupole coupling $\omega_Q^{(1)}$ vanishes in isotropic liquids, so the two peaks coincide. There is no quadrupolar splitting for spins-1 in isotropic liquids (see Figure 13.9a).[5]

Liquid crystals. A quadrupolar splitting $\omega_Q^{(1)}$ is observed in anisotropic liquids (see Figure 13.9b). The quadrupolar splitting is proportional to the nuclear quadrupole moment, and the motional average of the electric field gradient at the site of the nucleus (see Equation 9.23). The appearance of a ^{2}H quadrupolar splitting is a clear signature of a liquid crystal phase.[6]

Solid powders. In solids, the quadrupolar splitting $\omega_Q^{(1)}$ depends on the orientation of the electric field gradient tensor with respect to the external magnetic field (see Equation 13.5). In a powder, the molecules take a variety of orientations with respect to the magnetic field. This leads to a distribution of first-order splittings $\omega_Q^{(1)}$, and hence a broad spectrum with a characteristic shape. In the common case of a uniaxial electric field gradient tensor ($\eta_Q = 0$), the spectrum has a characteristic symmetric shape, called a *Pake doublet*[7] (see Figure 13.9c).

For a uniaxial electric field gradient tensor, the splitting between the two outermost shoulders of the spin-1 Pake doublet is equal to $3C_Q/2$, in units of hertz, where the quadrupole coupling constant is $C_Q = e^2qQ/h$. The splitting between the strong inner peaks is $3C_Q/4$, in units of hertz.

The strong inner peaks of the Pake doublet are generated by molecules for which the unique principal axis of the electric field gradient tensor is *perpendicular* to the magnetic field. The weaker outer shoulders of the Pake doublet correspond to molecules for which the unique principal axis of the electric field gradient tensor is *parallel* to the magnetic field:

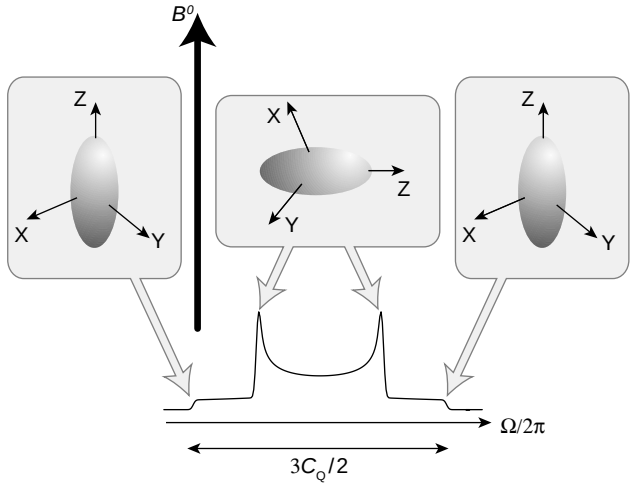

Figure 13.10
The main features of the spin-1 Pake pattern, and the corresponding orientations of the electric field gradient tensor.

The shoulders are weaker than the main peaks because it is much more likely that the unique electric field gradient principal axis is almost perpendicular to the field, rather than almost parallel to it.[8]

The symmetrical Pake doublet[9] is actually a superposition of two asymmetric spectral components, each generated by a different (−1)-quantum coherence. The underlying spectral components are made clearer in the following diagram:

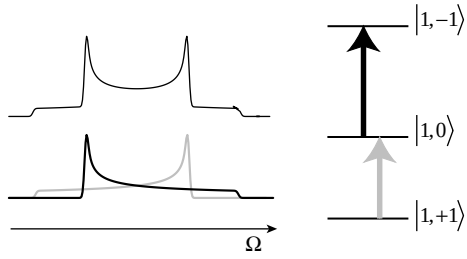

Figure 13.11
A Pake doublet has two components, one from each of the (−1)-quantum coherences.

The lineshape generated by each coherence has the same form as the powder pattern for a uniaxial CSA tensor (see Section 9.1).

A biaxial electric field gradient tensor ($\eta_Q \neq 0$) can arise if the local molecular motion does not have a high degree of symmetry. In that case the spectral lineshapes do not have the Pake form.

13.1.10 Quadrupolar echo

For rigid sites in deuterated organic solids, the full width of the ^{2}H spectrum is over 200 kHz. Such a broad spectrum corresponds to an FID with components that decay rapidly to almost zero within around 5 μs of the end of the pulse.[10]

In practice, the capture of a rapidly decaying NMR signal is exceedingly difficult, since the weak NMR signal coincides with the release of accumulated electrical energy from the tuned circuit in the probe at the end of the pulse. Electrical interference makes it essentially impossible to detect the weak NMR signal until around 5 μs after a pulse has finished, which is too late to detect most of the powder ^{2}H NMR signal.

This problem may be avoided by generating a spin echo, in order to displace the NMR signal to a region in time that is well separated from the end of the pulse. In the case of a spin-1 ensemble, a suitable spin echo is generated by a sequence of two strong $\pi/2$ pulses, with a relative phase shift of $\pi/2$:

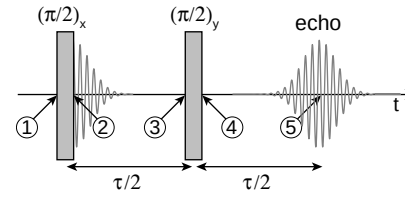

Figure 13.12
Spin-1 quadrupolar echo pulse sequence.

The interval between the two $\pi/2$ pulses is denoted $\tau/2$. The echo forms at a time $\tau/2$ after the end of the second pulse.

This type of spin echo is called a *quadrupolar echo*. In contrast to those described in Sections 12.2 and 12.4, the quadrupolar echo involves the refocusing of spin evolution under a *distribution of first-order quadrupolar interactions*, rather than a distribution in local magnetic fields or chemical shifts.

The two-pulse sequence in Figure 13.12 only generates a quadrupolar echo in the case of spin-1 systems. It does not work for higher spin quantum numbers.

To see how the quadrupolar echo works, consider the density operator at time point ③, which is at a time interval $\tau/2$ after the end of the first pulse. If relaxation is ignored, the ($\pm$1)-quantum coherences at this time point are given as follows:

$$\begin{aligned}
\rho_{\boxed{-1_{-1}}}\,③ &= \rho_{\boxed{-1_{-1}}}\,② \exp\{\mathrm{i}\Omega_{\boxed{-1_{-1}}}\,\tau/2\} = -\mathrm{i}\frac{1}{3\sqrt{2}}\mathbb{B}\exp\{\mathrm{i}\Omega_{\boxed{-1_{-1}}}\,\tau/2\} \\
\rho_{\boxed{-1_{+1}}}\,③ &= \rho_{\boxed{-1_{+1}}}\,② \exp\{\mathrm{i}\Omega_{\boxed{-1_{+1}}}\,\tau/2\} = -\mathrm{i}\frac{1}{3\sqrt{2}}\mathbb{B}\exp\{\mathrm{i}\Omega_{\boxed{-1_{+1}}}\,\tau/2\} \\
\rho_{\boxed{+1_{-1}}}\,③ &= \rho_{\boxed{+1_{-1}}}\,② \exp\{\mathrm{i}\Omega_{\boxed{+1_{-1}}}\,\tau/2\} = +\mathrm{i}\frac{1}{3\sqrt{2}}\mathbb{B}\exp\{\mathrm{i}\Omega_{\boxed{+1_{-1}}}\,\tau/2\} \\
\rho_{\boxed{+1_{+1}}}\,③ &= \rho_{\boxed{+1_{+1}}}\,② \exp\{\mathrm{i}\Omega_{\boxed{+1_{+1}}}\,\tau/2\} = +\mathrm{i}\frac{1}{3\sqrt{2}}\mathbb{B}\exp\{\mathrm{i}\Omega_{\boxed{+1_{+1}}}\,\tau/2\}
\end{aligned} \tag{13.24}$$

The coherence frequencies are given by Equation 13.11. If the chemical shift offset frequency Ω^0 is neglected,[11]

Equation 13.24 may be simplified as follows:

$$\begin{aligned}
\rho_{\boxed{-1_{-1}}}\textcircled{3} &= -\mathrm{i}\frac{1}{3\sqrt{2}}\mathbb{B}\exp\{\mathrm{i}\frac{1}{4}\omega_{\mathrm{Q}}^{(1)}\tau\} & \rho_{\boxed{-1_{+1}}}\textcircled{3} &= -\mathrm{i}\frac{1}{3\sqrt{2}}\mathbb{B}\exp\{-\mathrm{i}\frac{1}{4}\omega_{\mathrm{Q}}^{(1)}\tau\} \\
\rho_{\boxed{+1_{-1}}}\textcircled{3} &= +\mathrm{i}\frac{1}{3\sqrt{2}}\mathbb{B}\exp\{\mathrm{i}\frac{1}{4}\omega_{\mathrm{Q}}^{(1)}\tau\} & \rho_{\boxed{+1_{+1}}}\textcircled{3} &= +\mathrm{i}\frac{1}{3\sqrt{2}}\mathbb{B}\exp\{-\mathrm{i}\frac{1}{4}\omega_{\mathrm{Q}}^{(1)}\tau\}
\end{aligned} \tag{13.25}$$

Since the first-order quadrupolar coupling $\omega_{\mathrm{Q}}^{(1)}$ depends on molecular orientation, all coherences dephase in the complex plane during the first interval $\tau/2$. Note that the complex phase factors in Equation 13.25 depend on the satellite order of the coherences (lower subscript). The (-1)-quantum coherence $\rho_{\boxed{-1_{-1}}}$ has the same complex phase factor as the $(+1)$-quantum coherence $\rho_{\boxed{+1_{-1}}}$, and similarly for $\rho_{\boxed{-1_{+1}}}$ and $\rho_{\boxed{+1_{+1}}}$.

For this reason, it is convenient to group coherences according to the satellite order. The (± 1)-quantum part of the density matrix at time point ③ may be written in the following way:

$$\hat{\rho}_{\textcircled{3}} = -\mathrm{i}\frac{1}{3\sqrt{2}}\mathbb{B}\exp\{\mathrm{i}\frac{1}{4}\omega_{\mathrm{Q}}^{(1)}\tau\}\begin{pmatrix}0&0&0\\1&0&-1\\0&0&0\end{pmatrix} - \mathrm{i}\frac{1}{3\sqrt{2}}\mathbb{B}\exp\{-\mathrm{i}\frac{1}{4}\omega_{\mathrm{Q}}^{(1)}\tau\}\begin{pmatrix}0&-1&0\\0&0&0\\0&1&0\end{pmatrix} \tag{13.26}$$

The first term in the right-hand side of Equation 13.26 includes coherences with satellite order $q = -1$ and the second term includes coherences with satellite order $q = +1$.

Now consider the second $(\pi/2)_y$ pulse, which is also assumed to be strong. This pulse transforms the density operator as follows:

$$\hat{\rho}_{\textcircled{4}} = \widehat{R}_y(\pi/2)\hat{\rho}_{\textcircled{3}}\widehat{R}_y(\pi/2)^{\dagger}$$

where the spin-1 matrix representation of the rotation operator is given in Section 7.9.1:

$$\widehat{R}_y(\pi/2) = \frac{1}{2}\begin{pmatrix}1&-\sqrt{2}&1\\\sqrt{2}&0&-\sqrt{2}\\1&\sqrt{2}&1\end{pmatrix}$$

Straightforward matrix multiplication leads to the following properties:

$$\begin{aligned}
\widehat{R}_y(\pi/2)\begin{pmatrix}0&0&0\\1&0&-1\\0&0&0\end{pmatrix}\widehat{R}_y(\pi/2)^{\dagger} &= \begin{pmatrix}0&-1&0\\0&0&0\\0&1&0\end{pmatrix} \\
\widehat{R}_y(\pi/2)\begin{pmatrix}0&-1&0\\0&0&0\\0&1&0\end{pmatrix}\widehat{R}_y(\pi/2)^{\dagger} &= \begin{pmatrix}0&0&0\\1&0&-1\\0&0&0\end{pmatrix}
\end{aligned} \tag{13.27}$$

These are the central results leading to the spin-1 quadrupolar echo: the set of coherences with satellite order $q = +1$ is exchanged with the set of coherences with satellite order $q = -1$. These *coherence transfer processes* are depicted in Figure 13.13.

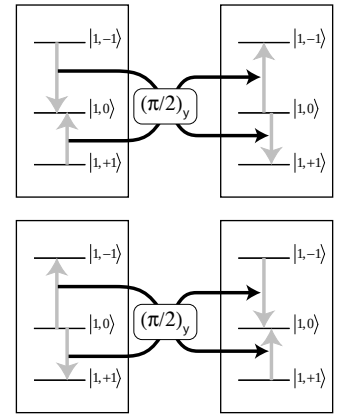

Figure 13.13
Coherence exchange processes induced by the second pulse in a quadrupolar spin echo.

Equations 13.26 and 13.27 may be combined to obtain the spin density operator after the second pulse:

$$\hat{\rho}_{④} = -\mathrm{i}\frac{1}{3\sqrt{2}}\mathbb{B}\exp\{-\mathrm{i}\frac{1}{4}\omega_{\mathrm{Q}}^{(1)}\tau\}\begin{pmatrix}0&0&0\\1&0&-1\\0&0&0\end{pmatrix} - \mathrm{i}\frac{1}{3\sqrt{2}}\mathbb{B}\exp\{\mathrm{i}\frac{1}{4}\omega_{\mathrm{Q}}^{(1)}\tau\}\begin{pmatrix}0&-1&0\\0&0&0\\0&1&0\end{pmatrix} \tag{13.28}$$

The (-1)-quantum coherences after the second pulse are therefore given by

$$\rho_{\boxed{-1_{-1}}}④ = -\mathrm{i}\frac{1}{3\sqrt{2}}\mathbb{B}\exp\{-\mathrm{i}\frac{1}{4}\omega_{\mathrm{Q}}^{(1)}\tau\}$$
$$\rho_{\boxed{-1_{+1}}}④ = -\mathrm{i}\frac{1}{3\sqrt{2}}\mathbb{B}\exp\{\mathrm{i}\frac{1}{4}\omega_{\mathrm{Q}}^{(1)}\tau\}$$

Further evolution for the interval $\tau/2$ refocuses the dispersion of phases, leading to:

$$\rho_{\boxed{-1_{-1}}}⑤ = \rho_{\boxed{-1_{-1}}}④\exp\{+\mathrm{i}\frac{1}{4}\omega_{\mathrm{Q}}^{(1)}\tau\} = -\mathrm{i}\frac{1}{3\sqrt{2}}\mathbb{B}$$
$$\rho_{\boxed{-1_{+1}}}⑤ = \rho_{\boxed{-1_{+1}}}④\exp\{-\mathrm{i}\frac{1}{4}\omega_{\mathrm{Q}}^{(1)}\tau\} = -\mathrm{i}\frac{1}{3\sqrt{2}}\mathbb{B}$$

The two (-1)-quantum coherences come into phase at the time point ⑤, leading to a spin density operator that is independent of the first-order quadrupole coupling $\omega_{\mathrm{Q}}^{(1)}$. This is the quadrupolar echo. Acquisition of the decaying NMR signal after the quadrupolar echo, followed by FT, generates a spin-1 NMR spectrum, undisturbed by interference from the r.f. pulses. An experimental example of a spectrum obtained this way is shown in Figure 13.14.

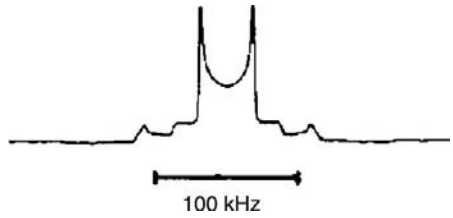

Figure 13.14 Experimental ^{2}H spectrum of deuterated poly(methylmethacrylate), showing two superimposed Pake patterns with different values of the quadrupole coupling constant C_Q. Adapted from M. H. Levitt, D. Suter and R. R. Ernst, *J. Chem. Phys.* **80**, 3064 (1984). Copyright 1984, American Institute of Physics.

A coherence transfer pathway diagram for the quadrupolar echo pulse sequence is shown below.

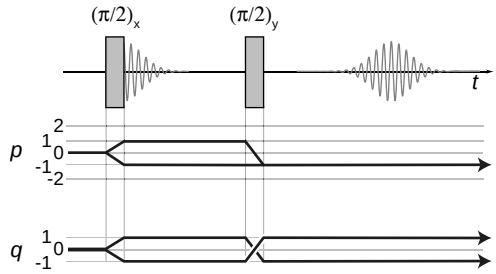

Figure 13.15
Coherence transfer pathway diagram for a quadrupolar spin echo.

The two staves depict the histories of coherence orders p and satellite orders q leading to the final NMR signal. The upper stave spans all orders p between -2 and $+2$, since the spin-1 density matrix may contain double-quantum coherences as well as populations and single-quantum coherences.

The upper stave shows that the pathway leading to the NMR signal starts with order 0, corresponding to thermal equilibrium populations, and terminates with order -1, corresponding to the quadrature-detected NMR signal. Double-quantum coherences are not involved. Note that the coherence transfer pathway for the quadrupolar echo involves both orders $p = \pm 1$ between the two pulses, unlike the Hahn echo (see Section 12.2.6), for which only the $(+1)$-quantum pathway forms an echo.

The lower stave shows the sign change of satellite order induced by the second $\pi/2$ pulse. It is this change in satellite order q that leads to the quadrupolar echo. The final NMR signal is induced by both (-1)-quantum coherences, with satellite orders $q = \pm 1$.

13.2 Spin $I = 3/2$

There is a large number of spins-3/2 isotopes in the periodic table (see Plate C). The alkali metals are especially well represented: ^{7}Li, ^{23}Na, ^{39}K and ^{87}Rb. There are also several halogen isotopes with spin-3/2: ^{35}Cl, ^{37}Cl, ^{79}Br and ^{81}Br. The semi-metal nuclides ^{69}Ga, ^{71}Ga and ^{75}As are particularly useful for the study of semiconductors. Other important spin-3/2 nuclides include the two copper isotopes ^{63}Cu and ^{65}Cu, the boron isotope ^{11}B, the gold isotope ^{197}Au, the iridium isotopes ^{191}Ir and ^{193}Ir, and the noble gas nuclides ^{21}Ne and ^{131}Xe.

13.2.1 Spin-3/2 energy levels

The quantum mechanics of a spin-3/2 nucleus may be developed on the same lines as for spin-1. In the case of spin-3/2, there are four eigenstates of angular momentum along the z-axis, denoted $|\frac{3}{2}, M\rangle$ where the quantum number M is equal to $+3/2$, $+1/2$, $-1/2$ or $-3/2$, and the Zeeman eigenstates have the following properties:

$$\begin{aligned} \hat{I}_z|\frac{3}{2}, M\rangle &= M|\frac{3}{2}, M\rangle \\ \hat{I}^2|\frac{3}{2}, M\rangle &= I(I+1)|\frac{3}{2}, M\rangle = \frac{15}{4}|\frac{3}{2}, M\rangle \end{aligned} \tag{13.29}$$

For a spin-3/2, the first-order quadrupolar Hamiltonian is given by

$$\begin{aligned} \widehat{\mathcal{H}}_{\mathrm{Q}}^{(1)} &= \omega_{\mathrm{Q}}^{(1)} \times \frac{1}{6}\left(3\hat{I}_z^2 - I(I+1)\widehat{1}\right) \\ &= \omega_{\mathrm{Q}}^{(1)} \times \frac{1}{6}\left(3\hat{I}_z^2 - \frac{15}{4}\widehat{1}\right) \qquad \text{(for spin } I = 3/2\text{)} \end{aligned} \tag{13.30}$$

where the first-order quadrupolar coupling $\omega_{\mathrm{Q}}^{(1)}$ is given by Equation 9.23.

In the case of a solid, the first-order quadrupolar coupling is given by

$$\begin{aligned} \omega_{\mathrm{Q}}^{(1)}(\theta_{\mathrm{Q}}) &= \frac{3\pi C_{\mathrm{Q}}}{2I(2I-1)}\left(3\cos^2\theta_{\mathrm{Q}} - 1\right) \\ &= \pi C_{\mathrm{Q}} \times \frac{1}{2}\left(3\cos^2\theta_{\mathrm{Q}} - 1\right) \qquad \text{(for spin } I = 3/2\text{)} \end{aligned} \tag{13.31}$$

assuming a uniaxial electric field gradient tensor ($\eta_{\mathrm{Q}} = 0$). Here, θ_{Q} is the angle between the major principal axis of the electric field gradient tensor and the magnetic field. Note that the first-order quadrupolar coupling for spin-3/2 is three times smaller that for spin-1, given the same quadrupole coupling constant C_{Q} (compare Equation 13.5 and 13.31).

The four Zeeman eigenstates $|\frac{3}{2}, M\rangle$ are eigenstates of the first-order quadrupolar Hamiltonian:

$$\widehat{\mathcal{H}}_{\mathrm{Q}}^{(1)}|\frac{3}{2}, M\rangle = +\frac{1}{2}\left(M^2 - \frac{5}{4}\right)\omega_{\mathrm{Q}}^{(1)}|\frac{3}{2}, M\rangle$$

leading to the following eigenequations:

$$\widehat{\mathcal{H}}_{\mathrm{Q}}^{(1)}|\frac{3}{2}, \pm\frac{3}{2}\rangle = +\frac{1}{2}\omega_{\mathrm{Q}}^{(1)}|\frac{3}{2}, \pm\frac{3}{2}\rangle \qquad \widehat{\mathcal{H}}_{\mathrm{Q}}^{(1)}|\frac{3}{2}, \pm\frac{1}{2}\rangle = -\frac{1}{2}\omega_{\mathrm{Q}}^{(1)}|\frac{3}{2}, \pm\frac{1}{2}\rangle$$

If the quadrupolar coupling $\omega_{\mathrm{Q}}^{(1)}$ is positive, then the energies of the outer states $|\frac{3}{2}, \pm\frac{3}{2}\rangle$ are shifted upwards in energy by $\omega_{\mathrm{Q}}^{(1)}/2$, while the energies of the inner states $|\frac{3}{2}, \pm\frac{1}{2}\rangle$ are shifted down in energy by the same amount (see Figure 13.16).

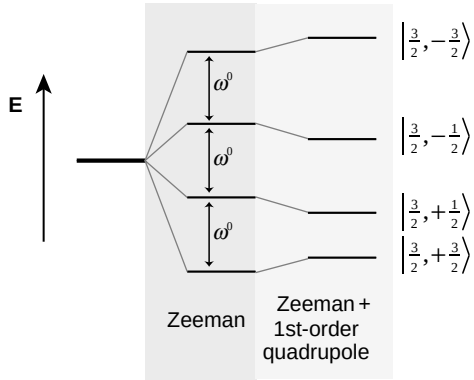

Figure 13.16
Energy levels of a spin-3/2 nucleus, in the case of positive gyromagnetic ratio.

13.2.2 Populations and coherences

The quantum state of a spin-3/2 ensemble may be written as a 4×4 density matrix, as follows:

$$\hat{\rho} = \overline{|\psi\rangle\langle\psi|} = \begin{pmatrix} \rho_{|+3/2\rangle} & \rho_{\boxed{+1_{+2}}} & \rho_{\boxed{+2_{+2}}} & \rho_{\boxed{+3_0}} \\ \rho_{\boxed{-1_{-2}}} & \rho_{|+1/2\rangle} & \rho_{\boxed{+1_0}} & \rho_{\boxed{+2_{-2}}} \\ \rho_{\boxed{-2_{-2}}} & \rho_{\boxed{-1_0}} & \rho_{|-1/2\rangle} & \rho_{\boxed{+1_{-2}}} \\ \rho_{\boxed{-3_0}} & \rho_{\boxed{-2_{+2}}} & \rho_{\boxed{-1_{+2}}} & \rho_{|-3/2\rangle} \end{pmatrix} \tag{13.32}$$

The populations of the four Zeeman states are denoted $\rho_{|+3/2\rangle}$, $\rho_{|+1/2\rangle}$, $\rho_{|-1/2\rangle}$ and $\rho_{|-3/2\rangle}$, and may be represented diagramatically as 'little balls' sitting on the corresponding energy level:

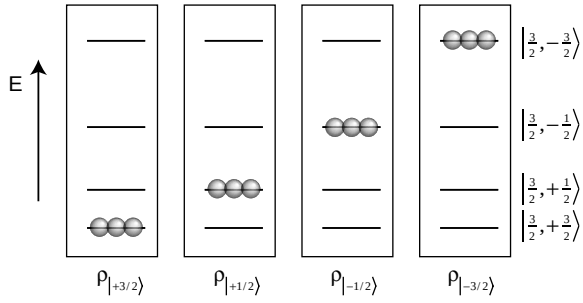

Figure 13.17
State populations for an ensemble of spins-3/2.

The 12 coherences of the spin-3/2 ensemble are labelled using the coherence order and satellite order, as defined in Equation 13.7. For example, the coherence $\rho_{\boxed{+1_{+2}}}$ is given by the following density matrix element:

$$\rho_{\boxed{+1_{+2}}} = \langle 3/2, +3/2|\, \hat{\rho}\, |3/2, +1/2\rangle$$

The two subscript labels of this coherence are derived as follows:

$$p = \left(\frac{3}{2}\right) - \left(\frac{1}{2}\right) = +1 \quad q = \left(\frac{3}{2}\right)^2 - \left(\frac{1}{2}\right)^2 = +2$$

The other labels in Equation 13.32 are derived in a similar way.

The spin-1 ensemble supports three (-1)-quantum coherences, denoted $\rho_{\boxed{-1_{-2}}}$, $\rho_{\boxed{-1_0}}$ and $\rho_{\boxed{-1_{+2}}}$:

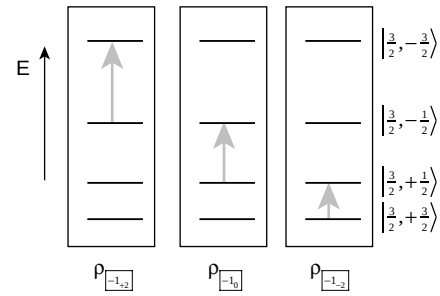

Figure 13.18
The (-1)-quantum coherences for an ensemble of spins-3/2.

The coherence $\rho_{\boxed{-1_0}}$ involves the two innermost eigenstates $|3/2, \pm 1/2\rangle$, and is particularly important, as discussed below. It is associated with the *central transition* of the spin-3/2 system.

The $(+1)$-quantum coherences $\rho_{\boxed{+1_{-2}}}$, $\rho_{\boxed{+1_0}}$ and $\rho_{\boxed{+1_{+2}}}$ may be represented by arrows running in the opposite direction to the (-1)-quantum coherences:

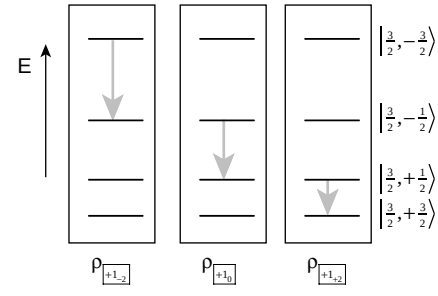

Figure 13.19
The $(+1)$-quantum coherences for an ensemble of spins-3/2.

The spin-3/2 ensemble may also support *double-quantum coherences* (with order $p = \pm 2$) and a pair of *triple-quantum coherences* (with order $p = \pm 3$). These may be depicted as follows:

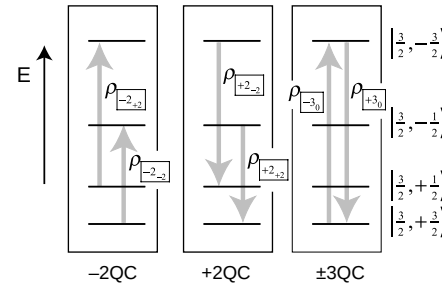

Figure 13.20
The (± 2)-quantum coherences and (± 3)-quantum coherences for an ensemble of spins-3/2.

These double- and triple-quantum coherences have no counterpart for spins-1/2.

The evolution frequencies of the spin-3/2 coherences are as follows:

$$\begin{aligned}
\Omega_{\boxed{-3_0}} &= 3\Omega^0 & \Omega_{\boxed{+1_{+2}}} &= -\Omega^0 - \omega_Q^{(1)} \\
\Omega_{\boxed{-2_{+2}}} &= 2\Omega^0 - \omega_Q^{(1)} & \Omega_{\boxed{+1_0}} &= -\Omega^0 \\
\Omega_{\boxed{-2_{-2}}} &= 2\Omega^0 + \omega_Q^{(1)} & \Omega_{\boxed{+1_{-2}}} &= -\Omega^0 + \omega_Q^{(1)} \\
\Omega_{\boxed{-1_{+2}}} &= \Omega^0 - \omega_Q^{(1)} & \Omega_{\boxed{+2_{+2}}} &= -2\Omega^0 - \omega_Q^{(1)} \\
\Omega_{\boxed{-1_0}} &= \Omega^0 & \Omega_{\boxed{+2_{-2}}} &= -2\Omega^0 + \omega_Q^{(1)} \\
\Omega_{\boxed{-1_{-2}}} &= \Omega^0 + \omega_Q^{(1)} & \Omega_{\boxed{+3_0}} &= -3\Omega^0
\end{aligned} \tag{13.33}$$

where Ω^0 is the chemically shifted resonance offset (see Equation 13.12). Note that the contribution from the quadrupolar coupling $\omega_Q^{(1)}$ is proportional to the satellite order of the coherence. The coherences $\rho_{\boxed{\pm 1_0}}$ and $\rho_{\boxed{\pm 3_0}}$ are not influenced by the first-order quadrupole interaction.

13.2.3 NMR signal

An expression for the NMR signal is derived by combining Equation 13.13 with the spin-3/2 matrix representation of the shift operator, as given in Section 7.9:

$$\hat{I}^+ = \begin{pmatrix} 0 & \sqrt{3} & 0 & 0 \\ 0 & 0 & 2 & 0 \\ 0 & 0 & 0 & \sqrt{3} \\ 0 & 0 & 0 & 0 \end{pmatrix} \tag{13.34}$$

Using $\langle \hat{I}^+ \rangle = \mathrm{Tr}\{\hat{I}^+ \hat{\rho}\}$ leads to the following expression for the spin-3/2 NMR signal:

$$s(t) \sim 2\mathrm{i} \exp\{-\mathrm{i}\phi_{\mathrm{rec}}\} \left(\sqrt{3}\rho_{\boxed{-1_{-2}}}(t) + 2\rho_{\boxed{-1_0}}(t) + \sqrt{3}\rho_{\boxed{-1_{+2}}}(t) \right) \quad \text{(for spin } I = 3/2\text{)} \tag{13.35}$$

Each (−1)-quantum coherence gives rise to an NMR signal, but the three coherences do not contribute equally. The central coherence $\rho_{\boxed{-1_0}}$ provides a more intense signal than the outer coherences $\rho_{\boxed{-1_{\pm 2}}}$.

Fourier transformation of $s(t)$ provides an NMR spectrum $S(\Omega)$ containing three Lorentzian peaks:

$$\begin{aligned}
S(\Omega) &= a_{\boxed{-1_{-2}}} \mathcal{L}(\Omega; \Omega_{\boxed{-1_{-2}}}, \lambda) + a_{\boxed{-1_0}} \mathcal{L}(\Omega; \Omega_{\boxed{-1_0}}, \lambda) + a_{\boxed{-1_{+2}}} \mathcal{L}(\Omega; \Omega_{\boxed{-1_{+2}}}, \lambda) \\
&= a_{\boxed{-1_{-2}}} \mathcal{L}(\Omega; \Omega^0 + \omega_Q^{(1)}, \lambda) + a_{\boxed{-1_0}} \mathcal{L}(\Omega; \Omega^0, \lambda) + a_{\boxed{-1_{+2}}} \mathcal{L}(\Omega; \Omega^0 - \omega_Q^{(1)}, \lambda)
\end{aligned} \tag{13.36}$$

The peak intensities are proportional to the (−1)-quantum coherence amplitudes at the beginning of the detection interval:

$$\begin{aligned}
a_{\boxed{-1_{-2}}} &= 2\mathrm{i}\sqrt{3} \exp\{-\mathrm{i}\phi_{\mathrm{rec}}\} \rho_{\boxed{-1_{-2}}}(0) \\
a_{\boxed{-1_0}} &= 4\mathrm{i} \exp\{-\mathrm{i}\phi_{\mathrm{rec}}\} \rho_{\boxed{-1_0}}(0) \\
a_{\boxed{-1_{+2}}} &= 2\mathrm{i}\sqrt{3} \exp\{-\mathrm{i}\phi_{\mathrm{rec}}\} \rho_{\boxed{-1_{+2}}}(0)
\end{aligned} \tag{13.37}$$

The NMR spectrum generated by a spin-3/2 ensemble is therefore a *triplet* with a splitting of $\omega_{\mathrm{Q}}^{(1)}$ between each of the components.

13.2.4 Single pulse spectrum

Consider a single-pulse experiment in which a strong $(\pi/2)_x$ pulse is applied to an ensemble of spins-3/2. The discussion below uses the timing diagram in Figure 13.7.

The thermal equilibrium density matrix contains populations satisfying the Boltzmann distribution, and no coherences. Within the high-temperature approximation, the thermal equilibrium populations are given by

$$\rho_{|+3/2\rangle} \cong \frac{1}{4}(1 + 3\mathbb{B}/2) \qquad \rho_{|-1/2\rangle} \cong \frac{1}{4}(1 - \mathbb{B}/2)$$
$$\rho_{|+1/2\rangle} \cong \frac{1}{4}(1 + \mathbb{B}/2) \qquad \rho_{|-3/2\rangle} \cong \frac{1}{4}(1 - 3\mathbb{B}/2)$$

The thermal equilibrium spin density operator at time point ① (before the pulse) is therefore given by

$$\hat{\rho}_{①} = \frac{1}{4}\widehat{1} + \frac{1}{4}\mathbb{B}\hat{I}_z \tag{13.38}$$

Suppose that the r.f. field is strong enough to satisfy the strong-pulse condition:

$$|\omega_{\mathrm{nut}}| >> |\omega_{\mathrm{Q}}^{(1)}| \tag{13.39}$$

In this case, the density operator after the pulse is given by

$$\hat{\rho}_{②} = \widehat{R}_x(\pi/2)\hat{\rho}_{①}\,\widehat{R}_x(\pi/2)^{\dagger} = \frac{1}{4}\widehat{1} - \frac{1}{4}\mathbb{B}\hat{I}_y \tag{13.40}$$

The case of a weak r.f. pulse is considered in Section 13.2.7.

The density matrix corresponding to Equation 13.40 may be derived using the spin-3/2 matrix representation of $\hat{I}_y$ given in Section 7.9. The result is as follows:

$$\hat{\rho}_{②} = \frac{1}{4}\begin{pmatrix} 1 & \mathrm{i}\mathbb{B}\frac{1}{2}\sqrt{3} & 0 & 0 \\ -\mathrm{i}\mathbb{B}\frac{1}{2}\sqrt{3} & 1 & \mathrm{i}\mathbb{B} & 0 \\ 0 & -\mathrm{i}\mathbb{B} & 1 & \mathrm{i}\mathbb{B}\frac{1}{2}\sqrt{3} \\ 0 & 0 & -\mathrm{i}\mathbb{B}\frac{1}{2}\sqrt{3} & 1 \end{pmatrix}$$

This shows that the double- and triple-quantum coherences are not excited by the pulse, and that the excited (-1)-quantum coherences are given by

$$\rho_{\boxed{-1_{+2}}}② = -\mathrm{i}\frac{1}{8}\sqrt{3}\,\mathbb{B}$$
$$\rho_{\boxed{-1_{0}}}② = -\mathrm{i}\frac{1}{4}\mathbb{B}$$
$$\rho_{\boxed{-1_{-2}}}② = -\mathrm{i}\frac{1}{8}\sqrt{3}\,\mathbb{B} \tag{13.41}$$

Note that the central coherence has a larger amplitude than the satellite coherences.

The effect of the strong pulse on the populations and coherences is as follows:

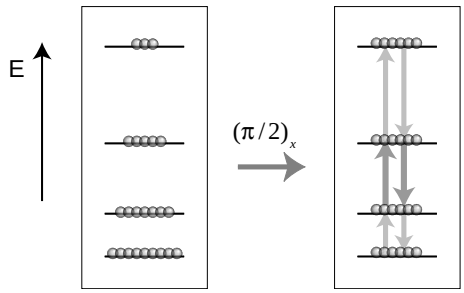

Figure 13.21
A strong $\pi/2$ pulse eliminates population differences and creates (± 1)-quantum coherences.

All populations are equalized, and (± 1)-quantum coherences are created. The stronger amplitudes of the central coherences are represented by the heavier arrows.

Equation 13.41 may be combined with Equations 13.36 and 13.37 to derive the NMR spectrum obtained by Fourier transforming the quadrature-detected NMR signal. If the receiver phase is zero ($\phi_{\text{rec}} = 0$), the result is

$$S(\Omega) = \frac{3}{4}\mathbb{B}\mathfrak{L}(\Omega; \Omega^0 + \omega_{\text{Q}}^{(1)}, \lambda) + \mathbb{B}\mathfrak{L}(\Omega; \Omega^0, \lambda) + \frac{3}{4}\mathbb{B}\mathfrak{L}(\Omega; \Omega^0 - \omega_{\text{Q}}^{(1)}, \lambda)$$

The NMR spectrum of a single spin-3/2 ensemble, excited by a strong $\pi/2$ pulse, is a 3:4:3 triplet, with a splitting of $\omega_{\text{Q}}^{(1)}$ between adjacent peaks:

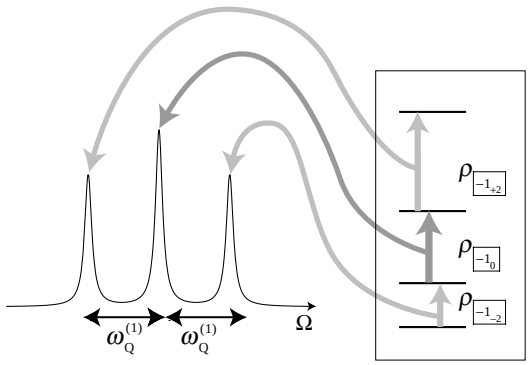

Figure 13.22
The spectrum of a spin-3/2 ensemble and the corresponding (-1)-quantum coherences.

The unequal peak intensities arise because (i) the satellite (-1)-quantum coherences have a smaller amplitude than the central (-1)-quantum coherence and (ii) the satellite (-1)-quantum coherences are less efficient in inducing an NMR signal than the central (-1)-quantum coherence. The peak intensity ratio 3 : 4 : 3 corresponds to the *squares* of the $\hat{I}^+$ matrix elements, which are given by $\{\sqrt{3}, 2, \sqrt{3}\}$ (see Equation 13.34).

The central peak of the spin-3/2 triplet is of particular importance and is called the *central transition*. The outer peaks are called *satellite transitions*.[12]

13.2.5 Spin-3/2 spectra for small quadrupole couplings

The first-order quadrupolar coupling $\omega_Q^{(1)}$ depends strongly on the phase of matter. This determines the nature of the spin-3/2 NMR spectrum.

Isotropic liquids. As in the spin-1 case, there is no quadrupolar splitting for spins-3/2 in isotropic liquids, since the three triplet components coincide:

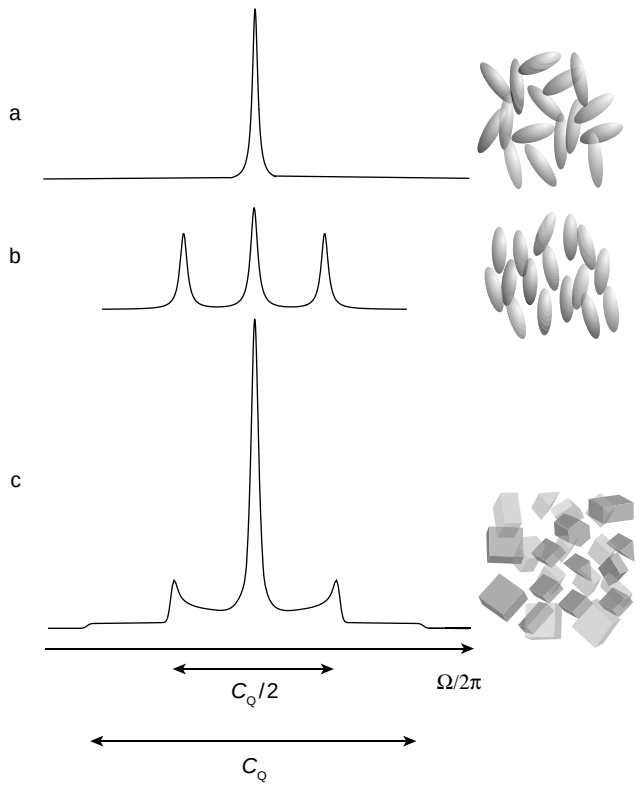

Figure 13.23
Typical appearance of spin-3/2 spectra for: (a) an isotropic liquid; (b) a nematic liquid crystal oriented along the magnetic field; (c) a solid powder for the case of a small quadrupole coupling constant C_Q.

Anisotropic liquids. The spectrum of spins-3/2 has the form of a 3:4:3 triplet in a nematic liquid crystal[6] (see Figure 13.23b). An experimental ^{23}Na spectrum showing the triplet structure is shown in Figure 13.24a.

Solid powders. In solids, the two satellites generate a broad Pake pattern, assuming a uniaxial electric field gradient tensor ($\eta_Q = 0$). The splitting between the 'parallel' shoulders is C_Q, in units of hertz, and the splitting between the 'perpendicular' peaks in the Pake pattern is $C_Q/2$. The quadrupole coupling constant is defined as usual by $C_Q = e^2qQ/h$. The central transition is not affected by the first-order quadrupolar coupling and gives rise to a strong narrow peak at the centre of the Pake pattern (see Figure 13.23c).

In practice, the satellite Pake pattern can be very difficult to observe, since it is so broad compared with the central transition. In many cases, only the central transition of spins-3/2 is observed in a solid, unless the quadrupole coupling constant C_Q is exceptionally small.

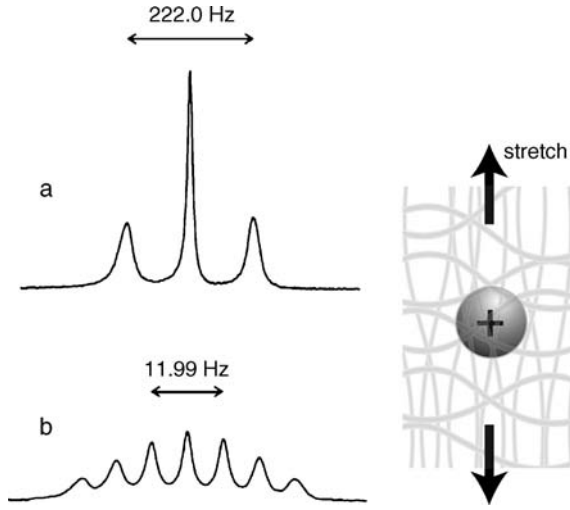

Figure 13.24 NMR spectra of alkali metal ions in a stretched gelatine gel. The mechanical stretching of the gel creates a slight anisotropy in the ionic environments, leading to a small quadrupole coupling C_Q. (a) ^{23}Na (spin $I = 3/2$) and (b) ^{133}Cs (spin $I = 7/2$). Adapted from P. W. Kuchel, B. E. Chapman, N. Müller, W. A. Bubb, D. J. Philp and A. M. Torres, *J. Magn. Reson.* **180**, 256–265 (2006), copyright Elsevier.

13.2.6 Second-order quadrupole couplings

If C_Q is large, the satellite transitions are too broad to be observed, and are also excited very inefficiently. In this case, only the central transition peak is observed. This peak is relatively narrow, since the central transition frequency $\Omega_{\boxed{-1_0}}$ is independent of the first-order quadrupolar interaction $\omega_Q^{(1)}$.

In the case of large C_Q, *second-order quadrupolar interactions* become important. The second-order quadrupolar coupling is proportional to the square of the first-order quadrupole coupling divided by the Larmor frequency (see Equation 9.25). Since the second-order quadrupolar coupling depends on molecular orientation, the central transitions of spins-3/2 display complicated broad lineshapes in powdered solids.

These second-order effects can be very considerable. It is not uncommon for second-order central-transition lineshapes to be hundreds of kilohertz wide.

The second-order quadrupolar broadening is usually undesirable, since it makes the spectra very complicated and obscures chemical shifts. Since the second-order coupling is inversely proportional to the static magnetic field (see Equation 9.25), it may be reduced in magnitude by increasing the static field. In general, the solid-state NMR spectroscopy of spins-3/2 (and half-integer spins in general) benefits greatly from using the highest possible magnetic field strengths.

Although the second-order quadrupolar broadening may be reduced by increasing the static magnetic field, it may not be eliminated completely in this way. A range of experimental methods are available for completely eliminating the second-order quadrupolar broadening,[13] greatly improving the chemical site resolution of half-integer quadrupolar NMR. One set of methods involves rotating the sample rapidly about two different axes, either simultaneously (*double rotation*, or *DOR*) or sequentially (*dynamic angle spinning*, or *DAS*). Another set of methods involves combining rapid sample rotation with pulse-induced coherence transfers. One variant is called multiple-quantum NMR (*multiple-quantum magic-angle-spinning* or *MQ-MAS*). Another method involves satellite coherences instead of multiple-quantum coherences, and

is called *satellite transition magic-angle-spinning* or *ST-MAS*. See *Further Reading* for a description of these techniques.

13.2.7 Central transition excitation

If the quadrupole coupling constant C_Q is very large, then practical r.f. field strengths are too weak to impose the strong-pulse condition of Equation 13.39, at least for the vast majority of molecular orientations. The analysis in Section 13.2.4 is therefore invalid in the case of strong quadrupolar coupling.

Consider the spin Hamiltonian during an r.f. pulse of phase $\phi_p = 0$. If the second-order quadrupolar coupling and chemical shifts are ignored, the total rotating-frame spin Hamiltonian is given by

$$\widehat{\mathcal{H}}_p = \widehat{\mathcal{H}}_Q^{(1)} + \omega_{nut}\hat{I}_x = \omega_Q^{(1)}\left(\hat{I}_z^2 - \frac{5}{4}\widehat{1}\right) + \omega_{nut}\hat{I}_x$$

The spin-3/2 matrix representation of this Hamiltonian is as follows:

$$\widehat{\mathcal{H}}_p = \begin{pmatrix} \frac{1}{2}\omega_Q^{(1)} & \frac{1}{2}\sqrt{3}\omega_{nut} & 0 & 0 \\ \frac{1}{2}\sqrt{3}\omega_{nut} & -\frac{1}{2}\omega_Q^{(1)} & \omega_{nut} & 0 \\ 0 & \omega_{nut} & -\frac{1}{2}\omega_Q^{(1)} & \frac{1}{2}\sqrt{3}\omega_{nut} \\ 0 & 0 & \frac{1}{2}\sqrt{3}\omega_{nut} & \frac{1}{2}\omega_Q^{(1)} \end{pmatrix} \tag{13.42}$$

Now suppose that the nutation frequency under the r.f. field is *weak* compared with the first-order quadrupolar coupling:

$$|\omega_{nut}| << |\omega_Q^{(1)}|$$

This is the opposite limit to that discussed in Section 13.2.4.

In the weak-pulse limit, the secular approximation may be applied to Equation 13.42. Off-diagonal matrix elements that connect large differences in diagonal elements are ignored (see Appendix A.6). This leads to the following approximate expression for the Hamiltonian during the pulse:

$$\widehat{\mathcal{H}}_p \cong \begin{pmatrix} \frac{1}{2}\omega_Q^{(1)} & 0 & 0 & 0 \\ 0 & -\frac{1}{2}\omega_Q^{(1)} & \omega_{nut} & 0 \\ 0 & \omega_{nut} & -\frac{1}{2}\omega_Q^{(1)} & 0 \\ 0 & 0 & 0 & \frac{1}{2}\omega_Q^{(1)} \end{pmatrix} \tag{13.43}$$

Suppose now that the pulse is applied to a thermal equilibrium spin density operator of the form

$$\hat{\rho}_{①} = \frac{1}{4}\widehat{1} + \frac{1}{4}\mathbb{B}\hat{I}_z$$

where the matrix representation of $\hat{I}_z$ is given by

$$\hat{I}_z = \begin{pmatrix} \frac{3}{2} & 0 & 0 & 0 \\ 0 & \frac{1}{2} & 0 & 0 \\ 0 & 0 & -\frac{1}{2} & 0 \\ 0 & 0 & 0 & -\frac{3}{2} \end{pmatrix} \tag{13.44}$$

Since Equations 13.43 and 13.44 are block diagonal, it is easy to show that the density operator after the pulse is given by

$$\begin{aligned} \hat{\rho} &= \frac{1}{4}\widehat{1} + \frac{1}{4}\mathbb{B}\exp\{-\mathrm{i}\widehat{\mathcal{H}}_\mathrm{p}\tau_\mathrm{p}\}\hat{I}_z\exp\{+\mathrm{i}\widehat{\mathcal{H}}_\mathrm{p}\tau_\mathrm{p}\} \\ &= \frac{1}{4}\widehat{1} + \frac{1}{4}\mathbb{B}\begin{pmatrix} \frac{3}{2} & 0 & 0 & 0 \\ 0 & \frac{1}{2}\cos(\beta_\mathrm{p}^\mathrm{C}) & +\mathrm{i}\frac{1}{2}\sin(\beta_\mathrm{p}^\mathrm{C}) & 0 \\ 0 & -\mathrm{i}\frac{1}{2}\sin(\beta_\mathrm{p}^\mathrm{C}) & -\frac{1}{2}\cos(\beta_\mathrm{p}^\mathrm{C}) & 0 \\ 0 & 0 & 0 & -\frac{3}{2} \end{pmatrix} \end{aligned} \tag{13.45}$$

where $\beta_\mathrm{p}^\mathrm{C}$ is the *central-transition flip angle*, given by

$$\beta_\mathrm{p}^\mathrm{C} = \omega_\mathrm{nut}^\mathrm{C}\tau_\mathrm{p} \tag{13.46}$$

and $\omega_\mathrm{nut}^\mathrm{C}$ is the *nutation frequency on the central transition*, given by

$$\omega_\mathrm{nut}^\mathrm{C} = 2\omega_\mathrm{nut} \qquad \text{(for spins } I = 3/2\text{)} \tag{13.47}$$

The excitation of the central-transition coherence is maximized for the central-transition flip angle $\beta_\mathrm{p}^\mathrm{C} = \pi/2$. This corresponds to a *selective* $\pi/2$ *rotation on the central transition of the spin-3/2 system*. Under these conditions, the population difference across the central transition is completely converted into central-transition (±1)-quantum coherences:

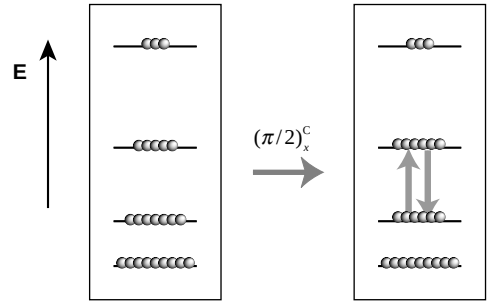

Figure 13.25
A selective $\pi/2$ pulse on the central transition converts the central transition population difference into central transition coherences.

Note that the populations of the outer levels are not perturbed by the selective pulse on the central transition.[14]

One curious feature should be noted carefully. Equation 13.47 shows that the central-transition nutation frequency in the selective pulse regime is *twice* that which would be expected for a strong pulse using the same r.f. field. This counter-intuitive effect may be rationalized by imagining that a strong, non-selective, pulse 'wastes' some of the r.f. power on exciting the satellite transitions. The pulse becomes twice as efficient when the r.f. field is concentrated on the central transition alone.

This effect often catches out inexperienced spectroscopists. For example, suppose that the ^{23}Na nutation frequency is calibrated by observing the pulse response in a solution of NaCl. In this case, the quadrupole coupling is zero, so the pulse operates in the 'strong-pulse' regime, and the nuclei respond according to the non-selective nutation frequency ω_{nut}. The NMR signal is maximized by choosing a pulse duration τ_{p} such that $\beta_{\text{p}} = \omega_{\text{nut}}\tau_{\text{p}} = \pi/2$. However, if the same pulse is used on a solid sample containing ^{23}Na ions in a high-C_{Q} environment, the ^{23}Na NMR signal vanishes! This is because the r.f. field is now selective on the central transition, with a central transition nutation frequency $\omega^{\text{C}}_{\text{nut}} = 2\omega_{\text{nut}}$. The central transition flip angle for the same pulse duration τ_{p} is $\beta^{\text{C}}_{\text{p}} = \omega^{\text{C}}_{\text{nut}}\tau_{\text{p}} = \pi$, which leads to a failure of central transition coherence excitation. The correct procedure is to *halve* the pulse duration on changing from the low-C_{Q} to the high-C_{Q} sample.

13.2.8 Central transition echo

The shifts caused by the second-order quadrupolar interaction lead to an inhomogeneous broadening of the central transition peak. This corresponds to a rapid decay of the NMR signal after the central-transition excitation pulse. The inhomogeneous decay may be refocused by applying a π pulse to the central transition, in order to generate a spin echo. In this respect, the second-order quadrupolar broadening for the central transition of spins $I = 3/2$ behaves in the same way as CSA broadening of spins $I = 1/2$ in powdered solids. In both cases, a π pulse leads to a spin echo.

⚠ The pulse duration must take into account the fact that the nutation frequency on the $I = 3/2$ central transition is twice the non-selective nutation frequency for the same r.f. field strength, as described above. A central-transition echo is induced by a pulse with a duration τ_{p} satisfying the condition $\omega^{\text{C}}_{\text{nut}}\tau_{\text{p}} = 2\omega_{\text{nut}}\tau_{\text{p}} = \pi$.

⚠ Do not confuse the central-transition spin echo for $I = 3/2$ with the non-selective spin echo for $I = 1$. Although the quadrupolar interaction is involved in both cases, the pulse sequences are completely different. The $I = 1$ echo involves two $\pi/2$ pulses, with a phase shift of $\pi/2$ (a '90–90 echo'), whereas the second pulse in the $I = 3/2$ sequence has a central-transition flip angle of π (a '90–180 echo').

13.3 Spin $I = 5/2$

The most important nuclides with spin $I = 5/2$ are ^{17}O, ^{25}Mg, ^{27}Al, ^{55}Mn, ^{121}Sb, ^{127}I and the two rhenium isotopes ^{185}Re and ^{187}Re.

^{17}O is the only stable oxygen isotope that is NMR active. It is, therefore, of great importance, despite its very low natural abundance and large quadrupole moment. It is feasible, although expensive, to enrich materials with ^{17}O so that NMR may be used to probe the local environments of the oxygen atoms in a molecule or mineral.

^{27}Al NMR is of great importance in inorganic chemistry. It is a relatively 'easy' spin-5/2 isotope, since it has a high natural abundance and a reasonably large gyromagnetic ratio.

The quantum mechanics of spins-5/2 may be developed in the same way as for spins-3/2. There are six Zeeman eigenstates, with the following properties:

$$\hat{I}_z|\frac{5}{2}, M\rangle = M|\frac{5}{2}, M\rangle$$
$$\hat{I}^2|\frac{5}{2}, M\rangle = I(I+1)|\frac{5}{2}, M\rangle = \frac{35}{4}|\frac{5}{2}, M\rangle$$

where $M = \{5/2, 3/2 \ldots -5/2\}$. The first-order quadrupolar Hamiltonian is given by

$$\begin{aligned}\widehat{\mathcal{H}}_{\mathrm{Q}}^{(1)} &= \omega_{\mathrm{Q}}^{(1)} \times \frac{1}{6}\left(3\hat{I}_z^2 - I(I+1)\widehat{1}\right) \\ &= \omega_{\mathrm{Q}}^{(1)} \times \frac{1}{2}\left(\hat{I}_z^2 - \frac{7}{4}\widehat{1}\right) \qquad \text{(for spin } I = 5/2)\end{aligned} \tag{13.48}$$

The first-order quadrupolar coupling is given by

$$\omega_{\mathrm{Q}}^{(1)}(\theta_{\mathrm{Q}}) = \frac{\pi C_{\mathrm{Q}}}{10} \times \frac{1}{2}\left(3\cos^2\theta_{\mathrm{Q}} - 1\right) \qquad \text{(for spin } I = 5/2) \tag{13.49}$$

assuming a uniaxial electric field gradient tensor ($\eta_{\mathrm{Q}} = 0$). Note the factor of 10 in the denominator of the right-hand side of Equation 13.49. The effect of the quadrupole coupling constant C_{Q} is scaled down strongly for spin-5/2.

The Zeeman eigenstates are also eigenstates of the first-order quadrupolar Hamiltonian, as follows:

$$\widehat{\mathcal{H}}_{\mathrm{Q}}^{(1)}|\frac{5}{2}, \pm\frac{5}{2}\rangle = +\frac{5}{3}\omega_{\mathrm{Q}}^{(1)}|\frac{5}{2}, \pm\frac{5}{2}\rangle$$
$$\widehat{\mathcal{H}}_{\mathrm{Q}}^{(1)}|\frac{5}{2}, \pm\frac{3}{2}\rangle = -\frac{1}{3}\omega_{\mathrm{Q}}^{(1)}|\frac{5}{2}, \pm\frac{3}{2}\rangle$$
$$\widehat{\mathcal{H}}_{\mathrm{Q}}^{(1)}|\frac{5}{2}, \pm\frac{1}{2}\rangle = -\frac{4}{3}\omega_{\mathrm{Q}}^{(1)}|\frac{5}{2}, \pm\frac{1}{2}\rangle$$

For spins-5/2, a positive first-order coupling $\omega_{\mathrm{Q}}^{(1)}$ increases the energy of the outer pair of states, while decreasing the energy of the inner four states (see Figure 13.26). This figure is appropriate for the ^{27}Al case, which has a positive gyromagnetic ratio. The arrangement of energy levels is inverted in the case of ^{17}O, which has a negative gyromagnetic ratio.

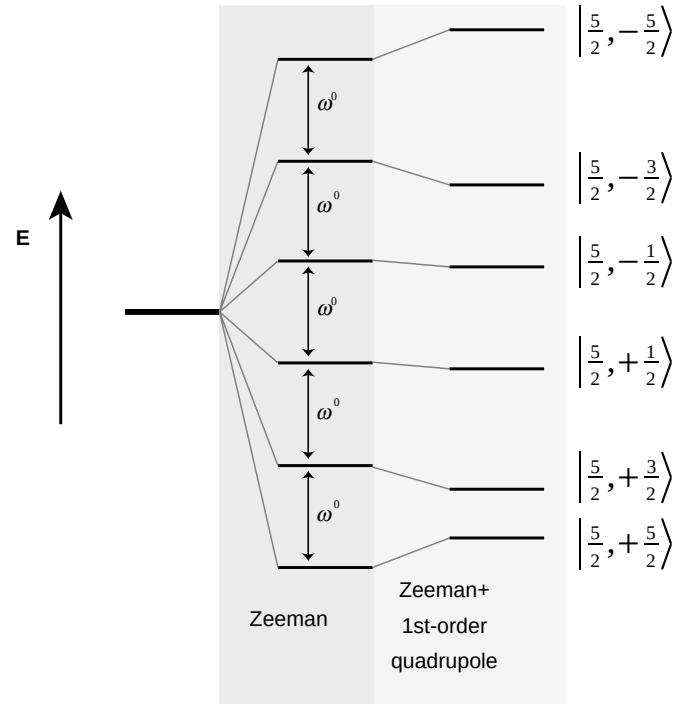

Figure 13.26
Energy levels of a spin-5/2 nucleus, for a positive gyromagnetic ratio.

The quantum state of a spin-5/2 ensemble may be represented by a 6×6 density matrix, comprising six populations on the diagonal, five (-1)-quantum coherences, five $(+1)$-quantum coherences, four (-2)-quantum coherences, four $(+2)$-quantum coherences, three (-3)-quantum coherences, three $(+3)$-quantum coherences, two (-4)-quantum coherences, two $(+2)$-quantum coherences, and a pair of coherences with order ± 5. The complete density matrix, including the satellite order indices, is as follows:

$$\hat{\rho} = \begin{pmatrix} \rho_{|+5/2\rangle} & \rho_{\boxed{+1_{+4}}} & \rho_{\boxed{+2_{+6}}} & \rho_{\boxed{+3_{+6}}} & \rho_{\boxed{+4_{+4}}} & \rho_{\boxed{+5_{0}}} \\ \rho_{\boxed{-1_{-4}}} & \rho_{|+3/2\rangle} & \rho_{\boxed{+1_{+2}}} & \rho_{\boxed{+2_{+2}}} & \rho_{\boxed{+3_{0}}} & \rho_{\boxed{+4_{-4}}} \\ \rho_{\boxed{-2_{-6}}} & \rho_{\boxed{-1_{-2}}} & \rho_{|+1/2\rangle} & \rho_{\boxed{+1_{0}}} & \rho_{\boxed{+2_{-2}}} & \rho_{\boxed{+3_{-6}}} \\ \rho_{\boxed{-3_{-6}}} & \rho_{\boxed{-2_{-2}}} & \rho_{\boxed{-1_{0}}} & \rho_{|-1/2\rangle} & \rho_{\boxed{+1_{-2}}} & \rho_{\boxed{+2_{-6}}} \\ \rho_{\boxed{-4_{-4}}} & \rho_{\boxed{-3_{0}}} & \rho_{\boxed{-2_{+2}}} & \rho_{\boxed{-1_{+2}}} & \rho_{|-3/2\rangle} & \rho_{\boxed{+1_{-4}}} \\ \rho_{\boxed{-5_{0}}} & \rho_{\boxed{-4_{+4}}} & \rho_{\boxed{-3_{+6}}} & \rho_{\boxed{-2_{+6}}} & \rho_{\boxed{-1_{+4}}} & \rho_{|-5/2\rangle} \end{pmatrix}$$

As usual, the observable (-1)-quantum coherences are the most important. Excitation with a $\pi/2$ pulse in the strong-pulse regime ($|\omega_{\text{nut}}| >> |\omega_{\text{Q}}^{(1)}|$) provides a five-peak spectrum, with intensities in the ratio 5:8:9:8:5, as shown below:

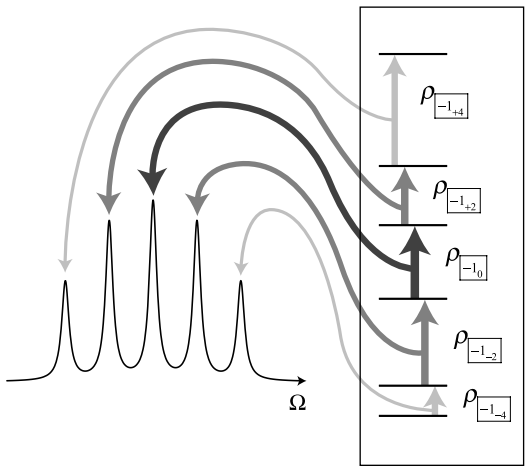

Figure 13.27
The spectrum of a spin-5/2 ensemble and the corresponding (−1)-quantum coherences.

The splitting between adjacent peaks is $\omega_{\mathrm{Q}}^{(1)}$, as for spins-1 and spins-3/2. The peak intensities correspond to the squares of the matrix elements of $\hat{I}^{+}$:

$$\hat{I}^{+} = \begin{pmatrix} 0 & \sqrt{5} & 0 & 0 & 0 & 0 \\ 0 & 0 & 2\sqrt{2} & 0 & 0 & 0 \\ 0 & 0 & 0 & 3 & 0 & 0 \\ 0 & 0 & 0 & 0 & 2\sqrt{2} & 0 \\ 0 & 0 & 0 & 0 & 0 & \sqrt{5} \\ 0 & 0 & 0 & 0 & 0 & 0 \end{pmatrix}$$

In isotropic liquids, the first-order quadrupolar coupling vanishes, so all five spectral peaks are coincident. For example, the NMR spectrum of ^{17}O-labelled water is a single line (the J-couplings to the protons are unresolved).

In anisotropic liquids, the five-peak multiplet of Figure 13.27 becomes visible.

In powdered solids, the satellite peaks from the $\rho_{\boxed{-1_{\pm 2}}}$ and $\rho_{\boxed{-1_{\pm 4}}}$ coherences are generally too broad to observe. The spectra are dominated by the central-transition peak from the coherence $\rho_{\boxed{-1_{0}}}$, for which the frequency is independent of the first-order quadrupole coupling $\omega_{\mathrm{Q}}^{(1)}$. Nevertheless, the central-transition peaks are broadened by the second-order quadrupole coupling $\omega_{\mathrm{Q}}^{(2)}$, which may be as large as hundreds of kilohertz, in the case of ^{17}O. An experimental example is shown in Figure 13.28.

As in the spin-3/2 case, the second-order quadrupole broadening may be reduced by using a strong static magnetic field, and may be eliminated entirely using methods such as DAS, DOR, MQ-MAS, or ST-MAS (see *Further Reading*).

When C_{Q} is large, r.f. pulses act selectively on the central transition, as described in Section 13.2.7. The central-transition nutation frequency is given by

$$\omega_{\mathrm{nut}}^{\mathrm{C}} = 3\omega_{\mathrm{nut}} \qquad \text{(for spins } I = 5/2\text{)} \tag{13.50}$$

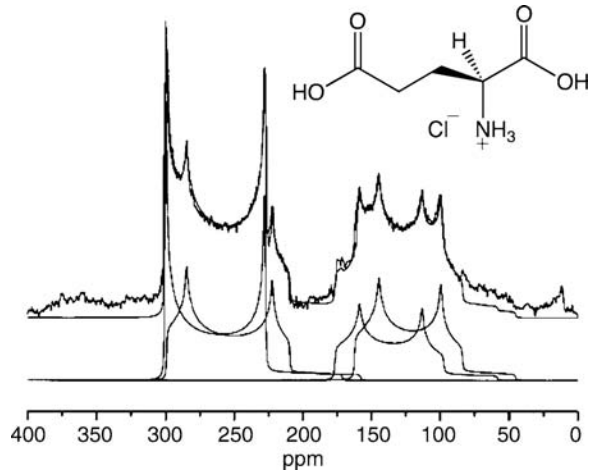

Figure 13.28 Solid-state magic-angle-spinning ^{17}O NMR spectra of ^{17}O-labelled L-glutamic acid hydrochloride obtained at a magnetic field of 14.1 T. All spectral features are generated by the ^{17}O central transition coherences; the satellite signals are too broad to be detected. The spectrum contains contributions from four different ^{17}O sites, with different quadrupole and chemical shift parameters. Each spectral contribution has a complicated shape due to second-order quadrupolar broadening. Simulations of the lineshape components are shown below the experimental data. Adapted from V. Lemaître, K. J. Pike, A. Watts, T. Anupõld, A. Samoson, M. E. Smith and R. Dupree, *Chem. Phys. Lett.* **371**, 91–97 (2003), copyright Elsevier.

For spins-5/2, the r.f. pulse is *three times* as effective when acting selectively on the central transition, compared with the non-selective regime.

13.4 Spins $I = 7/2$

Nuclear isotopes with spin $I = 7/2$ include ^{45}Sc, ^{51}V, ^{59}Co, ^{133}Cs, ^{139}La and ^{165}Ho.

Spin-7/2 nuclei have eight Zeeman energy levels, so the NMR spectrum contains contributions from seven (-1)-quantum coherences. In an isotropic environment, all seven peaks are superimposed, but a seven-peak multiplet is observed if the environment is anisotropic. Excitation in the strong-pulse regime provides a seven-peak multiplet with intensities in the ratio 7:12:15:16:15:12:7. These numbers are the squares of the $\hat{I}^+$ matrix elements. An experimental ^{133}Cs spectrum displaying a seven-peak multiplet is shown in Figure 13.24b.

In powdered solids, only the central transition is usually observed, if C_Q is large. In this regime, an r.f. pulse acts selectively on the central transition. The central-transition nutation frequency is

$$\omega_{\text{nut}}^{\text{C}} = 4\omega_{\text{nut}} \qquad \text{(for spins } I = 7/2\text{)} \tag{13.51}$$

Note the large enhancement factor for the central-transition nutation frequency.

13.5 Spins $I = 9/2$

Spin $I = 9/2$ isotopes include ^{83}Kr, ^{93}Nb, ^{115}In, and ^{209}Bi.

The $I = 9/2$ isotope ^{93}Nb is the most magnetic nuclide in the periodic table. The magnitude of the nuclear magnetic moment is given by

$$\langle \mu \rangle = \langle \hat{\boldsymbol{\mu}}^2 \rangle^{1/2} = \gamma \hbar \{ I(I+1) \}^{1/2}$$

Although the gyromagnetic ratio of ^{93}Nb is only 24% that of ^{1}H, the high nuclear spin of ^{93}Nb leads to a nuclear magnetic moment $\langle \mu \rangle$ that is about 50% greater than that of ^{1}H.

Notes

1. ^{14}N NMR is relatively straightforward if the nitrogen is in a sufficiently symmetrical environment (e.g. in the case of NH_4^+ ions), or if the molecular site has a high degree of mobility, so that the electric field gradient is averaged to a small value.

2. A general quantum state of a spin-1/2 nucleus may be depicted by drawing a polarization arrow pointing in the direction of defined $+\frac{1}{2}$ angular momentum. By extension, the general quantum state of a spin-1 nucleus may be depicted using *two* arrows, and the general quantum state of a spin-3/2 nucleus may be depicted using *three* arrows, and so on. This technique is sketched in R. Penrose, '*The Emperor's New Mind*', Oxford University Press, 1989, p. 353.

3. The use of the satellite order index was developed by S. Antonijevic and G. Bodenhausen, *J. Magn. Reson.* **180**, 297–304 (2006), following the early analysis of I. Solomon, *Phys. Rev.* **110**, 61 (1958).

4. The (± 2)-quantum coherences of spins $I = 1$ give rise to weak NMR signals at *twice* the Larmor frequency, in the case of large quadrupolar couplings. These peaks are called *overtones* and result from the breakdown of the secular approximation. The (± 2)-quantum overtone frequencies are insensitive to the first-order quadrupole coupling (see Equation 13.11). Overtone ^{14}N spectroscopy may be used to study peptide conformations (e.g. see R. Tycko and S. J. Opella, *J. Am. Chem. Soc.* **108**, 3531 (1986)).

5. The absence of a quadrupolar splitting for ^{2}H nuclei in isotropic liquids allows the ^{2}H resonance to be used for stabilizing the magnetic field in solution NMR experiments. See Chapter 4 Note 3.

6. There is a rich variety of liquid crystal phases, and not all of them give rise to the simple multiplets depicted in Figures 13.9 and 13.23. In general, more complex spectra are observed, which depend on the orientational distribution of the liquid crystal director axes with respect to the magnetic field.

7. The lineshape is named after its discoverer, George E. Pake (*J. Chem. Phys.* **16**, 327 (1948)).

8. The greater probability of perpendicular orientations compared with parallel orientations is discussed in Section 9.3.2.

9. This discussion of quadrupolar lineshapes neglects the influence of CSA. In the presence of CSA interactions, the contributions from the two (-1)-quantum coherences are different, giving rise to asymmetrical powder lineshapes.

10. The effective time origin of the ^{2}H NMR signal is actually at the *centre* of the r.f. pulse, so a reduction in the 'dead time' to zero would still not be good enough to detect an accurate powder NMR signal.

11. The description of the spin-1 quadrupolar echo is significantly more complicated if chemical shifts cannot be neglected. In that case, coherences must be followed individually, instead of grouping them together as in Equation 13.26. A full analysis distinguishes between coherence transfers that change both the coherence order and the satellite order (such as $\rho_{\boxed{+1_{+1}}} \Rightarrow \rho_{\boxed{-1_{-1}}}$) and coherence transfers that only change the satellite order (such as $\rho_{\boxed{-1_{+1}}} \Rightarrow \rho_{\boxed{-1_{-1}}}$). In the former case, a Zeeman echo is formed at the same time as the quadrupolar echo. This means that the chemical shift evolution refocuses at the same time as the first-order quadrupole evolution. In the second case, only a quadrupolar echo is formed. This means that the first-order quadrupole evolution refocuses, but the chemical shift evolution does not. The echo signal is a superposition of these different components.

12. Strictly speaking, the spectral peaks do not arise from *transitions*, but from *coherences*. Nevertheless, I retain the common terms *central transition* and *satellite transition*, for the sake of consistency with the literature.

13. Although techniques such as DOR and MQ-MAS remove second-order quadrupolar *broadening*, they do not remove *all* effects of the second-order quadrupolar interaction. There is also a *second-order quadrupolar shift*, which is analogous to a chemical shift, and which is not removed by DOR, MQ-MAS, and similar methods. This second-order shift is also observed in isotropic liquids where it is given the name 'dynamic frequency shift'.

14. Figure 13.25 suggests that the population difference across the central transition is enhanced if the populations are first equalized across each of the two satellite transitions. Saturation of the two satellite transitions by using a suitably modulated r.f. field may, therefore, be used to enhance the central-transition signal generated by a subsequent selective $(\pi/2)_x^C$ pulse. A number of experimental methods exploit this trick. One example is described in H. T. Kwak, S. Prasad, T. Clark and P. J. Grandinetti, *Solid State Nucl. Magn. Reson.* **24**, 71–77 (2003). See Exercise 13.1.

Further Reading

- A good introduction to the solid-state NMR of quadrupolar nuclei is given in M. J. Duer, *Introduction to Solid-State NMR Spectroscopy*, Blackwell Science, 2004.
- The following article is recommended as a good introduction to solid-state NMR in general, including a concise overview of quadrupolar NMR techniques: D. D. Laws, H.-M. L. Bitter and A. Jerschow, *Angew. Chem. Int. Ed.* **41**, 3096–3129 (2002).
- It needs a steady head to navigate the formal theory of quadrupolar NMR in solids. A reliable guide is provided by A. Jerschow, *Prog. NMR Spectrosc.* **46**, 63–78 (2005).
- A review of ^{23}Na NMR in anisotropic environments is given in R. Kemp-Harper, S. P. Brown, C. E. Hughes, S. Peter and S. Wimperis, *Prog. NMR Spectrosc.* **30**, 157–181 (1997).
- Techniques for the NMR of quadrupolar nuclei in solids are reviewed by M. E. Smith and E. R. H. van Eck, *Prog. NMR Spectrosc.* **34**, 159–201 (1999), and S. E. Ashbrook and M. J. Duer, *Concepts Magn. Reson. A* **28**, 183–248 (2006).
- An excellent review of satellite-transition magic-angle-spinning experiments is given in S. E. Ashbrook and S. Wimperis, *Prog. NMR Spectrosc.* **45**, 53–108 (2004).
- The following classic paper on quadrupolar echoes in solids is still instructive: I. Solomon, *Phys. Rev.* **110**, 61 (1958).

Exercises

13.1 Consider an ensemble of spin-I nuclei, where I is a half-integer greater than 1 (i.e. $I = 3/2$, or $5/2$, or $7/2$, etc.) The spin system is left to reach thermal equilibrium, and then all the satellite transitions are completely saturated by a suitably modulated r.f. field. What is the enhancement factor for the population difference across the central transition?

13.2 In Section 13.2.7, it is shown that the nutation frequency of the spin $I = 3/2$ central transition is enhanced by a factor 2 when the transition is excited selectively, compared with the non-selective case. What is the enhancement factor for general I (assuming that I is a half-integer greater than 1)?

13.3 The quadrupolar echo pulse sequence in Figure 13.12 uses two $\pi/2$ pulses with a relative phase shift of $\pi/2$. Show that the same sequence generates double-quantum coherence if the two pulses have the same phase.

13.4 How many peaks are observed for an ensemble of spin-9/2 nuclei in a slightly anisotropic environment? What are the relative intensities of the multiplet components for ideal strong-pulse excitation?